ABSTRACT

CHEE EUNICE Enhancing Biomimetic Function of Platelet-Like Particles. (Under direction of Dr. Ashley Brown)

Platelets hold crucial functions in the process of wound healing and immune responses. To achieve these functions, platelets travel in the vascular system in a rounded inactive state until they arrive at an injury site where they, subsequently, change morphology into a stellate shape and bind to various clotting components. Platelets bind to fibrinogen, generate thrombin on their surface, and enhance fibrin clot formation. Over time, platelets can then activate myosin machinery and pull fibrin fibers in to condense clots, thus inducing the process of clot retraction, which contributes to clot stability and healing. However, these processes can become compromised when platelets become depleted, such as in cases of traumatic bleeding. To address issues associated with platelet depletion, many platelet-mimetic products have been developed previously throughout the biomedical field but have been focused primarily on recapitulating the hemostatic activity of platelets. In contrast, our group has developed platelet-like particles (PLPs) that are capable of not only mimicking the shape and hemostatic abilities, but also the clot retraction function of natural platelets.

Despite these promising properties, PLPs still have some capacities that could be improved to improve their platelet-mimetic nature. PLPs consist of a highly deformable microgel coupled to a fibrin targeting motif (such as an antibody or peptide). However, unlike natural platelets, PLPs lack any antimicrobial function. Additionally, unlike natural platelets, current PLP formulations do not conditionally change shape in response to injury stimuli, but rather, only mimic activated platelet morphology. As a result, there is a need to investigate and develop alternative PLP formulations with enhanced functions. Thus, the purpose of the works described in this dissertation were to: 1) develop a PLP with antimicrobial capabilities and 2) develop PLPs

with wound-triggered shape changing capability. Additionally, this dissertation also explores long-term stability of the resulting enhanced function PLPs.

© Copyright 2022 by Eunice Chee

All Rights Reserved

Enhancing Biomimetic Function of Platelet-Like Particles

by
Eunice Chee

A dissertation submitted to the Graduate Faculty of
North Carolina State University
in partial fulfillment of the
requirements for the degree of
Doctor of Philosophy

Biomedical Engineering

Raleigh, North Carolina
2022

APPROVED BY:

_____	_____
Dr. Ashley Brown Committee Chair	Dr. Ke Cheng
_____	_____
Dr. Maureane Hoffman External Member	Dr. William Polacheck External Member
_____	
Dr. David Zaharoff	

BIOGRAPHY

Eunice was born and raised in the United States and has lived all over the country until settling down in Austin, Texas through completion of high school. She received a Bachelor of Science in Engineering in Biomedical Engineering from the University of Pennsylvania. In 2017, she became a doctoral student under the direction of Dr. Ashley Brown in the Joint Department of Biomedical Engineering at North Carolina State University and the University of North Carolina – Chapel Hill.

ACKNOWLEDGMENTS

The work presented in this thesis would not have been possible without the help of the many people I have had the pleasure of working with for the duration of my doctoral program. Firstly, I would like to thank Dr. Ashley Brown for not only providing me the great honor of working under her but also for being a wonderful, receptive, and insightful mentor. I truly enjoyed and appreciated hearing feedback from you in all our meetings! Thanks to your positive and motivating demeanor, I felt great motivation to push onwards as much as I could throughout the duration of my time working with you and the Advanced Wound Healing Laboratory.

I would also like to thank my committee members—Dr. William Polacheck, Dr. David Zaharoff, Dr. Ke Cheng, and Dr. Maureane Hoffman—for taking the time out of their busy schedules to provide me much appreciated insight and feedback owed to their individual field expertise. This thesis work could not attain the quality it has without your involvement.

To my fellow Advanced Wound Healing Laboratory members, thank you for your support and feedback over the last 5 years. To Erin, thank you for helping me learn the foundation protocols and knowledge for the antimicrobial PLP project; I learned much about the practices in our lab under your mentorship. To Seema, thank you for teaching me everything needed to fully characterize PLPs, both *in vitro* and *in vivo*, and for your patience and guidance. To Kim, thank you for being great moral support, helping with animal studies, and for your insights throughout my years as a part of our research group. To Emily, thank you for helping me out with animal studies and for helping me brainstorm through problems I encounter in the lab, especially when it came to Aim 2 experiments. To Dan, thank you for helping me get started and acquainted with basic particle synthesis. To Grant, thanks for being great company in the lab and for helping me through my many struggles with both AFM and the fluorescent microscope. To

Nina, thank you for also being great company in the lab; It's always a joy to chat with you and educational to hear about what goes on with the clinical side of things as of late. To Aryssa, Halston, and Ana: thanks for being great company in the lab even at odd hours, helping in a pinch, and for the shared sympathies in the continual process that research is! I wish you all the best in your experiments and progress towards your own theses! To our lab manager Jenn, thank you so much for all your help with all the animal studies, administrative matters, and lyophilizer maintenance. I could not have done so many of my experiments without your help keeping the lab stocked and years of animal study experience. You have been a great pleasure to work with.

To my fellow researchers at the BPC, it has been fun getting to know you all and learning what else goes on in the building. I have really enjoyed being a part of this collaborative community. Special thanks to Camillo for helping me get initially acquainted with the lyophilizer and its continued maintenance!

I would also like to thank the staff of the NCSU facilities. Without their help, there are many experiments that would not have been possible. From the AIF, I would like to thank Toby Tung, Christopher Winkler, and Yang Liu for their help with using the TEM. I would also like to thank Elaine Zhou for helping me become trained with using the cryoSEM and for her patience and understanding over the course of my time using the machine. From the CMIF, I would like to thank Marius Zareba and Eva Johannes for their help with using the confocal microscopy facilities. From Toxicology, I would like to thank Sandy Elliot for helping me conduct my infected dermal injury studies safely and with minimal impact on other projects. I would also like to thank the staff and Dr. Nikita George of LAR for accommodating the many survival liver laceration studies conducted in their facilities.

Finally, I would like to thank my parents for helping me find my way through life and supporting me through the duration of my program. Thank you for your insights from your own experiences as doctoral students and for your advice on how to ensure my doctoral program goes smoothly. Without your advice, I would have not enjoyed my time during my doctoral program as much.

TABLE OF CONTENTS

LIST OF TABLES

LIST OF FIGURES

CHAPTER 1

Introduction to Platelet Function in Wound Healing and Hemostasis and Overview of Platelet-Mimetic Materials and Biomimetic Antimicrobial Strategies

1.1 Platelet Function and Significance

Platelets are crucial to the wound healing process and are also involved in the response to pathogens, such as bacteria, working to both coordinate leukocytes and directly disrupt bacteria viability via production of antimicrobial peptides [3]. Platelets achieve their functions through a number of mechanisms including changing shape upon activation, exposing fibrin(ogen) receptors on their surfaces, binding to fibrin(ogen) at the wound site and promoting clot formation, and inducing clot retraction.

In the absence of injury, platelets will remain in a rounded inactive state. This shape facilitates the movement of platelets to vessel wall for adhesion to blood vessel walls, or margination. When injury occurs, margination allows platelets to approach and bind to injury sites and drive hemostasis through aggregation and promotion of fibrin formation. In the presence of coagulation factors, platelets undergo activation, activate cell surface receptors that bind to fibrin and undergo significant shape change, mediating the hemostasis process.

Hemostasis occurs through both primary and secondary hemostasis. During primary hemostasis [4], platelets aggregate and form a platelet plug to initially staunch bleeding. In secondary hemostasis, a fibrin clot forms that further contributes to cessation of bleeding. Additionally, the firm clot that forms serves as a provisional scaffold for later tissue repair. In this phase, thrombin generation on the platelet surface promotes rapid conversion of fibrinogen to fibrin. On a longer time-scale (i.e. hours after injury), platelets can also induce a process

known as clot retraction where they engage actin-myosin machinery to collapse or retract clots. Platelets bind to fibrin by using surface receptors (particularly integrin α2bβ3) that gain high binding affinity when platelets are activated and change shape. While in an activated state, platelets generate contractile forces in their actin-myosin cytoskeleton which get transferred to fibrin fibers through surface receptors and leads to platelets actively pulling and shortening fibrin fibers. As this process gets repeated, the fibrin becomes bundled where the platelet is and pulls in more fibers which leads to a summative response of bulk clot retraction across multiple platelets. [5-7] There has been much interest in better understanding the physiological role of clot retraction. Recent evidence suggests that clot retraction contributes to wound healing by increases clot stability [8,9]. Additionally, the condensed clot has higher stiffness, which can durotactically guide cells into the wound bed and enhance consequential healing [10]. Furthermore, the condensed clot size also allows for increased blood flow to the injured tissue. [4]

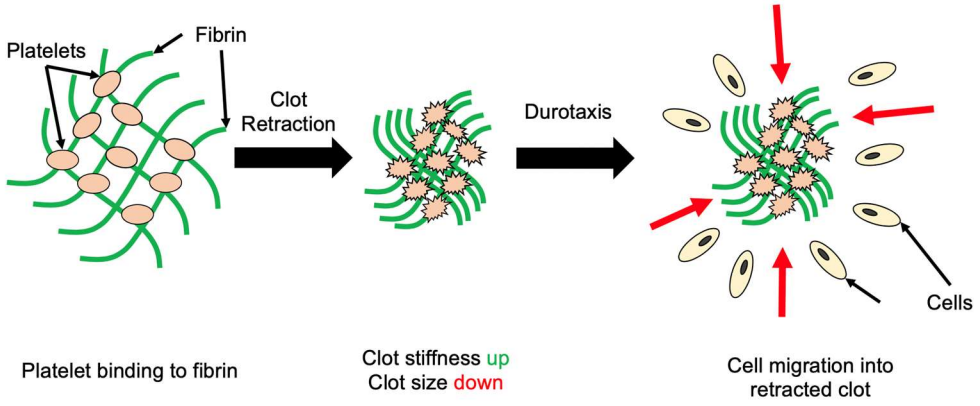

Figure 1.1 Schematic of clot retraction process. In clots formed at injury sites, platelets will bind to fibrin, activate their actin-myosin machinery and change shape. Through this process, platelets pull fibrin together to create a more condensed clot structure, resulting in higher stiffness and smaller clot size. Due to the higher stiffness of the condensed clot, cells migrate into the injury site by durotaxis.

Platelets can also partake in the immune response and participate in the immune response both indirectly and directly. The indirect participation of platelets in the immune response comes from directing many immune cell types, including neutrophils and monocytes, to aggregate around pathogens. Platelets can also directly partake in fighting infection by binding to bacteria and releasing antimicrobial compounds [3]

Platelets hold incredibly important functions to natural hemostasis, wound healing, and immune response. However, these functions can become compromised when platelets become depleted in certain situations, such as in traumatic bleeding, which remains the leading cause of death for people under the age of 45, in sepsis and infection, or in other conditions where hemostasis or platelet function is inhibited and contributes to impaired healing such as diabetes, or hereditary disorders (e.g.: von willebrand disease, hemophilia) [11-14]. Depletion of platelets can lead to unfavorable outcomes including decreased quality in healing, increased presence of viable bacteria in the blood (bacteremia), increased tissue damage and increased mortality [11,15]. As such, there is a great clinical need to address problems associated with platelet depletion.

1.2 Platelet Mimetic Strategies and Materials

To address clinical issues that result from platelet depletion, several platelet-mimetic strategies have been developed including natural platelet derived strategies, artificial platelets, and cloaking and active targeting drug delivery. Natural platelet derived strategies, such as platelet transfusion or lyophilized platelets, are based around creating derived substances from natural platelets. Platelet transfusion entails the use of allogenic platelets from an alternate source. Since platelet transfusions consist of natural platelets, all important functions and biologic compatibility is retained. However, they have extremely short shelf life (lasting up to 7 days at most), do not fully retain efficacy, and have immunogenicity issues due to not being

sourced from the patient. [4,16]Additionally, the availability of platelets is limited due to there being a lack of platelet donors. To address this issue, lyophilized platelets have been utilized. While storing in a lyophilized form increases the shelf life, lyophilized platelets were found to have short circulation time before clearance [17]. In addition, lyophilization does not remove the immunogenicity issues associated with allogenic platelets and can potentially lead to aggregation in the spleen [4,17,18].

Artificial platelets have also been investigated and tend to consist of particles or polymers coupled to bioactive motifs such as RGD peptides or antibodies that bind to platelets or coagulation factors. This design allows for reduced immunogenicity in comparison to the use of allogenic platelets. Additionally, artificial platelets have longer shelf lives and are easier to scale up, manufacture and tune. However, artificial platelets can have low clearance from physiological systems and do not recapitulate multiple platelet functions. [4] Many formulations of artificial platelets are focused on one aspect between mimicking shape, or mechanical properties.

Synthetic platelets developed by Mitragotri's group mimic the shape, size and flexibility of platelets by creating discoid particles. These discoid particles were created by stretching platelet-size matched particles into discoid shape, depositing proteins and polyelectrolytes in a layer by layer process with crosslinking of protein layers, and then finally removing the encased particle. These particles are capable of mimicking the mechanical stretching of natural platelets and were designed to target platelet thrombi by binding to GP1bα [19]. Another notable example of synthetic platelets is Synthoplate, developed by Sen Gupta's group, which consists of liposomes with binding motifs that target primary hemostasis markers (von Willebrand factor and collagen in particular) and mimic platelet hemostasis with demonstrated *in vivo* efficacy [20]. The Lavik group has also developed a synthetic platelet consisting of a poly(lactic-co-glycolic acid)-poly-L-lysine

(PLGA-PLL) main particle conjugated to polyethylene glycol (PEG) arms with RGD peptide ends. It was observed that these synthetic platelets can adhere to platelets, bind to clots and, mimic the hemostatic ability of platelets with significantly lower *in vivo* bleeding time [21]. Overall, many synthetic platelets are focused around mimicking the binding behaviors of platelets and their hemostatic ability.

Cloaking and active targeting drug delivery strategies have also been developed and consist of coupling drug delivery vessels to platelet binding motifs or platelet membranes. This type of strategy leads to increased targeting of drug delivery with less severe immune response than drug delivery without cloaking as well as improved circulation time [22]. However, cloaking strategies require the extraction of components from pre-existing platelets, which are not readily available. [4]

1.3 Ultra-Low Crosslinking (ULC) Microgel Platelet-like Particles

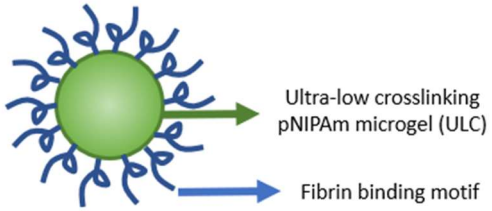

Figure 1.2: Composition of a platelet like particle (PLP). PLPs consist of a highly deformable microgel body coupled to a fibrin targeting motif on the acrylic acid co-polymer groups.

To address the issue of platelet depletion, our group has developed platelet-like particles (PLPs). As illustrated in **Figure 1.2**, PLPs consist of a highly deformable ultra-low crosslinking (ULC) microgel coupled to a fibrin-targeting antibody and can mimic platelets' ability to bind to fibrin, deform, and then retract clots. [23] This feature is thanks to the high deformability of the ULC and the high fibrin affinity of the fibrin-targeting antibody. To induce clot retraction, PLPs

bind to fibrin fibers and then deform and spread between bound fibers. Eventually, the microgel body will then return to a more energetically favorable state (its normally spherical morphology) and exert strain on the fibers it is bound to in the process. As a result of this strain, a microcollapse of the clot occurs. As this process occurs with multiple PLPs within the clot, eventually a bulk clot collapse is achieved. [23,24] In order for this process to occur, fibrin binding affinity must be high and the particle must highly deformable to achieve particle bridging of multiple fibrin fibers within the clot. If particle deformablity is decreased, for example through increased microgel crosslinking, or if the particle does not bind fibrin, PLP-mediated clot retraction is lost. This clot retraction is similar to natural platelet retraction as natural platelets will also bind to fibrin fibers, exert strain on fibers to induce a microcollapse that also results in a summative response of bulk clot retraction. [5] Despite these similarities, PLP clot retraction operates in a more passive manner relying on the microgel body to return to a base state as opposed to actively extending projections from the body like natural platelets. [5-7] Work in our group suggests that this clot retraction ability allows the PLPs to stabilize clots, increase clot stiffness and enhance cell migration by durotactic mechanisms. [8,10] This design additionally allows for PLPs to target sites of injury and enhance hemostasis *in vitro* and *in vivo*. While promising as a hemostatic and wound healing agent, PLPs still lack the ability to mimic some functions that are key to natural platelet function. In particular, PLPs, as is, are unable to fight infection or change shape conditionally. Both of these capacities are important functions of natural platelets. [3]

1.4 Antimicrobial Biomaterials

Drug resistant bacteria have become an ever-growing problem in clinics, affecting at least 2.8 million individuals annually [25]. Notable drug resistant strains include Methicillin-resistant

Staphylococcus aureus (MRSA) and drug -resistant *Streptococcus pneumoniae*, which led to about 323,000 infections and 900,000 infections in 2019 [25]. To combat infection by drug resistant variants, many material strategies have been investigated, ranging from delivery of alternative antimicrobial agents, such as antimicrobial peptides and nanometals, to modifying surfaces that known to be antimicrobial, such as insect wing surfaces and shark skin.

Current antimicrobial strategies include molecularly based strategies, biopolymers, and antimicrobial derived substances. Molecular strategies include the use of nanometals, antimicrobial peptides (AMPs), and bacteriophages, which are viruses that are directed to target bacteria. Biopolymer strategies are focused around modifying polymeric materials to bestow antimicrobial activity, including direct modification of molecular structure, incorporation of materials to induce migration of immune cells, or even the incorporation of antimicrobial substances. Antimicrobial derived substances refer to substances that are derived from naturally antimicrobial materials, such as platelet rich plasma (PRP) and essential oils. [26]

While these strategies provide alternatives to commonly used clinical drugs, there are some notable problems. Among molecular based strategies, nanometals and AMPs are frequently associated with high toxicity, be it toxic effects from direct interaction with these molecules or toxic byproducts from production methods. Additionally, AMPs have low *in vivo* efficacy and can be difficult to scale up. While bacteriophages have lower toxicity, bacteria have been recorded to develop resistance to them [27,28]. Biopolymer strategies can face similar issues as nanometals and AMPs due to residue of harsh reagents in synthesis methods. For derived substances, acquiring them can come with significant obstacle such as regulatory barriers for PRP or requirement of very specific fabrication process setups for Essential oils. Additionally, for PRP, antimicrobial efficacy can vary significantly [29].

Many biomimetic materials seek to address these issues, including investigating less harsh synthesis methods of nanometals, or incorporation of AMPs and nanometals into delivery vehicles. However, there are concerns that incorporation into other materials results in masking interaction surface area, leading to decreased efficacy compared to molecules alone. For bacteriophages, alternative functionalization has been investigated to enhance antimicrobial ability or biocompatibility, but the production methods require lots of time with low yields. Interestingly, there have also been more macroscale biomimetic approaches that work towards patterning materials with surface geometry mimicking those in animals to create antimicrobial surfaces, although these materials are not for internal physiological use [26].

1.5 Incorporation of Antimicrobial Materials into Microgels

While these antimicrobial materials do indeed affect drug resistant bacteria, it is also important to consider the ease of incorporation into pNIPAm microgels for the sake of developing an antimicrobial PLP. To make antimicrobial pNIPAm microgels, many methods incorporate nanometals or load the microgels with antimicrobial peptides (AMPs). Incorporation of nanometal is achieved through several different methods and has been utilized in many different constructions as well (e.g.: nanometal distributed throughout microgel, microgel shell with nanometal core, etc.). AMP incorporation is primarily achieved through loading.

Nanometal incorporation into pNIPAm microgels has been well documented in literature, with a variety of methods. These methods can be categorized into 3 main process characteristics: 1) nanometal seeding throughout microgel network, 2) encapsulation around nanometal particles, and 3) physical mixing or breathing in of nanometal particles. Nanometal seeding throughout microgel network entails allowing a metal ion dispersion to be loaded into microgels (where then the metal ions seep into crevices between polymer chains) and then conducting *in* situ reduction

with use of a reducing agent (e.g.: sodium borohydride for nanosilver fabrication) This type of method results in covalently bound nanometal particles that are distributed throughout the microgel. [30-32] Encapsulation around nanometal particles entails polymerizing microgels in the presence of an already prepared solution of nanometal particles, leading to the formation of microgel shells around nanometal particles. The composite nanometal microgels that result from these synthesis methods are assemblies with a nanometal core and microgel shell. [31-34] Physical mixing or breathing in of nanometal entails taking solutions of microgels and nanometals and allowing them to mix. This method type results in a composite microgel that has nanometal particles distributed throughout the microgel body but are not covalently bound. These nanometal composite microgels have also been reported to strongly retain incorporated nanometals. [35,36] Outside of these methods, microgels with surface-adhered nanometal rods have also been reported. [31,37] However, since nanometal rods physically cover the microgel surface, there is great potential for the nanorods to significantly interfere with the antibody targeting coupling process that is required for the work described herein.

Overall, nanometal composite microgels have been reported to retain many of the chemical properties of the polymers they have been incorporated into (e.g.: pH sensitivity, temperature sensitivity) while also gaining the associated properties of the incorporated nanometal (e.g.: antimicrobial activity for silver, optical properties). Applications of these nanometal composite microgels have been primarily focused on use for outside of the body such as for antifouling coatings, catalytic activity, detection of toxic substances, and optical applications. Additionally, it also notable that different microgel morphologies lead to differences in the ability of the microgels to serve as microreactors for the general synthesis of nanometal particles (i.e.: hollow

particles are considered better microreactors because the hollow morphology allows for larger reaction surface area for reduction of silver ions into nanosilver particles). [32,34,37,38]

The majority of incorporation of antimicrobial peptides into microgels consists of loading the AMPs into the microgels. [39-45] In these works, the microgel ultimately serves a delivery vehicle for AMPs. However, the main limitation of this incorporation is that the antimicrobial activity is only present until the loaded AMPs have all been released. In other words, microgels that have antimicrobial peptides incorporated by such methods cannot remain antimicrobial for an extended period of time. Additionally, work by Nyström et al demonstrated that although there is a way to surface conjugate AMPs onto microgels, the mechanism of antimicrobial activity can change depending on ionic presence in the environment. It was reported that at lower ionic presence, antimicrobial activity is based on contact, but at higher ionic presence the antimicrobial activity is based on release of AMPs instead. [46] Although this work was conducted in microgel layers, this difference of antimicrobial activity mechanism is still important to consider as it indicates that antimicrobial activity will ultimately be lost depending on the point of application. Additionally, it has been reported that composite microgels including AMPs still retain the associated toxicity. [47]It is also notable that outside of AMP delivery, the majority of applications for AMP incorporated microgels have been as surfaces/coatings. [47-49]

Thus, an antimicrobial PLP formulation that has nanometal incorporation made the most sense for this project. Nanometal incorporation methods are well-documented in literature, simple to conduct, and typically lead to highly stable nanometal composite microgels, meaning that the nanometal is not easily released and thus antimicrobial activity is retained for longer duration. In particular, methods that incorporate the nanometal throughout the microgel body were appealing for an antimicrobial PLP since these incorporation methods would not

significantly interfere with coupling of fibrin targeting motifs to the AAc groups of the microgel body.

1.6 Previous Work Towards Development of Antimicrobial PLPs

To develop antimicrobial PLPs, our group has previously developed nanogold composite PLPs. Two different types of nanogold composite PLPs were created based on different nanogold coupling types: non-covalently attached nanogold and covalently attached nanogold. Non-covalently attached nanogold composite microgels (ncNGCs) were created by resuspending poly-N-Isopropylacrylamide (pNIPAm) microgels in gold nanosphere solutions and allowing the microgels to "breathe in" the nanospheres. Covalently attached nanogold composite microgels (cNGCs) were created by tetra(hydroxymethyl)phosphonium chloride (THPC) mediated chemistry where nanogold was seeded on the microgels and then grown in size.

It was determined that the inclusion of nanogold did not significantly affect the PLP properties of the ncNGCs and cNGCs, with these composite nanogold microgels showing little difference in microgel size and clot retraction ability. Additionally, for the cNGCs an antimicrobial effect was detected, but it was not statistically significant [36]. Thus, the work of this dissertation sought to build up and optimize the antimicrobial activity for development of a different formulation of antimicrobial PLP using the results observed with nanogold composite PLPs as a foundation. In particular, based on the findings of cNGCs having better antimicrobial activity, this dissertation sought to make a formulation based on using a different nanometal that is also covalently incorporated.

1.7 Previous Work Towards Development of Shape Changing PLPs

Previously, our group has investigated creation of a shape changing PLP using a core-shell design. The core consisted of N-isopropylmethacrylamide (NIPMAm) crosslinked with N,N'-

(1,2-Dihydroxyethylene)bisacrylamide (DHEBA) and the shell consisted of a 2% BIS crosslinked shell. NIPMAm was selected as it is known to have little self-crosslinking, which means that a degradable NIPMAm particle will fully degrade. The inclusion of DHEBA makes it so that the NIPMAm core particle is degradable in the presence of sodium periodate.

The resulting core/shell (C/S) particle is nondeformable and rounded like an inactive platelet. After the core is degraded, a hollow particle is left behind. This hollow particle exhibits similar deformability to ULCs and similar morphology to activated platelets. It was also found that C/S-PLPs did not induce significant clot retraction while hollow-PLPs did. Additionally, following exposure to sodium periodate, the degraded C/S-PLPs were found to have retracted clots, demonstrating potential for triggered shape change. Furthermore, it was found that when applied to a full thickness dermal injury model, the stiff C/S-PLPs did not significantly improve wound healing outcomes while the deformable hollow-PLPs did [50]. These outcomes demonstrate the effect of the changing deformability of C/S-PLPs. The work of this dissertation sought to build upon the results of this work and create a shape changing PLP that degrades in the presence of thrombin, a more physiologically relevant molecule.

CHAPTER 2

Objectives

Platelets hold a crucial role in the wound healing process. Normally, platelets circulate throughout the body in an in active rounded state. Upon injury, platelets will become activated, taking on a stellate shape and displaying fibrin binding cell surface receptors. In this activated state, platelets are able to interact and bind with fibrin fibers in developing clots. However, when depleted, these functions are diminished. The focus of this work is the development of synthetic platelet-like-particles (PLPs) that can be used to replace and/or augment platelet function in situations of platelet depletion.

While previous designs of PLPs can recapitulate important platelet functions of hemostasis and clot retraction, many features of native platelets remain to be realized.[1] In particular, PLPs are not antimicrobial and do not have the ability to change morphology and deformability in response to injury stimuli. Thus, the long-term goal of this proposal is to develop next generation PLPs that better recapitulate platelet function. In order to bestow antimicrobial activity, nanosilver incorporation into PLPs was investigated. Additionally, 1st generation PLPs created from deformable ULCs display morphology mimicking activated platelets.[3,4] However, native platelets conditionally undergo a shape change following exposure to coagulation factors. Preliminary data demonstrates that nondeformable particles allow for better margination and clotting under high shear. Therefore, having a particle that can change deformability in response to injury could be beneficial. To create a PLP that better mimics natural platelet morphology, a shape-shifting architecture was designed to allow PLPs to retain a rounded morphology that is stiff until they come into contact with thrombin generated at wound sites.

The overarching hypothesis of this thesis is that the addition of a) nanosilver or b) wound-triggered shape change to PLPs will result in more platelet-mimetic particles without diminishing previously realized platelet-mimetic functions of hemostatic action, clot retraction, and enhanced healing. This thesis is divided into 2 specific aims with 2 subaims each: 1) to develop an antimicrobial PLP via nanosilver incorporation and 1a) evaluate its *in vitro* properties and 1b) *in vivo* performance in both absence and presence of bacterial infection (**Chapter 3**). 2) to develop a PLP with architectures facilitating wound triggered shape change and 2a) evaluate its *in vitro* properties, 2b) its *in vivo* performance (**Chapter 4**). Completion of these studies represents enhancement of functionality of an already promising platform of hemostatic and wound healing materials with wide range of impact for significant clinical issues.

CHAPTER 3

Nanosilver Composite pNIPAm Microgels for the Development of Antimicrobial Platelet-Like Particles

The goal of the studies outlined in this chapter was to demonstrate the antimicrobial capability of modified ULC-PLP technology. While the promise of ULC-based PLPs has been previously demonstrated [10], they lack several important of functions of native platelets, including the ability to fight off pathogens. In order to bestow antimicrobial capability to ULC-PLPs, nanosilver was incorporated into the ULC body by *in situ* reduction of silver ions. The influence of nanosilver incorporation on associated PLP performance was then evaluated. We were able to demonstrate that the nanosilver incorporation had little to no effects on previously demonstrated PLP hemostatic performance. Additionally, significantly reduced bacterial presence was observed *in vitro* and *in vivo*, and, thus, demonstrated that the ULC-PLP technology was successfully modified to include antimicrobial activity.

The work described in this chapter has been previously published in Journal of *Biomedical Materials Research Part B: Applied Biomaterials*: Chee E, Nandi S, Nellenbach K, Mihalko E, Snider DB, Morrill L, Bond A, Sproul E, Sollinger J, Cruse G, Hoffman M. Nanosilver composite pNIPAm microgels for the development of antimicrobial platelet-like particles. Journal of Biomedical Materials Research Part B: Applied Biomaterials. 2020 Aug;108(6):2599-609.

3.1 Introduction

Platelets are crucial to the wound healing process but can become depleted in traumatic injury or chronic wounds. Under normal conditions, platelets are able to bind to fibrin to promote

hemostasis and, over time, platelets engage their actin-myosin machinery to induce clot collapse through a process known as clot retraction. Beyond their role in hemostasis, platelets play important roles in promoting downstream healing through a variety of mechanisms including clot retraction and release of cytokines, growth factors, and antimicrobial agents [4] . Clot retraction leads to increased fibrin density, stabilization of the fibrin network, decreased external fibrinolysis and encourages cellular migration into wound beds [8]. Additionally, platelets fight off bacterial infection by both direct and indirect methods. Platelets themselves are capable of secreting naturally antimicrobial substances, including antimicrobial peptides, to directly disrupt bacterial membranes [3]. Platelets also bind to leukocytes and activate them towards infection combat [3] .

To address the issue of platelet depletion following trauma, our group has previously developed platelet-like particles (PLPs). PLPs consist of a highly deformable ultralow crosslinked microgel (ULC) conjugated to a fibrin targeting antibody. The combination of high microgel deformability with the high affinity to fibrin allows PLPs to recapitulate the natural platelet ability to enhance fibrin formation and, following clot formation, induce clot retraction. PLP fibrin binding enhances clot formation by stabilizing nascent clot formation and acting as nucleation sites for further polymer growth, without biochemically producing fibrin or coagulation factors themselves [23]. Clot retraction results in an increase in fibrin density, a decrease in overall clot size, increased clot stiffness, and increased clot stability. While PLP enhancement of clot formation is due only to the fibrin binding capability of the particles, PLP-mediated clot retraction is dependent on both fibrin-binding and a high degree of particle deformability [23]; while both highly crosslinked and ultralow crosslinked fibrin binding microgels enhance fibrin formation, only ultralow crosslinked fibrin binding microgels promote clot

retraction. We have previously shown that the unique clot retraction feature of the ultralow crosslinked fibrin binding particles enhances wound healing after cessation of bleeding. Previous work in our group demonstrates that this increased clot stiffness allows for enhanced healing by promoting durotaxis and enhanced cell infiltration into wound sites [10]. However, while natural platelets have antimicrobial activity, the base PLP design does not. Thus, the objective of this project is to incorporate antimicrobial metals into the base PLP design to bestow antimicrobial activity.

Incorporation of silver is a widely-used strategy for bestowing antimicrobial activity to biomaterials [51]. Most notably, silver is highly regarded for its ability to target a range of pathogenic organisms including a wide variety of species of bacteria, fungi and prokaryotes [52]. However, it is also known for having highly cytotoxic effects in high concentrations, especially in the form of ions or in bulk metal [53-55]. To circumvent these effects, nanosilver has been utilized to reduce the overall amount of silver used while increasing the surface area for interaction with bacteria. Therefore, nanosilver is a promising candidate for bestowing antimicrobial activity to PLPs as they have both been previously reported in literature as having antimicrobial activity without high *in vivo* toxicity when compared with their bulk metal counterparts [56]. In addition, nanosilver is able to disrupt bacterial metabolic processes by direct contact, which also allows for combat of infection by drug-resistant strains [56-58]. Indeed, nanosilver has been incorporated into many different materials to ward off infection by drug resistant bacteria including catheters and wound coverings for enhanced wound healing [57-59]. Additionally, incorporation of nanosilver into microgels has been previously investigated. However, these previous reports were targeted towards more chemically based applications such as catalytic enhancement or sensing of hydrogen peroxide [30,60]. Thus, the objective of these

studies was to combine PLPs with nanosilver to develop antimicrobial nanosilver microgel composites, while maintaining particle deformability to preserve PLP-mediated clot retraction. To that end, we fabricated nanosilver composite microgel PLPs and investigated particle deformability, clot retraction, antimicrobial activity, hemostasis after trauma, and healing after injury. These outcomes were evaluated via atomic force microscopy (AFM), confocal microscopy, colony forming unit (CFU) assays, a murine liver trauma model, and a murine full-thickness injury model in the absence or presence of infection, respectively.

3.2 Materials and Methods:

3.2.1 Composite Nanosilver ULC Microgel and PLP Synthesis

Ultralow crosslinked microgels (ULCs) were synthesized via a precipitation polymerization reaction of 100 mL of 140 mM monomer solution with 90% Poly(N-isopropylacrylamide) (NIPAm) and 10% Acrylic Acid (AAc). ULCs refer to the base microgel particle prior to incorporation with nanosilver and conjugation to fibrin-targeting antibody. Prior to the reaction, the solution was filtered using a 0.2 μm filter. AAc was added 10 min prior to initiation with 1 mM ammonium persulfate (APS) and then reacted for 6 hrs with nitrogen flux at 70°C. The end product was cooled overnight. For purification, the product mixture was first filtered through glass wool and then dialysis was performed using 1000 kDa tubing for 3 days with daily buffer changes. The solution was then lyophilized and resuspended in assay specific buffers for individual assays. To covalently attach nanosilver to ULCs, an *in situ* reduction procedure adapted from Liu et al. was used resulting in nanosilver conjugation to the amide groups of NIPAm [30]. 5 mL of 0.01 M $AgNO_3$ was added to 100 mL of 3.5 mg/mL purified ULCs and stirred. Under nitrogen purge, 0.16 M of $NaBH_4$ was added as a reducing agent and reacted for 10 min. The suspension was then purified by centrifugation and washed with ultrapure water

three times. To create PLPs, a sheep anti-fibrin Fragment E polyclonal antibody was coupled to the AAc groups of the ULCs or Ag-ULCs via EDC/NHS chemistry. PLPs refer to the products of the coupling of ULCs and fragment E antibody. PLPs were purified via dialysis against diH_20 using 1000 kDa dialysis tubing for 3 days with daily buffer changes. Particles were then concentrated via centrifugation. The products of Ag-ULC coupling are referred to as Ag-PLPs.

3.2.2 Analysis of Nanosilver Incorporation

Nanosilver incorporation into ULC microgels was analyzed via Transmission Electron Microscopy (TEM). Samples were prepared by dipping TEM grids into a 0.02 mg/mL suspension of microgel sample (ULC or Ag-ULC). The TEM grid was left in the microgel solution overnight and then allowed to air-dry for 24 hrs. All TEM imaging was conducted on a JEOL 2000fx TEM at 200 kV and 8000x magnification. Average nanosilver particles per microgel were obtained via manual counting.

3.2.3 Analysis of Microgel Deformability

Microgel hydrodynamic radius was determined by dynamic light scattering (DLS) and then compared to measurements of microgel spreading onto glass surfaces as determined via atomic force microscopy (AFM). To prepare microgel samples for DLS, microgel suspensions were diluted in 10 mM formate at pH 3.0; size was determined from 5 measurements of 30 sec intervals on a Malvern Zetasizer Nano S. For AFM, 100 μL of microgel samples were deposited onto cleaned cover glass and allowed to air dry overnight. Cover glass was cleaned by sonicating for 10 min via sequential cleaning with Alconox, deionized water, acetone, ethanol (200 proof), and isopropyl alcohol. Air topography imaging was then conducted on an MFP 3D Bio AFM (Asylum). Topography images and height trace data collected from AFM was then analyzed in ImageJ for particle height and diameter for 30 microgels per group.

3.2.4 Analysis of Antimicrobial Activity

To evaluate antimicrobial activity, relevant species of gram-positive (*Staphylococcus aureus*) and gram-negative (*Escherichia coli*) bacteria were cultured in the presence of ULCs, Ag-ULCs, or ampicillin. Escherichia coli (*E. coli*) Penicillin G and oxacillin-resistant FDA strain Seattle 1946 and Staphylococcus aureus (*S. aureus*) methicillin and oxacillin-resistant strain F-182 were obtained from ATCC. 200 μL of treatment (ULCs, Ag ULCs, ampicillin, control Mueller-Hinton broth) was added to 200 μL of 10^5 CFU/mL culture and cultured for 24 hrs at 37 °C with shaking at 180 rpm [36,61]. Microgel suspensions were added at 10 mg/mL and ampicillin was added at 100 μg/mL. Aliquots were taken from the bacteria culture at t = 0, 3, 6, 12, and 24 hrs. Aliquots were then deposited and spread onto Mueller-Hinton agar plates and incubated for 12-16 hrs at 37 °C in a humidified incubator. Resulting colonies were counted to quantify the number of bacteria present in each time point aliquot. This assay is based on previous work in our group with nanogold. [36]

3.2.5 Analysis of Anti-fibrin Fragment E Antibody per Ag-PLP Particle Content

To determine the amount of anti-fibrin Fragment E antibody coupled to Ag-PLPs, a known mass of Fragment E antibody and known particle concentration Ag-PLPs were conjugated to a VivoTag-S 750 nm fluorescent dye. Particle/mL concentration for Ag-PLPs was determined by NanoSight readings in 10 mM formate at pH 3 at 0.002 mg/mL Ag-PLPs. From this reading, a particle/mg concentration was then calculated. To conjugate the dye to free Fragment E antibody, 500 μL of 10 mg/mL anti-fibrin Fragment E antibody was added to 500 μL of 0.2 M pH 8.3 sodium bicarbonate buffer and 11.83 μL of 5 mg/mL 750 nm dye. The resulting solution was then shaken at room temperature for 1 hour. To conjugate the dye to the antibody components of Ag-PLPs, a similar procedure was used but with Ag-PLPs instead of the

antibody only solution. Purification was achieved by dialysis in ultrapure water at 4 °C for 72 hours. Conjugated antibodies were diluted to a range of 0-10 μg and added to a 96 well plate in duplicate to construct a fluorescence standard curve. Ag-PLPs were diluted to a range of 0-10^8 particles/mL and added to a 96 well plate in duplicate. The plate was then read for fluorescence on a Licor CLx. Signal readings from 800 nm channel were collected for each well and then divided by the well area. A standard curve for antibody fluorescence was then determined by plotting the mass in each well against an average of signal for the respective well. Amount of antibody per Ag-PLP particle was then calculated using an average of signal/area fluorescence reading of the Ag-PLP wells and the standard curve.

3.2.6 Analysis of Clot Retraction via Confocal Microscopy

To analyze the ability of PLPs and Ag-PLPs to include clot retraction, clots were polymerized in the presence or absence of PLPs or control non-binding microgel samples (ULCs) and then clot microstructure was analyzed via confocal microscopy [62]. Imaging by confocal microscopy allows for observation of how the clot structure changes in the presence of particle treatments. In particular, we focused on the density of the fibrin in the clot. Samples were prepared by depositing a 50 μL clot onto a microscope slide with two layers of double-sided tape. A coverslip was then placed on top of the tape. Clots were polymerized for at least 2 hrs. Clots consisted of 2 mg/mL fibrin (5% Alexa 488 labeled Fibrinogen), 0.1 U/mL thrombin, and 0.25 mg/mL of particles (ULC, Ag-ULC, PLP, or Ag-PLP). Clot structure was imaged using an LSM 880 Zeiss confocal microscope at 3 different sites of each clot and a minimum of 3 clots were analyzed per group. All images were taken using C-apochromat 40x/1.2 W Corr M27 objective with x3.1 zoom. Structural analysis was conducted by processing images in ImageJ to black and white, such that black is fibrin fibers and white is uncovered space. Area occupied by

black pixels and area occupied by white pixels were then measured using ImageJ's measure function. A fibrin density ratio was then calculated by dividing the black pixel area by the white pixel area as previously described [63].

3.2.7 Analysis of Bleeding Following Traumatic Injury:

A murine liver laceration traumatic injury model was used to analyze the ability of PLPs and Ag-PLPs to augment hemostasis following intravenous delivery. All studies were performed under protocols approved by the NCSU IACUC. 8-week-old male c57bl/6 mice were used for these studies. 5% isoflurane was used to anesthetize animals. Treatments were delivered via the jugular vein and were allowed to circulate for 5 min before inducing a liver laceration. Treatments included vehicle only, ULCs, PLPs, or Ag-PLPs. 10 mg/kg of each treatment was injected in 100 μL of sterile saline. Liver laceration was induced by creating a 10 mm cut along the left lobe to obtain ventral and dorsal laceration. Blood loss was monitored by placing gauze immediately adjacent to the laceration over the course of 10 min at the following timepoints: 10 second intervals for t = 0-30 sec, 30 second intervals for t = 1-3 min, and one-minute intervals for t = 3-10 min. Blood loss was determined from taking the difference in mass of gauze before and after blood collection at each time point and then normalized to body mass. This model was powered to total blood loss based on previous studies in our group. [10]

3.2.8 Analysis of Wound Healing Following Full-thickness Dermal Injury:

A murine full thickness dermal injury model was used to analyze the ability of PLPs and Ag-PLPs to modulate healing responses following topical application. All studies were performed under protocols approved by the NCSU IACUC. 8-week-old male c57bl/6 mice were used. 5% isofluorane was used to anesthetize animals and then a 4 mm biopsy punch was used to create two full dermal thickness wounds on the back of each mouse. Silicone rings were attached

with superglue to the skin surrounding the wound to ensure that wound closure was not confounded by the contraction of mouse skin [64] . Treatment groups included saline, fibrin-only, PLP, Ag-ULC and Ag-PLP. All particle treatments were applied to the wound within a fibrin gel based on previous *in vivo* studies from our group [10] demonstrating that delivery of PLPs via this method results in enhanced healing compared to delivery of PLPs alone. 10 μL clots were created with a composition of 2 mg/mL fibrin, 0.1 U/mL thrombin, and 0.25 mg/mL of particle treatments or saline for fibrin-only control. Wounds were imaged and covered using Opsite. Opsite was adhered to the silicone ring directly and care was taken to ensure that Opsite did not come into contact with the wound. 5 mg/mL Carprofen was administered to all mice for the first 5 days. Injuries were monitored over the course of 9 days with a daily change of Opsite to ensure wound cleanliness. 9 days post injury, mice were euthanized under carbon dioxide. The wound areas were then harvested, fixed in 10% formalin, and embedded in paraffin. All wounds were sectioned into 5 μm thick sections. Hematoxylin & Eosin (H&E) staining and immunohistochemistry staining were conducted to evaluate resulting tissue structure, distribution of particle treatments, and healing outcomes. Fibrin was labeled by monoclonal UC45 with secondary Alexa 594 antibody. PLPs were visualized by staining with a polyclonal anti-sheep 488 FITC-conjugated antibody to detect the fibrin specific antibody attached to the PLPs. To characterize CD31 production, skin sections were fluorescently labeled by DAPI for cell nuclei, and by clone SP38 monoclonal antibody to CD31 with secondary Alexa 594. All histology slides were imaged on an EVOS Auto FL microscope at 20x magnification. To evaluate wound healing outcomes, epidermal thickness was measured from H&E stained sections and total CD31+ area was measured from CD31 stained slides in ImageJ. CD31+ area quantification was performed by conducting particle analysis on the red channel with threshold of 0-50 following conversion to 8-

bit image. Gross images of the injuries were also analyzed for wound closure via area measurement and then calculating a percent closure normalized by Day 0 area. These images were analyzed with blinding for treatment by scrambling the order of images by random list generation. This model was powered to epidermal thickness based on previous studies in our group. [10]

3.2.9 Analysis of Wound Healing Following Full-thickness Dermal Injury in Presence of Infection:

To evaluate *in vivo* healing outcomes in the presence of infection, the same full dermal thickness model described above was used, but with an additional application of 25 μL of 2.5 x 10^7 CFU/mL suspension of F-182 strain *Staphylococcus aureus* and treatment groups of saline, PLP, or Ag-PLP. PLPs and Ag-PLPs were delivered in a clot consisting of 2 mg/mL fibrin, 0.1 U/mL thrombin, and 0.25 mg/mL particle treatment. As described for the uninfected model, wound closure was analyzed by measuring the open area of observed in images of wounds in ImageJ with random list generation for blinding to treatment. A percent change of area was then calculated. The same histological analysis methods as described for the uninfected full-thickness dermal model were conducted to evaluate wound healing outcomes in this infected model. For microscopic examination of infection, at least two 5 μm full-thickness (i.e. surface to subcutis) sections of skin collected at least 50 μm apart representing central portions of the wounded site were exposed to gram stain. Semi-quantitative scoring of gram stained sections was performed by a board-certified veterinary anatomic pathologist (i.e. Diplomate of the American College of Veterinary Pathologists) and severity scoring was assigned. Semi-quantitative wound infection severity scoring system was based on the criteria given by Schafer et al [65] and included scores of 1 for minimal, 2 for mild, 3 for moderate, 4 for marked, and 5 for severe. Wound infection score

was assigned based primarily upon location, distribution, and depth of bacteria, presence and relative number of gram positive-staining, less than 2 μm wide, cocci bacteria arranged in clusters (consistent with *Staphylococcus spp.*) or phagocytosed by leukocytes.

3.2.10 Statistical Analysis:

All statistical analysis was conducted using GraphPad Prism 8. Analysis of antimicrobial assays and wound closure used two-way ANOVA. Semi-quantitative histology severity scoring was evaluated by Kruskal-Wallis one-way ANOVA for nonparametric data. All other analyses used one-way ANOVA with Tukey's post-hoc test for multiple comparisons.

3.3 Results and Discussion

3.3.1 ULC Microgels Remain Deformable After Covalent Nanosilver Incorporation

To evaluate nanometal distribution, TEM was conducted. TEM images in **Figure 3.1** show nanosilver was successfully incorporated into the base ULCs and throughout the microgel particle. The average nanosilver content per microgel was 55±12 nanosilver particles (mean ± standard deviation; n=8). Deformability is a critical property of PLP clot retraction function. For this reason, we characterized deformability by comparing microgel hydrodynamic radius determined via DLS to spread particle size determined via AFM. In general, we saw indications of deformability across both microgel types, which remains consistent with expected behaviors for ULC microgels [66,67]. Z-average diameters in formate were as follows: 761±43 nm for ULCs and 608±9 nm for Ag-ULCs (**Table 3.1**).

Table 3.1 Summary of size data including DLS z-average readings in formate, dry diameter, and dry height

Microgel Type	Z-average size (nm)	Dry diameter (μm)	Dry height (μm)
ULC	761 ± 43	1.5 ± 2	15 ± 2
Ag-ULC	608 ± 9	1.6 ± 0.2	15 ± 3

AFM average dry diameters were 1.5±0.2 μm for ULCs and 1.6±0.2 μm for Ag-ULCs. AFM average dry heights were 15±2 nm for ULCs, 15±3 nm for Ag-ULCs. These results are summarized in **Figure 3.1**. Overall, Ag-ULCs showed deformability similar to unmodified ULCs.

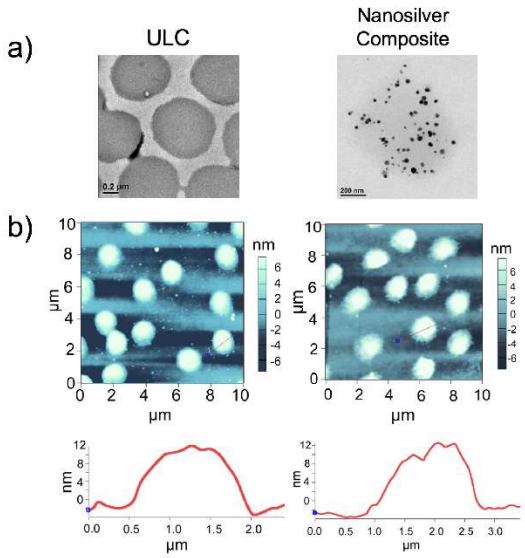

Figure 3.1: a) Representative TEM images of ultralow crosslinked microgels (ULCs) and covalent nanosilver composites. b) Representative AFM air topography images and height traces.

3.3.2 Analysis of Antimicrobial Activity

To evaluate *in vitro* antimicrobial activity, a colony forming unit assay (CFU) was conducted [36]. Average CFU/mL at 24 hrs for *E. coli* assays were: 1.48 x 10^{11} ± 2.21 x 10^{11} CFU/mL for control, 933 ± 902 CFU/mL for ampicillin, 5.27 x 10^{9} ± 1.63 x 10^{9} CFU/mL for

ULCs, and 0.00 CFU/mL for Ag-ULCs. Average CFU/mL at 24 hrs for *S. aureus* assays were: $1.78 \times 10^{11} \pm 1.89 \times 10^{11}$ CFU/mL for control, 0.00 CFU/mL for ampicillin, $6.33 \times 10^{10} \pm 9.10 \times 10^{10}$ CFU/mL for ULCs, and 0.00 CFU/mL for Ag-ULCs. For *E. coli* assays, significant differences in bacteria presence were observed at 24 hrs between controls and ampicillin, ULCs, and Ag-ULCs ($p< 0.01$). For *S. aureus* assays, significant differences in bacteria presence were observed at 24 hrs between controls and ampicillin and Ag-ULCs ($p<0.01$). Overall, results of the antimicrobial assay showed that Ag-ULCs completely reduce bacterial growth across all time points and in both species, displaying performance akin to that of ampicillin (**Figure 3.2**).

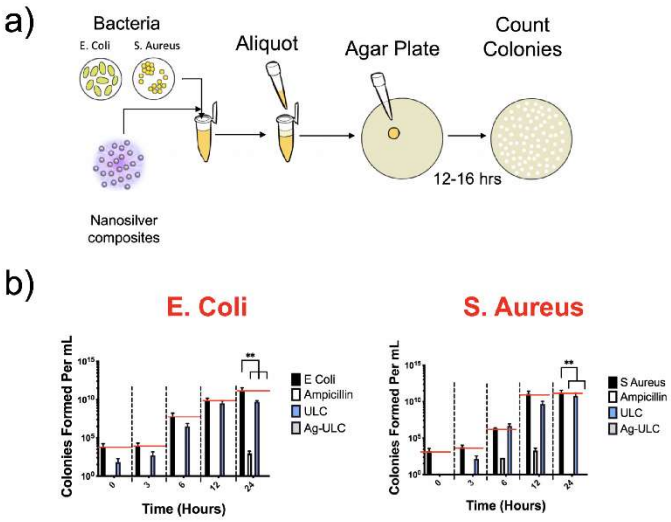

Figure 3.2: a) Schematic of the colony forming units (CFU) assay. b) Summary of CFU assay results. No bar for Ag-ULC is shown due to there being no bacterial presence detected at each time point. n = 3 assays. **p<0.01

3.3.3 Analysis of Anti-fibrin Fragment E Antibody per Ag-PLP Particle Content

To determine the amount of antibody per Ag-PLP particle, fluorescence of antibodies was measured and used to calculate a standard curve. From there, Ag-PLP fluorescence was measured and used to calculate an antibody per Ag-PLP particle content. The standard curve

calculated for antibody fluorescence is <Signal per Area> = 0.0003*<Antibody mass in ng> - 0.0108. The antibody per Ag-PLP particle was then determined to be 7.5 μg using the standard curve.

3.3.4 Analysis of Clot Retraction

To evaluate clot retraction, all microgel types were coupled to fibrin-targeting antibody by EDC/NHS chemistry to create PLPs. The resulting particles were then incorporated into clots and clot structure was analyzed via confocal microscopy 2 hrs after polymerization. All images were processed into black and white by ImageJ, with black representing fibrin fibers and white representing empty space to quantify fiber density. Average fiber density in clots were 1.95±0.37 for controls, 1.43±0.31 Ag-ULCs, 1.43±0.22 ULCs, 4.43±1.04 PLPs, and 4.70±0.77 Ag-PLPs. Representative images of clots including microgel treatments and corresponding fiber density measurements are summarized in **Figure 3.3**. Overall, PLP and Ag-PLPs had significantly higher fiber density than all other groups ($p<0.0001$ for control, Ag-ULC, and ULC groups compared to the PLP groups). No significant difference was observed between PLPs and Ag-PLPs, indicating that incorporation of nanosilver into the base PLP design does not greatly influence the ability of PLPs to induce clot retraction.

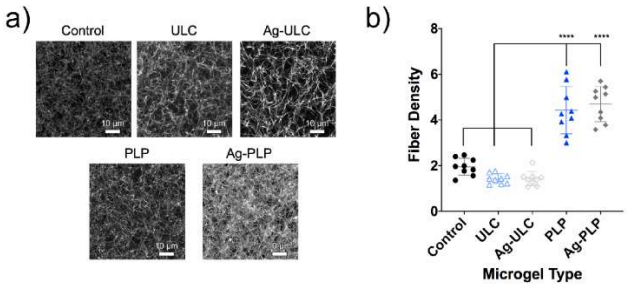

Figure 3.3: a) Representative confocal images of clots incorporated with ULCs, Ag-ULCs, PLPs, and Ag-PLPs. Images were taken at 63x with x3.1 zoom. b) Summary of fiber density data. n = 3 clots, 3 locations per clot ****=$p<0.0001$

3.3.5 Analysis of in vivo Bleeding Following Trauma

We next evaluated if incorporation of nanosilver into PLPs affected the hemostatic ability of the particles using a traumatic liver laceration injury model. In c57bl/6 mice, we measured total blood loss following intravenous injection of PLPs and Ag-PLPs. For overall blood loss, we saw statistically significant differences between the saline group and the PLP groups ($p<0.05$ between saline and PLP and Ag-PLP). The average blood loss (g blood loss/g animal) across groups were: saline: 0.015±0.005; ULC: 0.013±0.006; PLP: 0.007±0.002; and Ag-PLP: 0.007±0.002 (**Figure 3.4**). It is notable that no statistically significant difference was observed between the PLP and Ag-PLP groups. These results indicate that following incorporation of nanosilver into the base PLP design, Ag-PLPs retain the ability to decrease bleeding following trauma when injected intravenously.

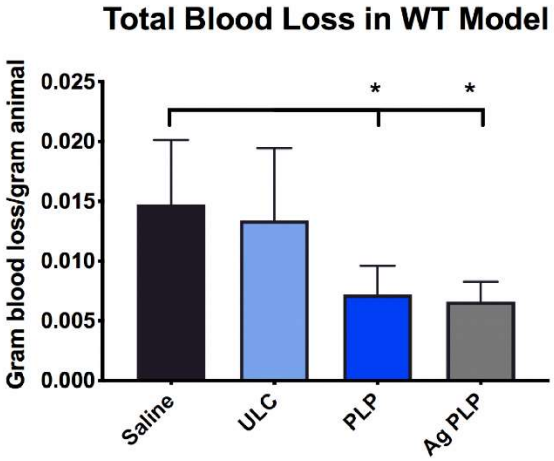

Figure 3.4: Summary of blood loss data. n= 5-7 per group *=$p<0.05$

3.3.6 Analysis of Healing Following Topical Application of PLPs in vivo

We next evaluated how incorporation of nanosilver into PLPs influences healing outcomes in a murine full thickness dermal injury model. PLPs, Ag-PLPs, or ULCs were applied

topically to full thickness dermal wounds in conjunction with a fibrin clot. Immunohistochemistry demonstrated that 9 days post injury, PLPs and Ag-PLPs could be observed in the wound site in conjunction with fibrin (**Figure 3.9**). Wound closure was evaluated daily for 9 days by measurement of wound area in ImageJ from gross images of the injuries and calculating a percent closure with normalization based around Day 0 wound area. While no significant differences were detected in percent wound closure over the course of 9 days (**Figure 3.10**), differences were observed in the histological outcomes.

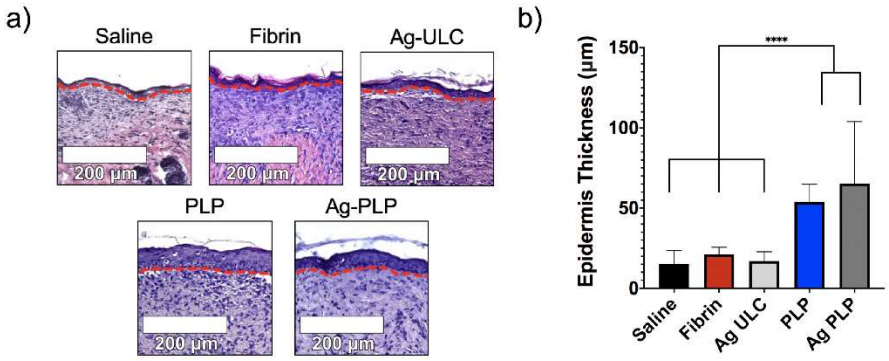

Figure 3.5: a) Representative images of H&E stained skin sections. Epidermis is outlined with red dotted lines. **b**) Summary of epidermal thickness analysis. n=3 wounds per group. ****=p<0.0001

9 days post injury, tissue was collected and processed to evaluate average epidermal thickness and angiogenesis (via analysis of CD31+ staining). Overall, PLPs and Ag-PLPs showed statistically significant differences ($p<0.0001$) in average epidermal thickness from control groups (saline and fibrin), and the non-fibrin binding microgel group (Ag-ULC; **Figure 3.5**). Average epidermal thickness was 15±8 µm in saline treated animals, 21±4 µm in fibrin only clot treated animals, 54±11 µm in PLP treated animals, 17±6 µm in Ag-ULC treated animals, and 65±39 µm in Ag-PLP treated animals. Overall, PLP groups also showed statistically significant differences in CD31+ area in comparison to control groups (saline and

fibrin) and the non-fibrin binding microgel group (Ag-ULC); $p<0.001$ saline vs. PLP and Ag-PLP; $p<0.01$ fibrin only vs. PLP and Ag-PLPs; $p<0.05$ Ag-ULC vs. PLP and Ag-PLP (**Figure 3.6**).

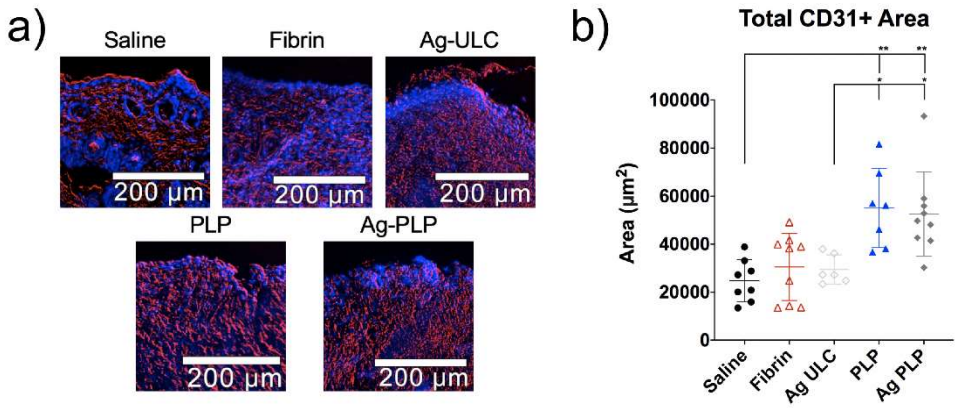

Figure 3.6: a) Representative images of wound sections analyzed with immunohistochemistry. Cell nuclei were stained blue with DAPI and CD31+ areas were stained red. b) Summary of total CD31+ staining 9 days post injury. n = 3 wounds/group *=$p<0.05$, **$p<0.01$

Average area covered by CD31+ tissue was 24,786±8,728 μm^2 in saline treated animals, 30,467±13,966 μm^2 in fibrin only clot treated animals, 55,065±16,448 μm^2 in PLP treated animals, 29,444±6,100 μm^2 in Ag-ULC treated animals, and 52,560±17,544 μm^2 in Ag-PLP treated animals. These results indicate that following incorporation of nanosilver into the base PLP design, Ag-PLPs retain the ability to improve wound healing outcomes, as indicated by increased epidermal thickness and angiogenesis compared to controls, following topical application to a full thickness wound.

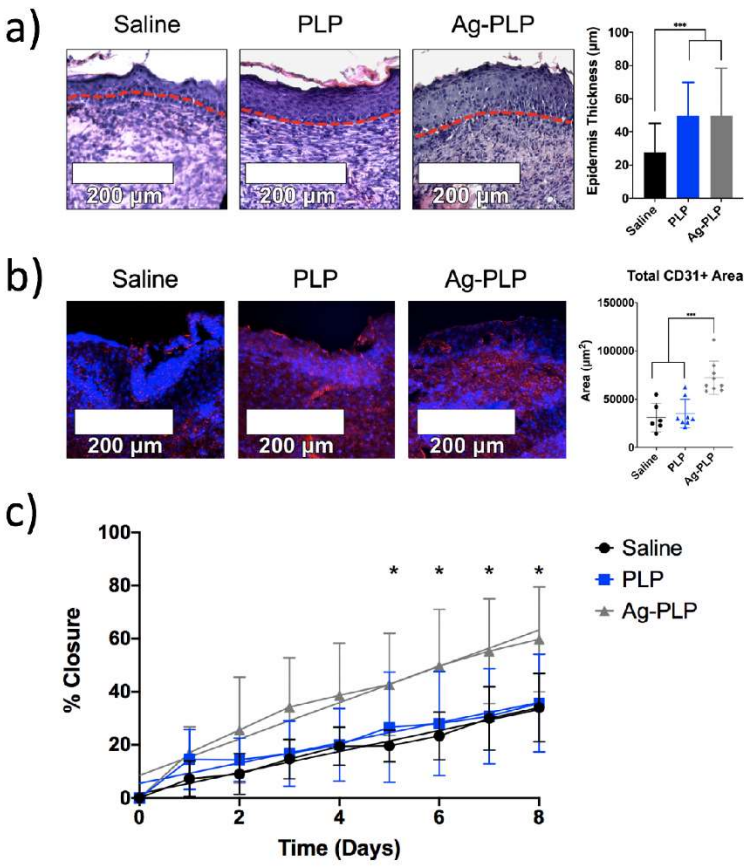

Figure 3.7: Infected injury wound healing outcomes. a) H&E images of wound sections from injuries infected with a drug resistant strain of *Staphylococcus aureus* (left) with epidermis outlined with a red dotted line. Summary of epidermis thickness measurements (right) shows improved re-epithelization in mice treated with PLPs and Ag-PLPs. n=3 wounds/group. ***=$p<0.001$ b) IHC images of wound sections from infected injuries (left) with blue staining for cell nuclei (DAPI) and red staining for CD31+ tissue. Summary of total CD31+ staining (right) shows enhanced CD31 staining only in mice treated with Ag-PLPs. n = 3 wounds/group. ***=$p<0.001$ c) Wound closure and wound closure rates. Injuries were imaged over the course of 9 days and measured for percent change in wound area. Statistically significant higher wound closure was observed starting on Day 5 in wounds treated with Ag-PLPs as well as a statistically significantly higher wound closure rate. n = 7-9 wounds/group. *=$p<0.05$

3.3.7 Analysis of Healing Following Topical Application of PLPs in the Presence of Infection in vivo

We next evaluated how incorporation of nanosilver into PLPs influences healing outcomes in a murine full thickness dermal injury model in the presence of infection. In these studies, the same murine full dermal thickness model described above was utilized in the presence of *Staphylococcus aureus* infection. Overall, Ag-PLPs showed significantly enhanced healing outcomes with improved wound closure, epidermal thickness, and CD31+ staining compared to control or PLP only groups (**Figure 3.7**). Wound closure was higher in wounds treated with Ag-PLPs, showing statistical significance starting Day 5 (20±6% for saline vs 27%±21% for PLP vs 43%±20% for Ag-PLP; $p<0.05$). Additionally, wounds treated with Ag-PLPs also resulted in significantly increased wound closure rates. Wound closure rates were as follows: 3.7±0.4 %/day for saline treatment, 3.8±0.7 %/day for PLP treatment, 6.8±0.8 %/day for Ag-PLP treatment ($p<0.05$).

Average epidermis thicknesses were 28±17 μm in saline treated wounds, 50±20 μm in PLP treated wounds, and 50±28 μm in Ag-PLP treated wounds. Overall, Ag-PLP and PLP treated wounds resulted in statistically significantly higher epidermal thickness compared to saline treated wounds ($p<0.0001$). Average total CD31 positive areas were 31,662±14,755 μm^2 in saline treated wounds, 35,197±14,844 μm^2 in PLP treated wounds, and 72,388±17,022 μm^2 in Ag-PLP treated wounds. Overall, wounds treated with Ag-PLPs displayed significantly higher CD31+ staining compared to saline or PLP groups ($p<0.001$). To evaluate persistent of bacteria in the tissue 9 days after injury, skin tissue sections were histochemically stained with Gram stain. *Staphylococcus aureus* infection was confined to less than 1 mm penetration to exposed

wounds. More specifically, the wound infection scoring was not significantly different for PLP and Ag-PLP treatment groups compared to the saline control (**Figure 3.8**).

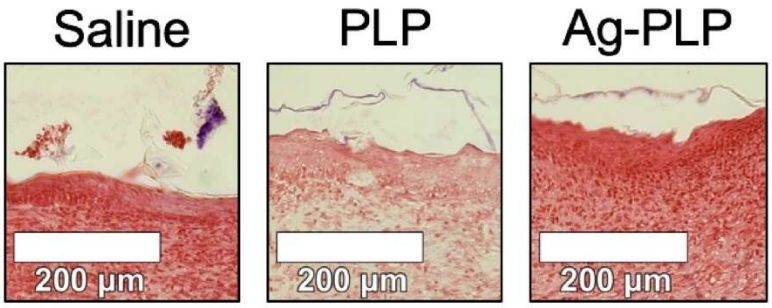

Figure 3.8: Gram stain of wound purposely infected with *Staphylococcus aureus*. Gram positive bacteria consistent with *Staphylococcus aureus* histochemically stained deep blue with methylene blue of the gram stain and failed to decolorize. The median score was none to mild severity of bacterial infection for all groups. Bacteria were not detected deeper than 1 mm in any of the wounded sites. There was no significant difference in the histopathology scoring when comparing saline control to PLP and Ag-PLP treatment groups ($p>0.05$; Krushal-Wallis one-way analysis of variance).

3.4 Conclusions and Greater Impact

Following trauma, platelets are depleted, and hemorrhage is a major problem in emergency medicine situations. Even if hemostasis is achieved, subsequent healing is often complicated by infection. Platelets are essential to the wound healing process due to their ability to stop bleeding, guide wound healing and fight infection. For this reason, we sought to develop a platelet-mimetic material capable of all these functions to stop bleeding and promote healing after trauma. We have demonstrated in these studies that fibrin binding covalent nanosilver composite PLPs are able to induce clot retraction and inhibit bacterial growth in suspension.

Previous studies with ULC-based PLPs demonstrated that microgel deformability and fibrin affinity are the contributors to the mimicry of clot retraction.

These results demonstrate that microgel deformability is retained following nanosilver incorporation, as evidenced by the ability to spread extensively on a glass surface (**Figure 3.1**). This deformability was sufficient to induce clot retraction, as evidenced by fibrin networks condensation when nanosilver composite microgels were coupled to a fibrin-binding antibody to a similar extent as our first generation PLPs (**Figure 3.3**). Ag-ULCs were also found to significantly reduce bacterial growth in suspension when compared to unmodified ULCs and nanogold incorporated ULCs in suspension. More specifically, no colony forming units were detected at all over the course of 24 hrs of bacterial culture. Previously, our group has explored the use of nanogold as an antimicrobial agent incorporated into PLPs. In these previous studies, we observed an antimicrobial effect from covalently incorporated nanogold ULC microgel composites while noncovalently incorporated nanogold ULC microgels composites had little to no antimicrobial effect. However, covalent nanogold composites were still not as effective as ampicillin[17] . We also have previously investigated the stability of nanometal into ULCs with non-covalent nanogold composite ULCs and found that even noncovalent nanometal composite ULCs remain stable with no significant differences reported in nanometal per microgel count[17] . Thus, we conclude that the Ag-ULCs are stable as well and do not release nanosilver. In these studies, we demonstrate that nanosilver incorporation into ULC microgels is a highly effective method for imparting antimicrobial activity to PLPs. This difference of antimicrobial activity aligns with previous findings that silver has higher antimicrobial activity than nanogold [56] .

We also demonstrated a retention of hemostatic ability and pro-healing activities *in vivo* for Ag-PLPs. Total blood loss observed from the liver laceration model demonstrates that Ag-

PLPs reduce the amount of blood loss to a similar extent as unmodified PLPs compared to saline controls. Additionally, in the uninfected full thickness dermal injury model, enhanced epidermal thickness and CD31+ tissue production was observed in wounds treated with Ag-PLPs while also demonstrating similar performance as unmodified PLPs. These results suggest that Ag-PLPs retained sufficient enough clot retraction ability following nanosilver incorporation to fully recapitulate the *in vivo* function we previously observed with unmodified PLPs. Furthermore, when treating wounds infected with *Staphylococcus aureus*, enhanced epidermal thickness was observed in wounds treated with Ag-PLPs and PLPs. However, only the wounds treated with Ag-PLPs showed increased rates of wound closure and enhanced CD31+ staining 9 days post-injury. This is likely the result of the Ag-PLPs reducing the presence of bacteria within the wound bed at early time points, thereby minimizing inflammation and promoting earlier migration of fibroblasts and other cell types into the wound bed required to rebuild the tissue. However, Gram stained images of sections of the wounds 9 days post injury show very little bacteria present in the wound itself in all conditions. It is likely that 9 days post-injury is enough time for the bacterial infection to be mostly cleared from the wound regardless of treatment. This should be analyzed further in future studies by evaluation of bacterial clearance at earlier time points and/or healing should be analyzed in the presence of higher levels of bacteria. Additionally, comparison to the inclusion of an equivalent amount of free nanosilver in the fibrin gel without PLPs would have provided further information regarding *in vivo* antimicrobial activity of Ag-PLPs. Furthermore, PLPs and Ag-PLPs do not degrade. Previous studies have shown no indication that they become engulfed by macrophages. We hypothesize that PLPs and Ag-PLPs may have sloughed off in the scab, but studies investigating the long-term in vivo effects in future studies are needed in order to truly determine clearance of PLPs and Ag-PLPs.

None-the-less the enhanced wound closure rates and increased angiogenesis observed in the presence of Ag-PLPs compared to PLPs or saline in the infected injury model support that Ag-PLPs are an effective method for promoting healing in infected wounds.

In conclusion, we were able to successfully fabricate antimicrobial composite nanosilver PLPs with all important PLP properties retained both *in vitro* and *in vivo*. In addition, we were demonstrated that Ag-PLPs have high levels of antimicrobial activity as evidenced by complete inhibition of bacterial growth *in vitro* in CFU assays and enhanced healing in infected injuries *in vivo.* Ag-PLPs were capable of significantly improving wound healing outcomes and outperformed first-generation PLPs with respect to CD31+ tissue staining when applied to infected injuries. With demonstrating retained PLP properties following nanosilver incorporation, future work will focus on evaluating long-term storage effects, safety, and efficacy of Ag-PLPs in larger animal models. Overall, Ag-PLPs show significant promise as an antimicrobial and hemostatic material for application to injuries following trauma.

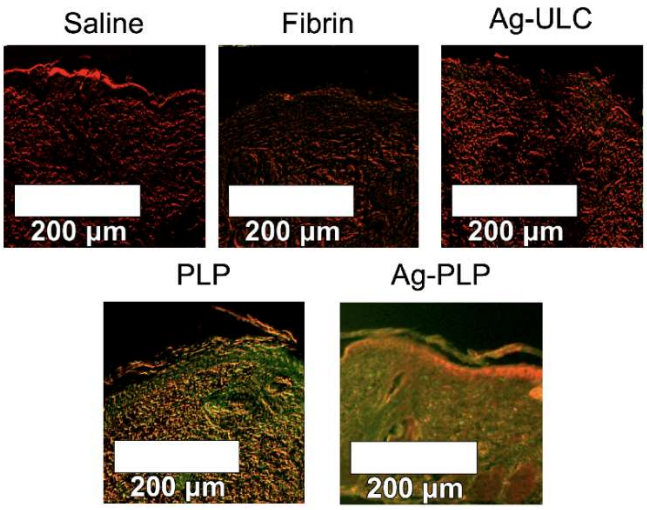

Figure 3.9: Immunohistochemistry conducted on wound sections with fluorescently stained fibrin shown in red and sheep fragment IgG on PLPs shown in green. The presence of green confirms the incorporation of PLPs and Ag-PLPs into fibrin in the wound site.

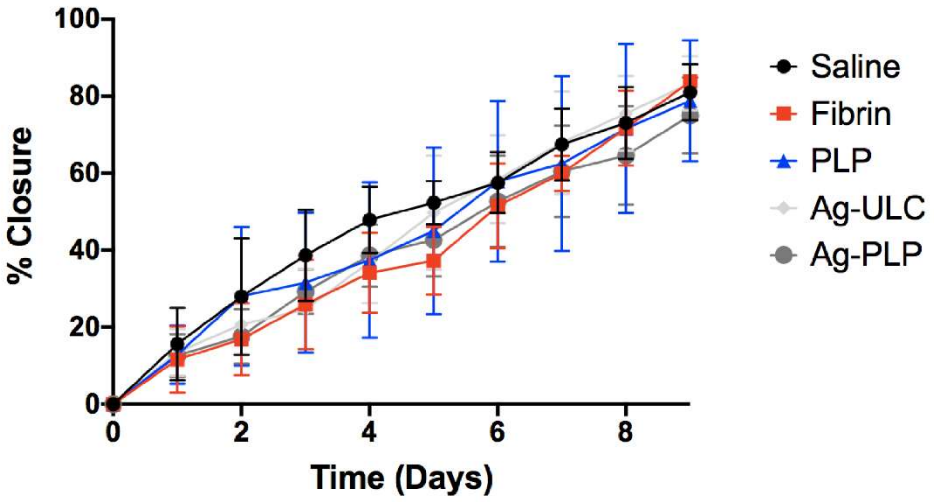

Figure 3.10: Wound closure and wound closure rates for uninfected dermal injuries. No significant differences in wound closure and wound closure rates were detected.

Acknowledgements: Funding was provided by the American Heart Association 16SDG29870005 and Predoctoral Fellowship 18PRE33990338, the National Science Foundation DMR CAREER 1847488, North Carolina State University Chancellor's Innovation Fund, and the Institutional National Research Service Award from the Office of the Director of National Institutes of Health to (NIH 2T32OD011130-11/12). This work was performed in part at the Analytical Instrumentation Facility (AIF) at North Carolina State University, which is supported by the State of North Carolina and the National Science Foundation (award number ECCS-1542015). The AIF is a member of the North Carolina Research Triangle Nanotechnology Network (RTNN), a site in the National Nanotechnology Coordinated Infrastructure (NNCI). Confocal microscopy was performed at the Cellular and Molecular Imaging Facility at NCSU.

CHAPTER 4

Wound-triggered Shape Change Microgels for the Development of Enhanced Biomimetic Function Platelet-like Particles

The goal of the studies outlined in this chapter was to demonstrate the feasibility of 1) creating a wound-triggered shape change microgel and 2) evaluate its associated *in vitro* and *in vivo* properties. PLPs demonstrate significant potential as a multifunctional hemostatic and wound healing material [10]. However, the constant deformability of the ULC body mimics only active platelet morphology. Thus, a PLP formulation with wound-triggered shape change was developed. We were able to demonstrate that thrombin-sensitive PLPs (TS-PLPs) do indeed have triggered shape change when exposed to thrombin and that the resulting shape change is sufficient enough to induce clot retraction *in vitro* and significantly stem bleeding and improve wound healing outcomes *in vivo*. Additionally, TS-PLPs did not display apparent off-target effects.

4.1 Introduction:

Under normal circumstances, platelets circulate in a rounded inactive state in the circulatory system. In this state, platelets can easily marginate or move to the vessel wall for attachment. When injury occurs, platelets are prompted by molecules, such as thrombin, to shift into a stellate shape and increase surface exposure of fibrin-binding surface receptors. In this activated state, platelets can mediate the hemostasis process and—following the formation of a fibrin clot—are able to utilize actin-myosin machinery to collapse clots, resulting in clot retraction. The resulting clot has a higher stiffness which is hypothesized to guide cells into the wound bed by durotaxis. As a result, clot retraction is hypothesized to lead to enhanced wound healing outcomes.

In conditions where platelets are depleted or hyporeactive, such as trauma, surgical associated bleeding, or chronic wounds, platelets are unable to carry about their functions, leading to inhibited hemostasis and wound healing. These outcomes are prevalent to traumatic injury, which remains the leading cause of death for people under age 45[12] , and chronic wounds, which can affect diabetics who consist of 34.2 million in the United States.[68]

To address the consequences of platelet depletion or hyporeactivity, many platelet-mimetic strategies have already been investigated. Platelet derived strategies are based on using derived substances from natural platelets, such as platelet transfusions and lyophilized platelets. However, these strategies have extremely short storage lifetime and are frequently associated with immunogenicity issues due to coming from allogeneic sources.[69] As an alternative, to natural platelet transfusions, artificial platelets have been a key area of development in recent year. Artificial platelets frequently consist of particles or polymers coupled to bioactive motifs such as RGD peptides or antibodies that bind to platelets or coagulation factors.[69] While the synthetic nature of these strategies allows for longer storage lifetime and easier scale up, artificial platelet strategies rarely mimic more than one platelet function.[69] Cloaking and active delivery strategies have also been investigated. These strategies consist of coupling drug delivery vessels to platelet binding motifs or platelet membranes. [69] While this construction allows for enhanced targeted delivery and reduced immune response when compared to uncloaked drug delivery, it requires the extraction of components from pre-existing platelets, which are not easily obtained or transported. [69]

As a treatment of the effects of platelet depletion, our group has developed platelet-like particles (PLPs) consisting of a microgel coupled to a fibrin-targeting antibody.[23] Previous work in our group has demonstrated that a highly deformable microgel is mimetic of active platelet

morphology and that when combined with high fibrin targeting affinity—such as what is provided by the fibrin-targeting antibody—can recapitulate the clot retraction ability of natural platelets. As a result of this particle design, PLPs can hone specifically to injuries and enhance subsequent healing. Previous work in our group has demonstrated that treatment by PLPs can lead to significantly reduced blood loss in traumatic injury and enhanced wound healing outcomes in full thickness dermal injuries. [10,23]

While PLPs are a promising material towards addressing the problems that come with platelet depletion, they still lack the ability to mimic platelet shape change in response to injury cues. Previously, we have investigated a shape changing PLP design consisting of a CoreShell architecture.[50] The core particle consists of N-isopropylmethacrylamide (NIPMAM) crosslinked with N,N-(1,2-Dihydroxyethylene)bisacrylamide (DHEBA). The shell particle consists of poly(N -isopropylacrylamide) (pNIPAm) crosslinked with 2% N,N' - methylenebisacrylamide (BIS). Due to the DHEBA, the core degrades in the presence of sodium periodate. Additionally, NIPMAM is known to have little self-crosslinking, meaning that degradation of NIPMAM cores is complete degradation. [70-73] When the core of a CoreShell particle is degraded, it leaves behind a deformable hollow particle. Findings from this work has shown that the CoreShell particle greatly resembles inactive platelet morphology and the hollow particle greatly resembles active platelet morphology. [50] When coupled to fibrin-targeting antibody and incorporated into clots, it was found that CoreShell particles do not induce significant changes in clot structure while hollow particles do induce a condensed clot, much like our base PLP technology. Additionally, when sodium periodate is added after incorporation of CoreShell particles into fibrin clots, the resulting clot structure was significantly more collapsed than control clot structure, demonstrating the potential for triggered shape change. [50] When applied to a full thickness

dermal injury murine model, hollow particles were found to significantly improve wound healing outcomes while CoreShell did not. This difference is consistent with the difference in deformability between the CoreShell and hollow particles. [50]

In this work, we built upon these findings and developed a thrombin-sensitive nanogel (TSN) from NIPMAM crosslinked with a thrombin-cleavable peptide sequence, enabling the particle to change shape in the presence of thrombin. (Figure 1A) In particular, we used the custom peptide sequence methacrylate-Gly-dPHe-Pro-Arg-Fly-Phe-Pro-Ala-Gly-Gly-Lys-methacrylate as it has seen previous use as part of a thrombin-cleavable bulk hydrogel already [74]. We then evaluated morphology and size of the thrombin-sensitive nanogels in the absence or presence of thrombin using AFM (Atomic Force Microscopy), Nanosight, and cryoSEM (cryogenic Scanning Electron Microscopy). To evaluate clot retraction, all particle treatments were coupled to a polyclonal Fragment E anti-fibrin antibody and incorporated into clots. The resulting clots were then imaged by confocal microscopy and analyzed for percent porosity. Finally, to evaluate *in vivo* hemostasis and wound healing, a murine liver laceration survival model was used. In the studies presented here, thrombin-sensitive PLPs (TS-PLPs) exposed to thrombin showed differences in morphology and clot retraction compared to non-exposed TS-PLPs. In addition, TS-PLPs demonstrated the ability to significantly stem bleeding in a traumatic injury model and significantly improve wound healing outcomes 1 week after injury.

4.2 Materials and Methods:

4.2.1 Thrombin-sensitive Nanogel (TSN) Synthesis

In order to add thrombin sensitivity to nanogels, the custom peptide sequence methacrylate-Gly-dPHe-Pro-Arg-Fly-Phe-Pro-Ala-Gly-Gly-Lys-methacrylate (ordered from GenScript at >95% purity) was incorporated. While stirred at 450 rpm, 85% NIPMAM and 5%

thrombin-cleavable peptide were incubated in 95 mM TEMED and put under nitrogen purge for 1 hr at room temperature. At 50 minutes into the purge, 10% Acrylic Acid was then added. The reaction was then initiated at room temperature with 125 mM ammonium persulfate (APS) and allowed to react for 24 hours at room temperature. The resulting reaction mixture was then purified by dialysis in ultrapure water in 1000 kDa dialysis tubing for 72 hours with water changes every 24 hours. The particle solution was then lyophilized and resuspended at desired concentrations with ultrapure water and stored at 4° C.

4.2.2 Size-matched Control Microgel Synthesis

To control for particle size effects, control microgels, size-matched to thrombin-sensitive nanogels, were synthesized. Ultralow crosslinking microgels (ULCs) and 7% crosslinked BIS (7% BIS) were selected as fully deformable and fully nondeformable controls, respectively. ULCs consisted of 90% Poly(N-isopropylacrylamide) (NIPAm) and 10% Acrylic Acid (AAc) and 7% BIS particles consisted of 83% NIPAm, 10% AAc, and 7% N,N' - methylenebisacrylamide (BIS). A100 mL precipitation synthesis of 140 mM monomer solutions and varying amounts of SDS (4 mM for ULCs, 2 mM SDS for 7% BIS) were filtered through a 0.2 um filter with AAc added 10 minutes prior to the addition of 1 mM ammonium persulfate (APS). The mixture was then allowed to react for 6 hours at 70° C flux with nitrogen purge. Resulting product solutions were then allowed to cool to room temperature and filtered against glass wool. Dialysis in 1000 kDa tubing against water was then conducted for 48 hours with 2 hour water changes for the latter 24 hours. The purified particle solutions were then frozen, lyophilized and resuspended at desired concentrations. Size-matched ULCs are sometimes referred to as small ULCs and size-matched 7% BIS microgels are sometimes referred to as small 7% BIS throughout this work.

4.2.3 Particle Size Characterization

Dilutions of particle solutions were analyzed on a Malvern NanoSight NS300 for hydrodynamic radius characterization with size and distribution determined from 10 measurements of 30 seconds or 5 measurements of 60 sec. Particle size and morphology was also analyzed via atomic force microscopy (AFM) imaging. For AFM imaging, cover glass was cleaned by sonication in a sequence of solutions for 10 minutes per solution. The sequence of solutions is as follows: Alconox, deionized water, acetone, ethanol (200 proof), and isopropyl alcohol. 50 μL of particle suspension was then deposited onto cleaned cover glass and allowed to air-dry overnight. The cover glass is then mounted onto a microscope slide using epoxy. Air topography imaging was then conducted on a MFP 3D Bio AFM (Asylum). Topography and height trace images were then analyzed in ImageJ for particle diameter and height for at least 30 microgels per group.

4.2.4 Particle Morphology

Particle morphology was analyzed by cryogenic scanning electron microscopy (cryoSEM) on a JEOL 7600F with Gatan Alto and Horiba CL Detector at 5 kV acceleration beam. 10 uL of particle solutions were deposited into the sample holder and plunged into nitrogen slush. Samples were then fractured and sputtered with gold.

4.2.5 Analysis of Thrombin-induced Degradation

Nanogel solutions were incubated with thrombin solutions for final thrombin concentrations of 50 U/mL or 75 U/ml and a final 0.5 mg/mL particle concentration for a total of 1 mL of solution. 100 μL time point aliquots were and analyzed for deformability, size and distribution, and morphology using AFM, Nanosight, and cryoSEM respectively. For AFM and Nanosight, aliquots were diluted 1:10 and analyzed as described in particle size characterization

methods. For cryoSEM, a 1:4 dilution of TSNs in water to 100 U/mL thrombin was created with 50 µL timepoint aliquots collected for total volume 400 µL for a final particle concentration of ~1.2 mg/mL. Timepoints were as follows for AFM and Nanosight: t = 0, 2 hr, 4 hr, 24 hr, 48 hr, 96 hr, 1 wk. For cryoSEM, the timepoints were t = 0, 2 hr, 6 hr, 24 hr, 48 hr, 96 hr, 1 wk.

4.2.6 Analysis of Thrombin-sensitive Nanogel Penetration

To model the potential for thrombin to fully penetrate the thrombin-sensitive nanogels, nanogel solutions were lyophilized and then resuspended at 10 mg/mL in 5 uM 70 kDa FITC labeled dextran. 70 kDa dextran was selected as a model molecule, because 70 kDa is close to the molecular size of thrombin (72 kDa). After 24 hours, 10 µL of the suspension was deposited onto cleaned cover glass, allowed to dry, mounted to a microscope slide and then imaged on a LSM 880 confocal microscope. The resulting images were then analyzed by fluorescent trace on ImageJ. This procedure was also repeated on nanogels that have been exposed to thrombin for 24 hours and 48 hours.

4.2.7 Coupling of Anti-fibrin Antibody to Particles to Create Platelet-like-Particles (PLPs)

To create PLPs, a sheep anti-fibrin Fragment E polyclonal antibody was coupled to the AAc groups by EDC/NHS chemistry. PLPs refer to the products of the coupling of particles and fragment E antibody. PLPs were purified by dialysis against diH20 using 1,000 kDa dialysis tubing for 24 hours. The product was then lyophilized for 24-48 hours. PLP particles were then weighed and resuspended at 10 mg/mL. Products of anti-fibrin antibody coupling to particles are referred to as <particle type>-PLPs (e.g.: thrombin-sensitive nanogels conjugated to anti-fibrin Fragment E = thrombin-sensitive PLP).

4.2.8 Clot Retraction Analysis

Treatment clots were made of 2 mg/ml fibrin, 0.1 U/ml thrombin, 0.25 mg/ml of particles (TS-PLP, small ULC-PLP, small 7% BIS-PLP, or ULC-PLP) and 10% volume 10X HEPES buffer and allowed to polymerize for 48 hours. Control clots were created similarly without the presence of particles. To control for any clot retraction due to additional thrombin, +thrombin counterparts were included. All clots were made with total of 150 μL volume. 2 hours into the polymerization an overlay of 50 μL of 100 U/mL thrombin was added to +thrombin counterparts. Clots were then imaged on a JEOL 7600F with Gatan Alto and Horiba CL Detector at 5 kV acceleration beam. Each group had 3 clots with multiple sites imaged for analysis. Images were then cropped to a 30 μm by 30 μm area with a percent porosity calculated by a ratio of black pixel area to total image pixel area. Black pixel area was measured in ImageJ.

4.2.9 In vivo Hemostatic Performance and Wound Healing Outcome Evaluation

To evaluate *in vivo* hemostatic performance and wound healing outcomes, C57/bl6 mice were anesthetized with 2% isofluorane. All studies were conducted under approval by NCSU IACUC protocol. Treatments were administered by tail vein injection and allowed to circulate for 5 minutes. Treatment groups for this study were Saline, ULC-PLP, TS-PLP and 7% BIS-PLP. All PLP-based groups were administered intravenously at 100 μL of 5 mg PLPs/kg animal suspended in sterile saline. The liver of each mouse was then exposed. A liver laceration of 0.5 cm length was then made extending from the apex of the exposed liver lobe (Figure 4A) and blood was collected onto pre-weighed filter paper and parafilm. Bleeding over time was imaged at t=0, 30 s, 1 min, 2 min, 3 min, 4 min, and 5 min. At t=5 min, the filter paper and parafilm assembly was then measured. The liver was then returned to the abdomen and mice were aseptically sutured closed. Mice were then monitored daily for 1 week for body weight and signs

of pain. After 1 week, mice were then sacrificed, and organs (wound site, healthy liver lobe, kidney, spleen, and heart) were harvested for histology. Blood loss was evaluated by determining the weight of blood collected onto the filter paper and parafilm assembly and normalizing the resulting mass by the respective animal's body weight. Filter paper area covered in blood (referred to as a bleeding area) was measured from each image taken during the bleeding assay using ImageJ. This model was powered to blood loss based on previous studies in our group.

4.2.10 Histological Analysis of Wound Healing Outcomes Following Liver Laceration

Histological analysis was conducted with hematoxylin & eosin (H&E) staining and immunofluorescent labeling for platelets, fibrin, particle treatments, and cell nuclei. To label platelets, monoclonal anti-integrin beta 3/CD61 SJ19-09 antibody from Novus Biologicals was used as primary antibody with secondary Alexa 594 antibody. To label fibrin, monoclonal UC45 was used as primary antibody with secondary Alexa 594 antibody. To label particle treatments, a polyclonal anti-sheep 488 FITC-conjugated secondary antibody was used, tagging the fibrin specific antibody attached to particles. Cell nuclei were labeled by DAPI. Images were captured on an EVOS Auto FL microscope at 4x magnification for H&E stained wounds and 10x magnification for all other organs and fluorescently labeled wounds. For each fluorescently labeled wound, 3 images at different sites were taken.

To quantify wound healing outcomes, wound area and fluorescence thresholding area were measured on ImageJ. Wound area was measured from H&E stained sections. Total areas for fibrin, particle presence, and CD61+ expression were measured by conducting particle analysis on 8-bit images with a threshold of 0-10 for fibrin (red channel), 0-30 for particle treatments (green channel), and 0-6 for CD61+ area (red channel).

4.2.11 Histological Analysis of Off-target Effects

To quantify off-target effects and clotting, peripheral organ (healthy liver lobe, heart, lung, kidney, spleen) sections were fluorescently labeled for fibrin and particles using the same methods described for fluorescent labeling for wounds. Fibrin and particle presence were also quantified using the same methods.

4.2.12 Statistical Analysis

All statistical analysis was conducted in GraphPad Prism 9. Bleeding area vs. time data was analyzed by two-way ANOVA. All other data was analyzed by one-way ANOVA with Tukey's post hoc test for multiple comparisons.

4.3 Results and Discussion

4.3.1 Size Evaluation of Thrombin-sensitive Nanogels

Unmodified thrombin-sensitive nanogels were determined to have average dry diameter of 0.33±0.05 µm and average dry height of 33±10 nm. When imaged for morphology on cryoSEM, the thrombin-sensitive nanogels displayed a rounded morphology. **(Figure 4.1)**

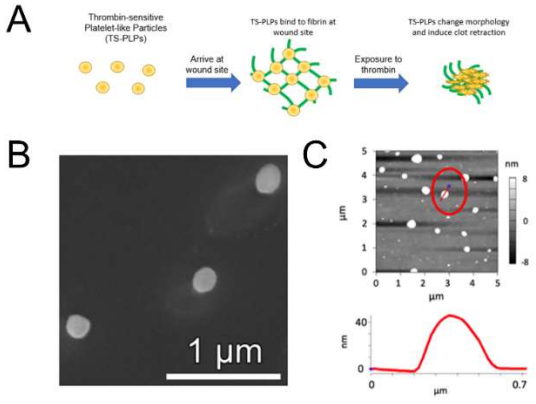

Figure 4.1: A) Schematic of TS-PLP Function. B) Representative cryoSEM image. When unmodified, TSNs exhibit rounded morphology C) Representative AFM image and height trace

When exposed to 50 U/mL and 75 U/mL thrombin, population distribution markers on Nanosight show significantly decreased size starting from t = 2 hr. However, size increased after 24 hours for 75 U/mL thrombin, potentially due to decreased crosslinks leading to increased swelling. AFM data with 50 U/mL thrombin shows no significant changes in particle diameter until t=4 hr and t-96 hr. In the presence of 50 U/ml thrombin, particle height also significantly decreased starting from t=2 hr. (**Figure 4.7**) Size increases at later time points, in combination with decreasing particle height may indicate swelling and increased deformability. This change in particle behavior was further confirmed with imaging of aliquots on cryoSEM for morphology. At later time points, the thrombin-sensitive nanogels displayed more stellate like morphology, much like active platelet morphology and ULCs. (**Figure 4.2**)

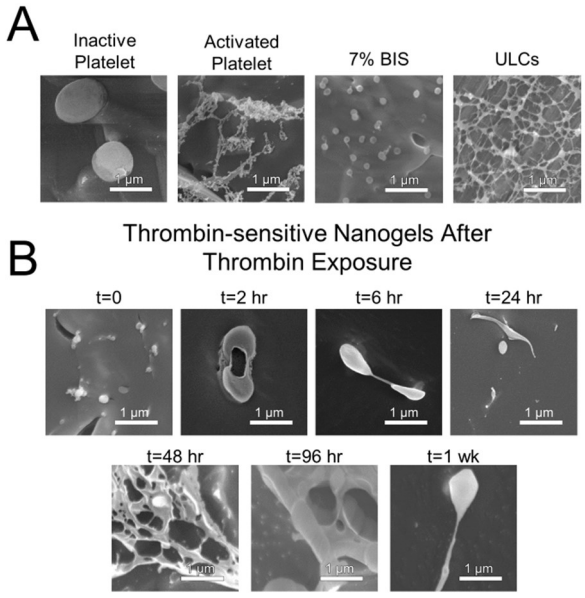

Figure 4.2: A) Representative cryoSEM images of inactive platelet, activated platelets, and size-matched control 7% BIS crosslinked and ultralow crosslinked (ULC) microgels. Scale bar = 1 µm B) Representative cryoSEM images of thrombin-sensitive nanogels (TSNs) at various time points following exposure to 75 U/mL thrombin.

4.3.2 Thrombin-sensitive Nanogel Loading Behavior

Because NIPMAM does not undergo self-crosslinking, complete degradation of particles was expected [70-73]. However, thrombin degradation assays showed that particles did not fully degrade. Thus, loading behavior was investigated to determine thrombin penetration. Fluorescent levels were observed to be higher at the edges of nanogels and lower in the center. (**Figure 4.8**) This observation indicates that there may be limited penetration into the center of the nanogel, explaining why complete degradation was not observed.

4.3.3 Clot Retraction Analysis

With confirming that the nanogels can change deformability in the presence of thrombin, we then sought to evaluate if this was sufficient to induce clot retraction. Clots including no particles (control), TS-PLPs, size-matched ULC-PLPs (small ULC-PLPs), size-matched 7% BIS-PLPs (small 7 BIS-PLPs) and ULC-PLPS were created, with +thrombin counterparts receiving a 100 U/mL thrombin overlay. All clots were then imaged on cryoSEM for clot structure. **(Figure 4.3)** The resulting images were then analyzed for % porosity, which is defined as black pixel area/total image pixels.

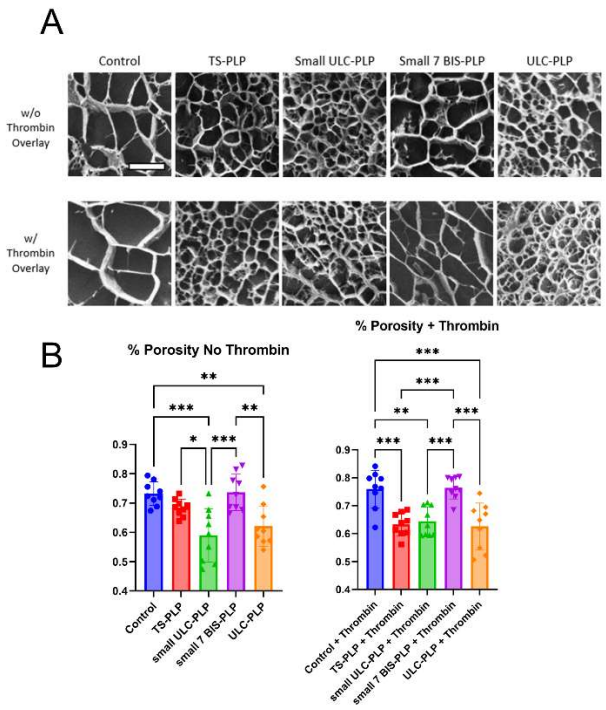

Figure 4.3: A) Representative cryoSEM images of fibrin clots polymerized in the presence of TS-PLPs, small ULC-PLPs, small 7 BIS-PLPs, and ULC-PLPs. Each image is 30 µm x 30 µm. Scale bar = 10 µm B) Mean percent porosity for each group of clots. Notably, significantly lower percent porosity was observed in small ULC-PLP and ULC-PLP groups in clots with no thrombin overlay but not in clots incorporated with TS-PLPs. After a thrombin overlay, significantly lower percent porosity was also observed in clots with TS-PLPs incorporated in addition to the ULC-PLP groups. n=9 images per group (3 images per clot, 3 clots per group). * = $p \leq 0.05$, ** = $p \leq 0.01$, *** = $p \leq 0.001$

For clots without a thrombin overlay, average % porosity was determined to be 0.73 ± 0.04 for control, 0.68 ± 0.03 for TS-PLPs, 0.59 ± 0.09 for small ULC-PLPs, 0.74 ± 0.06 for small 7 BIS-PLPs, and 0.62 ± 0.07 for ULC-PLPs. For clots with a thrombin overlay, average % porosity was determined to be 0.76 ± 0.07 for control, 0.63 ± 0.04 for TS-PLPs, 0.64 ± 0.05 for

small ULC-PLPs, 0.76 ± 0.04 for small 7 BIS-PLPs, and 0.63 ± 0.08 for ULC-PLPs. Without the addition of a thrombin overlay, it was found that clots with TS-PLPs incorporated do not have significantly lower % porosity whereas clots with small ULC-PLPs ($p \leq 0.001$) and ULC-PLPs have significantly lower % porosity ($p \leq 0.01$). Thus, the ULC-PLP particle types perform as we expect. With the addition of a thrombin overlay, in contrast, clots with TS-PLPs demonstrate a significantly lower % porosity ($p \leq 0.001$), on par with lower % porosity observed in clots with small ULC-PLPs ($p \leq 0.001$) and ULC-PLPs ($p \leq 0.001$).

4.3.4 Analysis of in vivo Hemostasis Following Traumatic Liver Laceration

We next evaluated the hemostatic ability of the TS-PLPs in a survival traumatic liver laceration model. Average blood loss (g blood loss/g animal) was $5.2 \times 10^{-3} \pm 3.1 \times 10^{-3}$ for saline treated animals, $1.3 \times 10^{-3} \pm 0.78 \times 10^{-3}$ for TS-PLP treated animals, $2.0 \times 10^{-3} \pm 0.96 \times 10^{-3}$ for size-matched ULC-PLP treated animals, and $2.8 \times 10^{-3} \pm 1.1 \times 10^{-3}$ for size-matched 7% BIS-PLP treated animals. Average bleeding area was 6.7 ± 2.9 cm^2 for saline treated animals, 1.8 ± 0.7 cm^2 for TS-PLP treated animals, 2.7 ± 1.8 cm^2 for size-matched ULC-PLP treated animals, and 4.0 ± 1.2 cm^2 for size-matched 7% BIS-PLP treated animals.

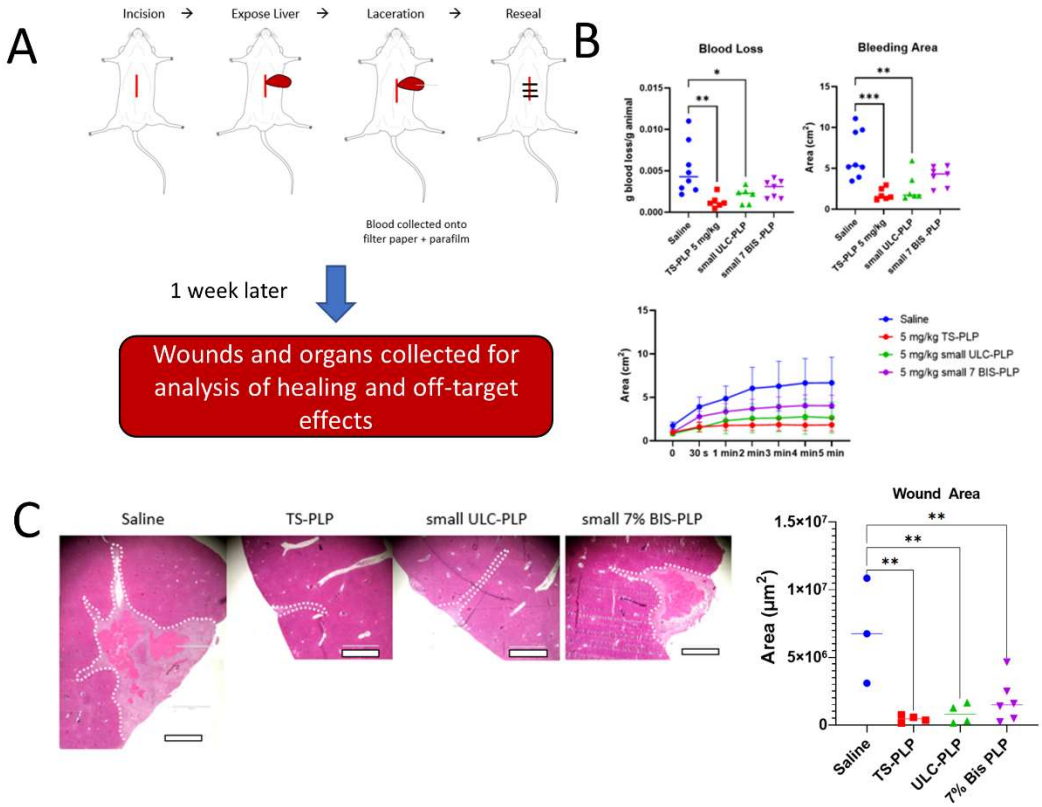

Figure 4.4: A) Schematic of survival liver laceration model B) Summary of blood loss data. Mice treated with TS-PLPs displayed significantly lower blood loss and bleeding area. Mice treated with TS-PLPs and size-matched ULC-PLPs displayed significant decreases in bleeding compared to control animals. n=6-8 animals per group. C) H&E stained wound sections with summary of wound area measurements. Scale bar = 1000 µm. Mice treated with all hemostatic particles had significantly lower average wound area when compared to saline mice, though the standard deviation was lowest in the TS-PLP group. n=3-6 mice per group. * = $p \leq 0.05$, ** = $p \leq 0.01$, *** = $p \leq 0.001$

In mice treated with TS-PLPs, significantly lower blood loss and bleeding area were observed, when compared to saline. Additionally, TS-PLPs reduce bleeding to similar extent as ULC-PLPs. (**Figure 4.4)**

4.3.5 Analysis of in vivo Wound Healing Outcomes Following Traumatic Liver Laceration

To evaluate wound healing outcomes, wound area was measured from H&E stained sections, fibrin positive area, CD61+ area, and particle presence were measured from immunofluorescent stained sections. Average wound area was $6.9 \times 10^6 \pm 3.9 \times 10^6$ μm^2 for saline treated animals, $0.5 \times 10^6 \pm 0.3 \times 10^6$ μm^2 for TS-PLP treated animals, $0.8 \times 10^6 \pm 0.7 \times 10^6$ μm^2 for size-matched ULC-PLP treated animals, and $1.8 \times 10^6 \pm 1.6 \times 10^6$ μm^2 for size-matched 7% BIS-PLP treated animals. Average fibrin area was 4585 ± 1417 μm^2 for saline treated animals, 16458 ± 11202 μm^2 for TS-PLP treated animals, 3725 ± 2058 μm^2 for size-matched ULC-PLP treated animals, and 3414 ± 3140 μm^2 for size-matched 7% BIS-PLP treated animals. Average CD61+ area was 4762 ± 3353 μm^2 for saline treated animals, 2545 ± 2585 μm^2 for TS-PLP treated animals, 3945 ± 1739 μm^2 for size-matched ULC-PLP treated animals, and 5668 ± 5305 μm^2 for size-matched 7% BIS-PLP treated animals. Average particle presence area was 0 μm^2 for all treatment groups.

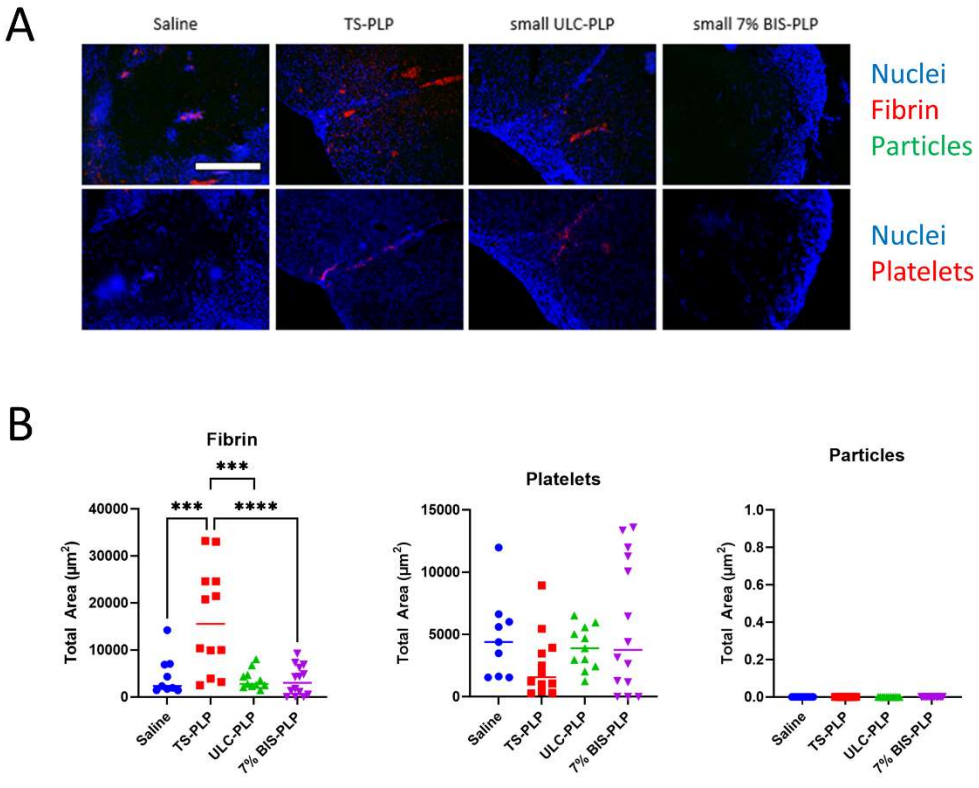

Figure 4.5: A) Representative IHC wound sections where cell nuclei, fibrin and particles were fluorescently labeled (top row) and where cell nuclei and platelets were fluorescently labeled (bottom row). Scale bar = 400 µm B) Summary of total area of fibrin, particles, and platelet presence (CD61+). Mice treated with TS-PLPs were observed to have both significantly higher fibrin presence while there were no significant differences observed in platelet presence and particle presence. n=3 images per wound and 3-5 animals per group. * = $p \leq 0.05$, *** = $p \leq 0.001$

Overall, significantly lower wound areas and CD61+ expression were observed in animals treated with TS-PLPs, size-matched ULC-PLPs, and size-matched 7% BIS-PLPs. However, fibrin presence was significantly higher only in animals treated with TS-PLPs and size-matched ULC-PLPs. The higher presence of fibrin one week after injury indicates that

animals treated with this therapy exhibit *in vivo* clot stability. Additionally, no significant differences were observed in particle presence across all groups, indicating that any particles administered to mice have left the injury site 1 week post-injury (**Figure 4.5**).

4.3.6 Analysis of Safety and Potential Off-target Effects

To evaluate potential off-target effects, peripheral organs were stained by H&E for tissue morphology and fluorescently labeled for fibrin and particles and measured for fibrin-positive and particle presence areas. Across all organs, tissue morphology looked normal and no significant differences in fibrin and particle presence were detected between treatment groups (**Figure 4.6)**.

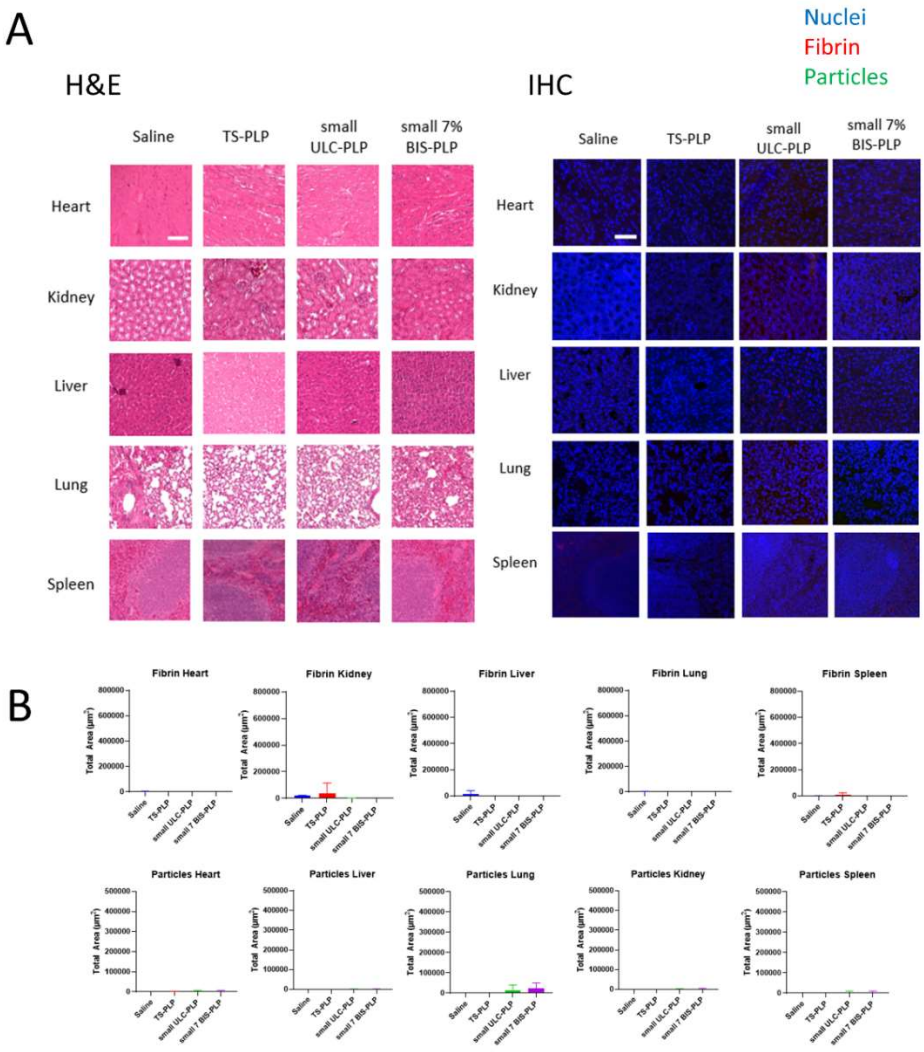

Figure 4.6: Summary of off-target effects studies. A) Representative images of both H&E to characterize gross tissue morphology and fluorescently labeled peripheral organs for fibrin and particle presence. Images are 400 μm x 400 μm. Scale bar = 100 μm B) Summary of total area for fibrin and particle presence, separated by organ type. Fibrin and particle presence were measured by converting individual channel images to 8-bit grayscale and then thresholding with a minimum of 0-16. The resulting image was then converted to binary and analyzed by particle analysis in ImageJ. For each organ type, n=3-5 animals per group. Overall, no significant differences in both fibrin and particle presence were observed with relatively low total area detected (compared to total area detected in wounds).

4.4 Conclusions and Greater Impact

PLPs are a promising material that seek to address the issues associated with platelet depletion in conditions such as traumatic injury and are capable of homing specifically to injuries while being able to mimic natural platelet clot retraction. However, PLPs lack the natural platelet ability to conditionally change shape after activation of the coagulation cascade. To address this shortcoming, we developed a thrombin-sensitive formulation capable of mimicking this conditional change shape based on the presence of thrombin. In these studies, we were able to demonstrate that these thrombin-sensitive PLPs (TS-PLPs) can induce clot retraction in the presence of thrombin and to similar extent as our current PLP technology while also demonstrating triggered shape change.

Prior to exposure to thrombin, TS-PLPs have a rounded shape and does not have significant deformability as indicated by the relatively high particle height, compared to previous findings with ULC-PLPs [10,36,67] (**Figure 4.1**). After exposure to thrombin, TS-PLPs then change shape, displaying morphology most like activated platelets and small ULC-PLPs at t=48 hrs. (**Figure 4.2**) Only in this morphology were TS-PLPs capable of significantly retracting the clot structure like ULC-PLPs (**Figure 4.3**).

Additionally, TS-PLPs demonstrated significant hemostatic ability and wound healing enhancement *in vivo*. TS-PLPs and ULC-PLPs decreased bleeding significantly compared to control animals treated with saline. Interesting, 7% BIS-PLPs had a lower mean bleeding time than control animals, but bleeding was not significantly different between the two groups. Other studies by our group using larger 7% BIS-PLPs and ULC-PLPs did not demonstrate differences in bleeding outcomes between these groups, but did show differences in clot retraction. These results suggest that both particle size and deformability synergistically can influence hemostatic

outcomes, and this relationship should be studied in more detail in future studies. Additionally, TS-PLPs demonstrated hemostatic ability to greater statistical significance than size-matched ULC-PLPs when compared to blood loss in mice treated with saline, although direct comparison between TS-PLPs and size-matched ULC-PLPs is not statistically significant. 7 days after injury, significantly lower wound area was observed in injury sites of mice treated with all PLP groups, However, only mice treated with TS-PLPs were observed to have significantly enhanced fibrin presence, potentially indicating greater *in vivo* fibrin stability.

While these studies describe a platelet-mimetic particle that conditionally changes shape in response to wound triggers, to create a more "platelet-like" particle, there are still aspects that could be further optimized. For example, while TS-PLPs do indeed change shape as a result of thrombin exposure, high concentrations of thrombin are required, and the degradation of crosslinks occur over long time scales. However, it is also possible that thrombin levels within clots may be at even higher levels and thus lead to more immediate TS-PLP shape change. Potential future studies to address this issue could involve further investigation of thrombin-degradation and interaction with TS-PLPs at more physiologically relevant concentrations and potentially coupling TS-PLPs to thrombin delivery systems [75]. Furthermore, the minimum thrombin concentration needed to induce TS-PLP shape change is currently unknown. Additionally, it is unknown if the current design allows for retention of thrombin within the microgel for extended periods of time. If this is the case, the microgel may act as a source of thrombin within the wound site for some time after injury. Thus, some other potential directions for future work could entail evaluating these parameters. Additionally, *in vivo* studies with more immediate end point could potentially enlighten the exact mechanisms as to why TS-PLPs were able to stem bleeding immediately.

In conclusion, we were able to successfully fabricate a wound-triggered shape changing PLP with TS-PLPs. As demonstrated in this work, TS-PLPs will remain in a rounded morphology, similar to inactive platelets. Following exposure to thrombin, TS-PLPs then change into a stellate morphology, like inactive platelets. In this degraded state, TS-PLPs can induce clot retraction and stem bleeding to similar extent as ULC-PLPs. Additionally, TS-PLPs were demonstrated to have improved wound healing outcomes in a survival liver laceration mouse model. Although further optimization of some aspects is still needed, TS-PLPs, nonetheless, demonstrated promising qualities as a hemostatic and wound healing material. Future work will focus on optimizing the thrombin-based degradation of TS-PLPs either by determining a formulation that will work at more physiologically relevant thrombin concentrations or coupling to a thrombin delivery system, evaluating long-term storage effects, safety and efficacy of TS-PLPs.

Acknowledgements: Funding was provided by the National Science Foundation DMR CAREER 1847488. This work was performed in part at the Analytical Instrumentation Facility (AIF) at North Carolina State University, which is supported by the State of North Carolina and the National Science Foundation (award number ECCS-2025064). The AIF is a member of the North Carolina Research Triangle Nanotechnology Network (RTNN), a site in the National Nanotechnology Coordinated Infrastructure (NNCI). The authors acknowledge the use of the Cellular and Molecular Imaging Facility (CMIF) at North Carolina State University, which is supported by the State of North Carolina and the National Science Foundation.

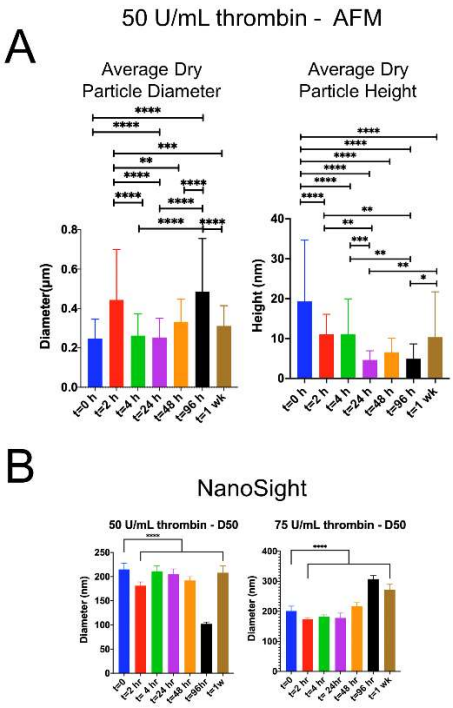

Figure 4.7: Summary of TSN particle size changes over time. A) Average dry diameter and height for TSNs exposed to 50 U/mL thrombin. As time since thrombin exposure increases, particle diameter increases and particle height decreases. For dry diameter, significantly higher diameter is observed at both t=24 hrs and t=96 hrs with an overall trend of increasing particle diameter. For dry height, significantly lower particle height is detected as early as t=2 hr. B) Average median wet diameter (D50). With 50 U/mL thrombin, a significant difference in particle size change was detected with a general trend of increasing median particle size. With 75 U/mL thrombin exposure, a much more noticeable increase in average TSN size was observed at later timepoints (t=96 hr, 1 wk) * = $p \leq 0.05$, ** = $p \leq 0.01$, *** = $p \leq 0.001$, **** = $p \leq 0.0001$

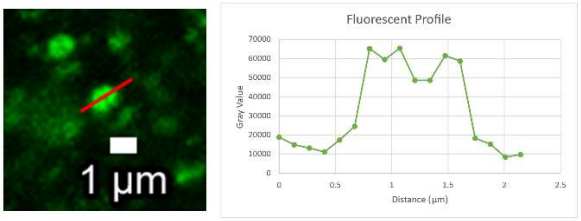

Figure 4.8: Representative confocal image of unmodified TSN loaded with 70 kDa FITC labeled dextran (left). Fluorescent profile of 70 kDa loaded TSN indicates that there is lower signal in the middle of the particle compared to the edges, indicating that the 70 kDa dextran does not fully penetrate the particle. Since 70 kDa is close to the molecular size of thrombin, these observations may indicate that thrombin does not fully penetrate the nanogels, potentially explaining why full particle degradation is not observed.

CHAPTER 5

Conclusions and Future Directions

5.1 Summary of Findings

This dissertation was dedicated to creating enhanced function formulations of PLPs to allow for great biomimetic capability. In particular, these studies were focused on adding the ability to fight infections and the ability to conditionally change shape. The objective of the studies conducted were divided into two specific aims, presented in Chapters 3-4. Aim 1 was focused on developing a PLP with antimicrobial activity and achieved this through the incorporation of nanosilver into the ULC microgel body. Aim 1 was divided into further sub-aims, with Aim 1A being focused on the fabrication of nanosilver composite ULCs and evaluation of their associated *in vitro* performance and Aim 1B being focused on the evaluation of the associated *in vivo* performance and properties both in the absence and presence of bacterial infection. Aim 2 was focused on developing a PLP formulation with triggered chape change and achieved this through the incorporation of a thrombin-cleavable peptide as a crosslinker into the nanogel body. Aim 2 was divided into similar sub-aims with Aim 2A focusing on the fabrication of a thrombin-sensitive PLP and associated *in vitro* properties and Aim 2B focusing on the evaluation of the TS-PLPs *in vivo*.

The studies conducted for Chapter 3 focused on first fabricating an antimicrobial nanosilver composite ULC (Ag-ULC), then evaluating its associated *in vitro* properties including particle size, deformability and clot retraction ability, and then finally evaluating *in vivo* performance in a mouse dermal injury model without bacterial infection and a model with bacterial infection. Because the combination of particle deformability and fibrin binding affinity of the fibrin-targeting antibody was found in first generation PLPs to both be required for clot

retraction, it was crucial to determine what effects the incorporation of nanosilver might have on particle deformability. To incorporate nanosilver into ULCs, an *in situ* reduction of silver ions by sodium borohydride was conducted. The resulting Ag-ULCs were found to share similar diameter, height and hydrodynamic diameter measured via DLS at pH 3 compared with unmodified ULCs, averaging about 1.6 μm in diameter, 15 nm in height, and 500 nm pH 3 diameter. Nanosilver presence was confirmed by TEM, shown as black dots. To evaluate clot retraction ability, Ag-ULCs were conjugated to fibrin targeting fragment E antibody and incorporated into clots. It was observed that clots with Ag-ULCs had significantly denser clot structure compared to control clots and that the fibrin density was similar to clots with ULC-PLPs. To evaluate *in vitro* antimicrobial activity, a colony forming assay was conducted using drug resistant strains of *Escherichia choli* and *Staphylococcus aureus*. These bacteria were cultured in the presence of Ag-ULCs over the course of 24 hours at 37^{o}C and it was observed that no colonies grew from any of the timepoint aliquots where Ag-ULCs were present across both species of bacteria cultured. These findings in combination with similarities in particle size properties, demonstrate that Ag-ULCs retain the properties and performance of ULCs following the nanosilver incorporation while demonstrating significant antimicrobial properties.

To evaluate *in vivo* hemostatic ability, a liver laceration mouse model was used, with treatments administered intravenously and particle treatments being administered at 10 mg particle/kg animal. It was observed that mice treated with Ag-PLPs had significantly less blood loss than mice treated with saline. The reduced blood loss is also similar to the blood loss observed in mice treated with ULC-PLPs. To evaluate effects of Ag-PLPs on wound healing outcomes, a full thickness dermal injury mouse model was used, with treatments delivered in a fibrin clot. 9 days after surgery, significantly thicker epidermal thickness and higher CD31

expression was observed in wounds treated with Ag-PLPs, compared to wounds treated with fibrin. Additionally, the enhanced wound healing outcomes in wounds treated with Ag-PLPs were observed to be similar to wound healing outcomes in wounds treated with ULC-PLPs. Across these two animal models, Ag-PLPs demonstrated similar performance as ULC-PLPs, indicating that Ag-PLPs also retain base ULC-PLP performance *in vivo*. To evaluate *in vivo* wound healing outcomes in the presence of bacterial infection, the same mouse dermal injury model was used with an additional application of 2.5 x 10^7 CFU/mL suspension of *S. aureus* prior to application of treatment clots. 9 days after surgery, it was observed that wounds treated with Ag-PLPs and ULC-PLPs both had enhanced epidermal thicknesses. However, only wounds treated with Ag-PLPs had enhanced CD31 expression in addition. Furthermore, significantly higher wound closure was observed in wounds treated with Ag-PLPs, starting from t=5 days onwards. Overall, Ag-PLPs significantly enhance wound healing outcomes in the presence of infection, indicating that Ag-PLPs can significantly fight off infection *in vivo*. In Chapter 3, a PLP formulation with antimicrobial activity was successfully fabricated and evaluated to have similar properties as ULC-PLPs while also demonstrating significant ability to combat infection both *in vitro* and *in vivo*. Thus, Ag-PLPs are more mimetic of actual platelets than ULC-PLPs due to the added antimicrobial capacity, which allows Ag-PLPs to assist in the host response to bacterial infection.

With the findings of Chapter 3 establishing a PLP formulation with the ability to fight infection, the studies conducted for Chapter 4 focused on the development of thrombin-sensitive PLPs as a PLP formulation with triggered shape change. Thrombin-sensitive nanogels (TSNs) were fabricated by a precipitation synthesis of NIPMAM, Acrylic Acid as a copolymer and a thrombin-cleavable peptide as a crosslinker. TSNs were then evaluated for morphology on

cryoSEM and dry particle size on AFM in the presence or absence of thrombin. When unmodified (i.e. not exposed to thrombin), TSNs were found to have a rounded morphology with an average particle diameter of about 330 nm and average particle height of 33 nm measured via AFM. To determine morphology changes over time in the presence of thrombin, TSNs were exposed to 75 U/mL thrombin and then imaged on cryoSEM at various time points over the course of 1 week. It was observed that the morphology of TSNs changes from rounded like inactive platelets to stellate and network-like, similar to the morphology of active platelets and ULCs, especially at t= 48 hours. To evaluate if the observed shape change can induce clot retraction when formulated into PLPs, TSNs were conjugated to a fibrin targeting fragment E antibody to create TS-PLPs and then incorporated into clots. To test thrombin-triggered shape change, TS-PLP containing clots with a thrombin overlay were characterized as well. Without a thrombin overlay, it was observed that clots with TS-PLPs did not have significantly different clot structure than control clots. As expected based on previous results, clots with size-matched ULC-PLPs and regular ULC-PLPs did exhibit significantly more condensed clot structure. However, with a thrombin overlay, clots with TS-PLPs displayed significantly lower % porosity and thus more condensed clot structure than control clots, with similar % porosity as the ULC-PLP groups. With a thrombin overlay, the clot retraction induced by TS-PLPs was similar to that observed in clots with ULC-PLPs. These findings demonstrate that TS-PLPs do indeed have triggered shape change and that this shape change is sufficient enough to induce significant clot retraction.

To evaluate *in vivo* performance and properties of TS-PLPs, a survival liver laceration mouse model was used. Particle treatments were administered intravenously at 5 mg/kg and allowed to circulate for 5 minutes prior to inducing laceration. Blood was then collected onto a pre-weighed

assembly of filter paper and parafilm with photos taken over the course of 5 minutes. The area covered in blood was then measured for a bleeding area in ImageJ. It was observed that TS-PLPs and size-matched ULC-PLPs significantly reduced blood loss compared to saline controls. To evaluate wound healing outcomes and potential off-target effects, organs and wounds were harvested from the mice 1 week after the initial liver laceration and histologically analyzed. Wound healing outcomes were evaluated by wound area measurement on H&E stained sections, fluorescently labeled fibrin and CD61 (to evaluate platelets). Particle presence was also evaluated by fluorescently labeling the fibrin targeting antibody. It was observed that mice treated with TS-PLPs and size-matched ULC-PLPs had significantly lower blood loss and bleeding area compared to mice treated with saline. Additionally, although comparison between blood loss in TS-PLP and size-matched ULC-PLP treated mice is not statistically significant, it is still noteworthy that mice treated with TS-PLPs exhibited greater statistical significance in blood loss and bleeding area when compared to mice treated with saline. For wound healing outcomes, wound area was statistically significantly lower in all particle treated mice compared to saline treated animals. However, fibrin was statistically significantly higher only in mice treated with TS-PLPs, indicating that animals treated with this therapy exhibit better clot stability *in vivo*. These findings indicate that TS-PLPs are capable of significant hemostatic ability and enhanced wound healing outcomes. For off targeting effects, no significant differences were detected for either fibrin or particle presence across all groups for each organ, indicating no noticeable off target effects. Overall, these findings indicate that TS-PLPs do indeed exhibit triggered shape change and that the shape change can significantly retract clots. Additionally, TS-PLPs demonstrated significant hemostatic ability and enhanced wound healing outcomes with minimal off target effects. In Chapter 4, a PLP formulation with wound-triggered shape change was

successfully fabricated with the development of thrombin-sensitive PLPs and evaluated to have triggered-shape change when exposed to thrombin. It was also found that this shape change was sufficient enough to induce significant clot retraction *in vitro* and sufficient enough to lead to enhanced hemostasis and wound healing outcomes *in vivo* without off target effects. These findings demonstrate that TS-PLPs are indeed a PLP formulation that can conditionally change shape in the presence of injury markers (specifically thrombin in this case) and thus more closely mimic platelet wound-triggered shape change.

5.2 Limitations and Challenges

These enhanced function PLP formulations have been demonstrated to not only perform similarly as their base ULC-PLP counterparts, but also demonstrate the ability to achieve their intended secondary function. For Ag-PLPs, it was determined that the nanosilver incorporation did not affect the associated ULC-PLP performance while being able to significantly fight off infection. For TS-PLPs, it was determined that they do not change shape until exposed to thrombin, and when they are exposed to thrombin, the resulting shape change is enough to induce similar in vitro clot retraction and in vivo hemostasis and enhanced wound healing outcomes. However, there are limitations to consider in both current PLP and study designs.

Although Ag-PLPs were observed to be able to fight off *in vivo* infection, it is worth noting that the injury model they were used in was one of acute infection, where bacteria were applied at the same time as with treatments. Furthermore, due to the length of the experiment, we were unable to detect bacteria by Gram stain, as shown by the lack of purple bacteria in **Figure 3.8** and hypothesize that bacteria may have sloughed off in the scab or may have even cleared by host animal immune response. Additionally, although nanometals are well-recorded as an antimicrobial agent, some studies have found that bacteria are capable of developing resistance

to nanometals [76]. Long-term and/or multiple doses of Ag-PLPs need to be evaluated in future studies. These studies also did not evaluate any off-target effects that Ag-PLPs may induce, which is important to evaluate for safety and eventual clinical translation.

For TS-PLPs, although the ability for thrombin-triggered shape change was observed, the time scale required to achieve sufficient shape change particle deformability is on the scale of days. While the shape change is not needed for hemostasis it is expected to contribute to enhanced healing outcomes, since our previous work has shown that deformable PLPs enhance dermal healing to a greater extent than non-deformable particles. Overall, the healing outcomes between TS-PLPs and ULC-PLPs were similar in our model, indicating that this design was sufficient to at least match our previous design. However, it should be noted that these prior studies did use larger ULC-PLPs (~1μm instead of ~300nm in diameter), and it is likely that size plays a role in the observed responses as well. Having faster shape change could potentially enhance the wound healing kinetics of the TS-PLPs. Additionally, the production of larger TS-PLPs should be explored in the future as well. Furthermore, the thrombin concentrations needed to induce the shape change in TS-PLPs are higher than physiological concentrations in circulation. However, at the wound site the thrombin concentrations would be expected to be much higher. Also, there has not been significant investigation of potential cytotoxicity or immune response in the presence of TS-PLPs, which are crucial evaluation points for safety.

Across both particle formulations, long-term effects remain mostly unevaluated at this time. For Ag-PLPs, some storage effects have been evaluated as shown in Appendix B.3, but there is still a need to evaluate if the nanosilver content, antimicrobial activity, and clot retraction ability are all retained. For both PLP types it is important to evaluate long-term effects to ensure that the performance observed in the studies for Chapters 3 and 4 are retained.

5.3 Clinical and Engineering Significance

Although nanosilver composite pNIPAm microgels have been fabricated and investigated in literature before, the majority of these applications have been more focused on chemical applications, particularly as catalytic materials where the microgel is used as a stabilizing agent for the nanosilver [77-80]. Thus, Ag-PLPs presents innovation in the field by expanding the potential applications of nanosilver composite microgels to a wound healing and biomedical space. Additionally, because PLPs can be applied both topically and intravenously, Ag-PLPs, with their ability to fight infection, could potentially be used to treat infections in many different injury sites, ranging from surface injuries such as chronic wounds or burns to more internal infections, or even as emergency hemostatic use that comes with built in infection prevention.

Many platelet-mimetic materials are focused on only recapitulating the hemostatic ability of platelets. As previously discussed, however, platelets achieve some of their important functions in the hemostatic and wound healing process by their ability to conditionally change shape and retract clots. PLPs in general have been highly innovative in this field with being a material that can retract clots. Thus, TS-PLPs are an innovative material in this field by not only being able to mimic clot retraction but also to mimic the conditional shape of platelets. It is also worth noting that current TS-PLPs do not require delivery of external coagulation or chemical signals to achieve the enhanced wound healing outcomes observed in Chapter 4. An additional innovation in this work is that the *in vivo* studies associated with Chapter 4 used a survival liver laceration model in mice, which is notable as most survival liver laceration rodent models in literature typically use rats [81-85]. One mouse survival liver laceration model has been found in literature, but it entailed cutting off 75% of a liver lobe and re-sealing mice with absorbent

material inside, which can be incredibly stressful or uncomfortable for the animals [86]. Thus, what makes the survival liver laceration model used for Chapter 4 innovative is its less harsh requirements to detect significant differences in bleeding and that it is conducted in an animal that is not usually used for this type of injury model. As a result, the studies for Chapter 4 have added a potential animal model for other investigators in the field to use.

5.4 Future Directions

Although the materials developed as part of this dissertation demonstrated significant promise in their hemostatic and wound healing applications, and expand the applications of their material types, there remain many aspects to be further optimized and explored. Ag-PLPs have demonstrated significant ability to fight off infection *in vivo*, but the infected injury model they were tested in was only for a model of acute infection, which is not necessarily reflective of clinically treated cases of bacterial infection. As such, a potential direction that can be taken for future work with Ag-PLPs is study of Ag-PLPs in animal models of long-term infection. Additionally, it has been recorded that some bacteria can indeed develop resistance to antimicrobial nanometals, nanosilver included, which lends to a need to investigate potential resistance to Ag-PLPs [76].

As mentioned previously in this dissertation, the conditions needed for significant shape change in TS-PLPs could be further optimized. Because of this limitation, future work can be dedicated to exploring alternative formulations, such as changing the amount of thrombin-cleavable peptide crosslinker or coupling TS-PLPs to previously described delivery systems loaded with thrombin[75]. Additionally, there is also a need to determine a minimum thrombin concentration to induce TSN shape change and to better understand if TSNs promote thrombin retention and/or prolonged activity. To that end, further directions for future work could entail

evaluating these parameters through conducted thrombin degradation assays at differing thrombin concentrations or evaluating behavior of TSNs in the presence of fluorescently labeled thrombin or a fluorescently labeled thrombin substrate. Furthermore, the current iteration of TSNs are smaller than platelets or first generation ULC-PLPs. The effect of these particle size discrepancies on TSN performance is unknown. Thus, another direction for future work is to determine particle size-related effects by exploring alternative formulations such as readjusting reagent concentrations or changing the main polymer from pNIPMAM to pNIPAm, the latter of which is used in our current ULC-PLP formulation.

Finally, across both PLP formulations, future work can also be focused on more thoroughly evaluating the long-term storage effects as well as safety and efficacy. For Ag-PLPs, preliminary study indicates that particle size remains relatively stable over the course of 1 month, but further investigation is needed to determine if associated nanometal content, antimicrobial activity and clot retraction ability are affected by the differing storage conditions. For TS-PLPs, future work on this front would entail determining what effects different storage conditions could have on the shape change ability as well as associated clot retraction performance. There is also potential to explore loading of these PLP formulations with other chemical markers as multi-functional delivery platforms to better imitate the ability of platelets to provide additional coagulation factors. Overall, there are still many aspects to explore to further enhance the biomimetic function of PLPs as well as many formulations to further develop.

In conclusion, the work presented in this dissertation has developed new platelet-like particle formulations that add additional functions to create multifunctional PLPs that are even more mimetic of natural platelets and not only achieve enhanced hemostasis and wound healing outcomes but also mimic platelets' ability to fight infection and conditionally change shape.

Because of these multifunctional aspects, the PLPs developed in this work have added platelet-mimetic materials that can mimic several functions in a field where most work focuses on only one: the hemostatic ability of platelets.

REFERENCES:

1. Senet P, Bon F, Benbunan M, et al. Randomized trial and local biological effect of autologous platelets used as adjuvant therapy for chronic venous leg ulcers. *Journal of vascular surgery*. 2003;38(6):1342-1348.

2. Ivanova EP, Hasan J, Webb HK, et al. Natural bactericidal surfaces: Mechanical rupture of pseudomonas aeruginosa cells by cicada wings. *Small*. 2012;8(16):2489-2494.

3. Koupenova M, Clancy L, Corkrey HA, Freedman JE. Circulating platelets as mediators of immunity, inflammation, and thrombosis. *Circ Res*. 2018;122(2):337-351.

4. Nandi S, Brown AC. Platelet-mimetic strategies for modulating the wound environment and inflammatory responses. *Exp Biol Med*. 2016;241(10):1138-1148.

5. Kim OV, Litvinov RI, Alber MS, Weisel JW. Quantitative structural mechanobiology of platelet-driven blood clot contraction. *Nature communications*. 2017;8(1):1-10.

6. Jansen EE, Hartmann M. Clot retraction: Cellular mechanisms and inhibitors, measuring methods, and clinical implications. *Biomedicines*. 2021;9(8):1064.

7. Tucker KL, Sage T, Gibbins JM. Clot retraction. In: *Platelets and megakaryocytes.* Springer; 2012:101-107.

8. Tutwiler V, Peshkova AD, Le Minh G, et al. Blood clot contraction differentially modulates internal and external fibrinolysis. *Journal of Thrombosis and Haemostasis*. 2019;17(2):361-370.

9. Samson AL, Alwis I, Maclean JA, et al. Endogenous fibrinolysis facilitates clot retraction in vivo. *Blood, The Journal of the American Society of Hematology*. 2017;130(23):2453-2462.

10. Nandi S, Sproul EP, Nellenbach K, et al. Platelet-like particles dynamically stiffen fibrin matrices and improve wound healing outcomes. *Biomaterials science*. 2019;7(2):669-682.

11. Page MJ, Pretorius E. A champion of host defense: A generic large-scale cause for platelet dysfunction and depletion in infection. . 2020;41(03):302-319.

12. Ten leading causes of death and injury. Centers for Disease Control and Prevention Web site. https://www.cdc.gov/injury/wisqars/LeadingCauses.html. Updated 2019. Accessed Dec 9, 2019.

13. Arrieta-Blanco JJ, Oñate-Sánchez R, Martínez-López F, Oñate-Cabrerizo D, Cabrerizo-Merino MC. Inherited, congenital and acquired disorders by hemostasis (vascular, platelet & plasmatic phases) with repercussions in the therapeutic oral sphere. *Medicina Oral, Patologia Oral y Cirugia Bucal*. 2014;19(3):e280.

14. Rand ML, Leung R, Packham MA. Platelet function assays. *Transfusion Apheresis Sci*. 2003;28(3):307-317.

15. HO-TIN-NOÉ B, Demers M, Wagner DD. How platelets safeguard vascular integrity. *Journal of Thrombosis and Haemostasis*. 2011;9:56-65.

16. Hux BD, Martin LG. Platelet transfusions: Treatment options for hemorrhage secondary to thrombocytopenia. *Journal of Veterinary Emergency and Critical Care*. 2012;22(1):73-80.

17. Fischer TH, Merricks E, Bellinger DA, et al. Splenic clearance mechanisms of rehydrated, lyophilized platelets. *Artificial Cells, Blood Substitutes, and Biotechnology*. 2001;29(6):439-451.

18. Cap AP, Perkins JG. Lyophilized platelets: Challenges and opportunities. *Journal of Trauma and Acute Care Surgery*. 2011;70(5):S59-S60.

19. Doshi N, Orje JN, Molins B, Smith JW, Mitragotri S, Ruggeri ZM. Platelet mimetic particles for targeting thrombi in flowing blood. *Adv Mater*. 2012;24(28):3864-3869.

20. Gupta AS, Pawlowski C, Sekhon UD, et al. SynthoPlate: A platelet-inspired hemostatic nanotechnology for treatment of bleeding complications. . 2016.

21. Bertram JP, Williams CA, Robinson R, Segal SS, Flynn NT, Lavik EB. Synthetic platelets: Nanotechnology to halt bleeding. *Science translational medicine*. 2009;1(11):11ra22.

22. Hu Q, Sun W, Qian C, Wang C, Bomba HN, Gu Z. Anticancer platelet-mimicking nanovehicles. *Adv Mater*. 2015;27(44):7043-7050.

23. Brown AC, Stabenfeldt SE, Ahn B, et al. Ultrasoft microgels displaying emergent platelet-like behaviours. *Nature materials*. 2014;13(12):1108.

24. Nandi S, Sommerville L, Nellenbach K, et al. Platelet-like particles improve fibrin network properties in a hemophilic model of provisional matrix structural defects. *J Colloid Interface Sci*. 2020;577:406-418.

25. Antibiotic/antimicrobial resistance: Biggest threats and data. Centers for Disease Control and Prevention Web site. https://www.cdc.gov/drugresistance/biggest_threats.html. Updated 2021. Accessed April 20, 2022.

26. Chee E, Brown AC. Biomimetic antimicrobial material strategies for combating antibiotic resistant bacteria. *Biomaterials Science*. 2020;8(4):1089-1100.

27. Labrie SJ, Samson JE, Moineau S. Bacteriophage resistance mechanisms. *Nature Reviews Microbiology*. 2010;8(5):317.

28. Loc-Carrillo C, Abedon ST. Pros and cons of phage therapy. *Bacteriophage*. 2011;1(2):111-114.

29. Fernandez-Moure JS, Van Eps JL, Cabrera FJ, et al. Platelet-rich plasma: A biomimetic approach to enhancement of surgical wound healing. *J Surg Res*. 2017;207:33-44.

30. Liu Y, Liu X, Yang J, Lin D, Chen X, Zha L. Investigation of ag nanoparticles loading temperature responsive hybrid microgels and their temperature controlled catalytic activity. *Colloids Surf Physicochem Eng Aspects*. 2012;393:105-110.

31. Begum R, Naseem K, Farooqi ZH. A review of responsive hybrid microgels fabricated with silver nanoparticles: Synthesis, classification, characterization and applications. *J Sol Gel Sci Technol*. 2016;77(2):497-515.

32. Arif M, Farooqi ZH, Irfan A, Begum R. Gold nanoparticles and polymer microgels: Last five years of their happy and successful marriage. *Journal of Molecular Liquids*. 2021;336:116270.

33. Li L, Niu R, Zhang Y. Ag–Au bimetallic nanocomposites stabilized with organic–inorganic hybrid microgels: Synthesis and their regulated optical and catalytic properties. *RSC advances*. 2018;8(22):12428-12438.

34. Bandyopadhyay S, Sharma A, Glomm WR. The influence of differently shaped gold nanoparticles functionalized with NIPAM-based hydrogels on the release of cytochrome C. *Gels*. 2017;3(4):42.

35. Farooqi ZH, Siddiq M. Temperature-responsive poly (N-isopropylacrylamide-acrylamide-phenylboronic acid) microgels for stabilization of silver nanoparticles. *J Dispersion Sci Technol*. 2015;36(3):423-429.

36. Sproul EP, Nandi S, Chee E, et al. Development of biomimetic antimicrobial platelet-like particles comprised of microgel nanogold composites. *Regenerative Engineering and Translational Medicine*. 2019:1-11.

37. Karg M, Lu Y, Carbo-Argibay E, et al. Multiresponsive hybrid colloids based on gold nanorods and poly (NIPAM-co-allylacetic acid) microgels: Temperature-and pH-tunable plasmon resonance. *Langmuir*. 2009;25(5):3163-3167.

38. Din MI, Khalid R, Akbar F, Ahmad G, Najeeb J, Nisa Hussain ZU. Recent progress of poly (N-isopropylacrylamide) hybrid hydrogels: Synthesis, fundamentals and applications–review. *Soft Materials*. 2018;16(3):228-247.

39. Nordström R, Nyström L, Ilyas H, et al. Microgels as carriers of antimicrobial peptides–effects of peptide pegylation. *Colloids Surf Physicochem Eng Aspects*. 2019;565:8-15.

40. Borro BC, Bohr A, Bucciarelli S, et al. Microfluidics-based self-assembly of peptide-loaded microgels: Effect of three dimensional (3D) printed micromixer design. *J Colloid Interface Sci*. 2019;538:559-568.

41. Nordström R, Nyström L, Andrén OC, et al. Membrane interactions of microgels as carriers of antimicrobial peptides. *J Colloid Interface Sci*. 2018;513:141-150.

42. Nordström R, Browning KL, Parra-Ortiz E, et al. Membrane interactions of antimicrobial peptide-loaded microgels. *J Colloid Interface Sci*. 2020;562:322-332.

43. Singh S, Datta A, Borro BC, et al. Conformational aspects of high content packing of antimicrobial peptides in polymer microgels. *ACS applied materials & interfaces*. 2017;9(46):40094-40106.

44. Kłodzińska SN, Molchanova N, Franzyk H, Hansen PR, Damborg P, Nielsen HM. Biopolymer nanogels improve antibacterial activity and safety profile of a novel lysine-based α-peptide/β-peptoid peptidomimetic. *European Journal of Pharmaceutics and Biopharmaceutics*. 2018;128:1-9.

45. Parilti R, Caprasse J, Riva R, et al. Antimicrobial peptide encapsulation and sustained release from polymer network particles prepared in supercritical carbon dioxide. *J Colloid Interface Sci*. 2018;532:112-117.

46. Nyström L, Strömstedt AA, Schmidtchen A, Malmsten M. Peptide-loaded microgels as antimicrobial and anti-inflammatory surface coatings. *Biomacromolecules*. 2018;19(8):3456-3466.

47. Li S, Dong S, Xu W, et al. Antibacterial hydrogels. *Advanced science*. 2018;5(5):1700527.

48. Keskin D, Zu G, Forson AM, Tromp L, Sjollema J, van Rijn P. Nanogels: A novel approach in antimicrobial delivery systems and antimicrobial coatings. *Bioactive materials*. 2021;6(10):3634-3657.

49. Nyström L, Malmsten M. Surface-bound microgels—From physicochemical properties to biomedical applications. *Adv Colloid Interface Sci*. 2016;238:88-104.

50. Sproul EP, Nandi S, Roosa C, Schreck L, Brown AC. Biomimetic microgels with controllable deformability improve healing outcomes. *Advanced Biosystems*. 2018;2(10):1800042.

51. Sim W, Barnard RT, Blaskovich M, Ziora ZM. Antimicrobial silver in medicinal and consumer applications: A patent review of the past decade (2007–2017). *Antibiotics*. 2018;7(4):93.

52. Cameron P, Gaiser BK, Bhandari B, Bartley PM, Katzer F, Bridle H. Silver nanoparticles decrease the viability of cryptosporidium parvum oocysts. *Appl.Environ.Microbiol.* 2016;82(2):431-437.

53. Hunt PR, Marquis BJ, Tyner KM, et al. Nanosilver suppresses growth and induces oxidative damage to DNA in caenorhabditis elegans. *Journal of Applied Toxicology*. 2013;33(10):1131-1142.

54. Sussman EM, Casey BJ, Dutta D, Dair BJ. Different cytotoxicity responses to antimicrobial nanosilver coatings when comparing extract-based and direct-contact assays. *Journal of Applied Toxicology*. 2015;35(6):631-639.

55. Hadrup N, Loeschner K, Bergström A, et al. Subacute oral toxicity investigation of nanoparticulate and ionic silver in rats. *Arch Toxicol*. 2012;86(4):543-551.

56. Rajendran NK, Kumar SSD, Houreld NN, Abrahamse H. A review on nanoparticle based treatment for wound healing. *Journal of Drug Delivery Science and Technology*. 2018;44:421-430.

57. Liu M, Liu T, Chen X, et al. Nano-silver-incorporated biomimetic polydopamine coating on a thermoplastic polyurethane porous nanocomposite as an efficient antibacterial wound dressing. *Journal of nanobiotechnology*. 2018;16(1):89.

58. Papi M, Palmieri V, Bugli F, et al. Biomimetic antimicrobial cloak by graphene-oxide agar hydrogel. *Scientific reports*. 2016;6(1):12.

59. Wu K, Yang Y, Zhang Y, Deng J, Lin C. Antimicrobial activity and cytocompatibility of silver nanoparticles coated catheters via a biomimetic surface functionalization strategy. *International journal of nanomedicine*. 2015;10:7241.

60. Han D, Zhang QM, Serpe MJ. Poly (N-isopropylacrylamide)-co-(acrylic acid) microgel/ag nanoparticle hybrids for the colorimetric sensing of H 2 O 2. *Nanoscale*. 2015;7(6):2784-2789.

61. Mohamed MM, Fouad SA, Elshoky HA, Mohammed GM, Salaheldin TA. Antibacterial effect of gold nanoparticles against corynebacterium pseudotuberculosis. *International journal of veterinary science and medicine*. 2017;5(1):23-29.

62. Sproul EP, Hannan R, Brown AC. Characterization of fibrin-based constructs for tissue engineering. In: Chawla K, ed. *Biomaterials for tissue engineering.* Springer; 2018:85-99.

63. Nellenbach K, Guzzetta NA, Brown AC. Analysis of the structural and mechanical effects of procoagulant agents on neonatal fibrin networks following cardiopulmonary bypass. *Journal of Thrombosis and Haemostasis*. 2018;16(11):2159-2167.

64. Dunn L, Prosser HC, Tan JT, Vanags LZ, Ng MK, Bursill CA. Murine model of wound healing. *JoVE (Journal of Visualized Experiments)*. 2013(75):e50265.

65. Schafer KA, Eighmy J, Fikes JD, et al. Use of severity grades to characterize histopathologic changes. *Toxicol Pathol*. 2018;46(3):256-265.

66. Joshi A, Nandi S, Chester D, Brown AC, Muller M. Study of poly (n-isopropylacrylamide-co-acrylic acid)(pnipam) microgel particle induced deformations of tissue-mimicking phantom by ultrasound stimulation. *Langmuir*. 2018;34(4):1457-1465.

67. Bachman H, Brown AC, Clarke KC, et al. Ultrasoft, highly deformable microgels. *Soft Matter*. 2015;11(10):2018-2028.

68. National diabetes statistics report. Centers for Disease Control and Prevention Web site. https://www.cdc.gov/diabetes/data/statistics/statistics-report.html. Updated 2020. Accessed Jun 9, 2020.

69. Nandi S, Brown AC. Platelet-mimetic strategies for modulating the wound environment and inflammatory responses. *Exp Biol Med*. 2016;241(10):1138-1148.

70. Smith MH, South AB, Gaulding JC, Lyon LA. Monitoring the erosion of hydrolytically-degradable nanogels via multiangle light scattering coupled to asymmetrical flow field-flow fractionation. *Anal Chem*. 2009;82(2):523-530.

71. Clarke KC, Dunham SN, Lyon LA. Core/shell microgels decouple the pH and temperature responsivities of microgel films. *Chemistry of Materials*. 2015;27(4):1391-1396.

72. Gaulding JC, South AB, Lyon LA. Hydrolytically degradable shells on thermoresponsive microgels. *Colloid Polym Sci*. 2013;291(1):99-107.

73. South AB, Lyon LA. Direct observation of microgel erosion via in-liquid atomic force microscopy. *Chemistry of Materials*. 2010;22(10):3300-3306.

74. Du H, Li C, Luan Y, et al. An antithrombotic hydrogel with thrombin-responsive fibrinolytic activity: Breaking down the clot as it forms. *Materials Horizons*. 2016;3(6):556-562.

75. Gupta AS, Girish A, Jolly K, et al. Intravenous nanomedicine for targeted delivery of thrombin to augment hemostasis. *Blood*. 2021;138:1029.

76. Gunawan C, Marquis CP, Amal R, Sotiriou GA, Rice SA, Harry EJ. Widespread and indiscriminate nanosilver use: Genuine potential for microbial resistance. *ACS nano*. 2017;11(4):3438-3445.

77. Naseem K, Begum R, Farooqi ZH, Wu W, Irfan A. Core-shell microgel stabilized silver nanoparticles for catalytic reduction of aryl nitro compounds. *Applied Organometallic Chemistry*. 2020;34(9):e5742.

78. Begum R, Farooqi ZH, Aboo AH, Ahmed E, Sharif A, Xiao J. Reduction of nitroarenes catalyzed by microgel-stabilized silver nanoparticles. *J Hazard Mater*. 2019;377:399-408.

79. Farooqi ZH, Begum R, Naseem K, et al. Fabrication of silver nanoparticles in pH responsive polymer microgel dispersion for catalytic reduction of nitrobenzene in aqueous medium. *Russian Journal of Physical Chemistry A*. 2016;90(13):2600-2608.

80. Brändel T, Sabadasch V, Hannappel Y, Hellweg T. Improved smart microgel carriers for catalytic silver nanoparticles. *ACS omega*. 2019;4(3):4636-4649.

81. Gaharwar AK, Avery RK, Assmann A, et al. Shear-thinning nanocomposite hydrogels for the treatment of hemorrhage. *ACS nano*. 2014;8(10):9833-9842.

82. Komatsu S, Nagai Y, Naruse K, Kimata Y. The neutral self-assembling peptide hydrogel SPG-178 as a topical hemostatic agent. *PLoS one*. 2014;9(7):e102778.

83. Li Y, Wang X, Fu Y, Wei Y, Zhao L, Tao L. Self-adapting hydrogel to improve the therapeutic effect in wound-healing. *ACS applied materials & interfaces*. 2018;10(31):26046-26055.

84. Banihashemi M, Safari A, Nezafat N, et al. Effect of fibrin packing on managing hepatic hemorrhage and liver wound healing in a model of liver stab wound in rat. *Bulletin of Emergency & Trauma*. 2017;5(1):18.

85. Paydar S, Nezhad GSM, Karami MY, et al. Stereological comparison of imbibed fibrinogen gauze versus simple gauze in external packing of grade IV liver injury in rats. *Bulletin of Emergency & Trauma*. 2019;7(1):41.

86. Dyer M, Haldeman S, Gutierrez A, Kohut L, Gupta AS, Neal MD. Uncontrolled hemorrhagic shock modeled via liver laceration in mice with real time hemodynamic monitoring. *JoVE (Journal of Visualized Experiments)*. 2017(123):e55554.

87. Nandi S, Brown AC. Characterizing cell migration within three-dimensional in vitro wound environments. *JoVE (Journal of Visualized Experiments)*. 2017(126):e56099.

88. Ligon BL. Penicillin: Its discovery and early development. . 2004;15(1):52-57.

89. Chaplin DD. Overview of the immune response. *J Allergy Clin Immunol*. 2010;125(2):S3-S23.

90. Ergene C, Yasuhara K, Palermo EF. Biomimetic antimicrobial polymers: Recent advances in molecular design. *Polymer Chemistry*. 2018;9(18):2407-2427.

91. Ganesh SD, Saha N, Zandraa O, Zuckermann RN, Sáha P. Peptoids and polypeptoids: Biomimetic and bioinspired materials for biomedical applications. *Polymer Bulletin*. 2017;74(8):3455-3466.

92. Wang J, Vermerris W. Antimicrobial nanomaterials derived from natural products—A review. *Materials*. 2016;9(4):255.

93. Espina L, Pagán R, López D, García-Gonzalo D. Individual constituents from essential oils inhibit biofilm mass production by multi-drug resistant staphylococcus aureus. *Molecules*. 2015;20(6):11357-11372.

94. Hassan M, Kjos M, Nes IF, Diep DB, Lotfipour F. Natural antimicrobial peptides from bacteria: Characteristics and potential applications to fight against antibiotic resistance. *J Appl Microbiol*. 2012;113(4):723-736.

95. Anitua E, Aguirre JJ, Algorta J, et al. Effectiveness of autologous preparation rich in growth factors for the treatment of chronic cutaneous ulcers. *Journal of Biomedical Materials Research Part B: Applied Biomaterials: An Official Journal of The Society for Biomaterials, The Japanese Society for Biomaterials, and The Australian Society for Biomaterials and the Korean Society for Biomaterials*. 2008;84(2):415-421.

96. Driver VR, Hanft J, Fylling CP, Beriou JM. A prospective, randomized, controlled trial of autologous platelet-rich plasma gel for the treatment of diabetic foot ulcers. *Ostomy Wound Management*. 2006;52(6):68.

97. Elbourne A, Crawford RJ, Ivanova EP. Nano-structured antimicrobial surfaces: From nature to synthetic analogues. *J Colloid Interface Sci*. 2017;508:603-616.

98. Michalska M, Gambacorta F, Divan R, et al. Tuning antimicrobial properties of biomimetic nanopatterned surfaces. *Nanoscale*. 2018;10(14):6639-6650.

99. Sakamoto A, Terui Y, Horie C, et al. Antibacterial effects of protruding and recessed shark skin micropatterned surfaces of polyacrylate plate with a shallow groove. *FEMS Microbiol Lett*. 2014;361(1):10-16.

100. Pogodin S, Hasan J, Baulin VA, et al. Biophysical model of bacterial cell interactions with nanopatterned cicada wing surfaces. *Biophys J*. 2013;104(4):835-840.

101. Bazaka K, Jacob MV, Chrzanowski W, Ostrikov K. Anti-bacterial surfaces: Natural agents, mechanisms of action, and plasma surface modification. *Rsc Advances*. 2015;5(60):48739-48759.

102. Reddy ST, Chung KK, McDaniel CJ, Darouiche RO, Landman J, Brennan AB. Micropatterned surfaces for reducing the risk of catheter-associated urinary tract infection: An in vitro study on the effect of sharklet micropatterned surfaces to inhibit bacterial colonization and migration of uropathogenic escherichia coli. *Journal of endourology*. 2011;25(9):1547-1552.

103. Chung KK, Schumacher JF, Sampson EM, Burne RA, Antonelli PJ, Brennan AB. Impact of engineered surface microtopography on biofilm formation of staphylococcus aureus. *Biointerphases*. 2007;2(2):89-94.

104. Efimenko K, Finlay J, Callow ME, Callow JA, Genzer J. Development and testing of hierarchically wrinkled coatings for marine antifouling. *ACS applied materials & interfaces*. 2009;1(5):1031-1040.

105. Kung M, Lin P, Peng S, et al. Biomimetic polymer-based ag nanocomposites as a antimicrobial platform. *Applied Materials Today*. 2016;4:31-39.

106. GhavamiNejad A, Park CH, Kim CS. In situ synthesis of antimicrobial silver nanoparticles within antifouling zwitterionic hydrogels by catecholic redox chemistry for wound healing application. *Biomacromolecules*. 2016;17(3):1213-1223.

107. Wang R, Li J, Chen W, et al. A biomimetic Mussel-Inspired ε-Poly-l-lysine hydrogel with robust Tissue-Anchor and Anti-Infection capacity. *Advanced Functional Materials*. 2017;27(8):1604894.

108. Meng H, Forooshani PK, Joshi PU, et al. Biomimetic recyclable microgels for on-demand generation of hydrogen peroxide and antipathogenic application. *Acta biomaterialia*. 2019;83:109-118.

109. Cheng D, He M, Li W, et al. Hydrothermal growing of cluster-like ZnO nanoparticles without crystal seeding on PET films via dopamine anchor. *Appl Surf Sci*. 2019;467:534-542.

110. McDonnell G. The use of hydrogen peroxide for disinfection and sterilization applications. *PATAI'S Chemistry of Functional Groups*. 2009:1-34.

111. Nadagouda MN, Varma RS. Green synthesis of silver and palladium nanoparticles at room temperature using coffee and tea extract. *Green Chem*. 2008;10(8):859-862.

112. Singh J, Dutta T, Kim K, Rawat M, Samddar P, Kumar P. 'Green'synthesis of metals and their oxide nanoparticles: Applications for environmental remediation. *Journal of nanobiotechnology*. 2018;16(1):84.

113. Cruz D, Falé PL, Mourato A, Vaz PD, Serralheiro ML, Lino ARL. Preparation and physicochemical characterization of ag nanoparticles biosynthesized by lippia citriodora (lemon verbena). *Colloids and Surfaces B: Biointerfaces*. 2010;81(1):67-73.

114. Njagi EC, Huang H, Stafford L, et al. Biosynthesis of iron and silver nanoparticles at room temperature using aqueous sorghum bran extracts. *Langmuir*. 2010;27(1):264-271.

115. Kahrilas GA, Wally LM, Fredrick SJ, Hiskey M, Prieto AL, Owens JE. Microwave-assisted green synthesis of silver nanoparticles using orange peel extract. *ACS Sustainable Chemistry & Engineering*. 2013;2(3):367-376.

116. Jain D, Kachhwaha S, Jain R, Srivastava G, Kothari SL. Novel microbial route to synthesize silver nanoparticles using spore crystal mixture of bacillus thuringiensis. . 2010.

117. Parikh RY, Singh S, Prasad B, Patole MS, Sastry M, Shouche YS. Extracellular synthesis of crystalline silver nanoparticles and molecular evidence of silver resistance from morganella sp.: Towards understanding biochemical synthesis mechanism. *ChemBioChem*. 2008;9(9):1415-1422.

118. Mandal D, Bolander ME, Mukhopadhyay D, Sarkar G, Mukherjee P. The use of microorganisms for the formation of metal nanoparticles and their application. *Appl Microbiol Biotechnol*. 2006;69(5):485-492.

119. Ebrahiminezhad A, Bagheri M, Taghizadeh S, Berenjian A, Ghasemi Y. Biomimetic synthesis of silver nanoparticles using microalgal secretory carbohydrates as a novel anticancer

and antimicrobial. *Advances in Natural Sciences: Nanoscience and Nanotechnology*. 2016;7(1):015018.

120. Schmidt NW, Wong GC. Antimicrobial peptides and induced membrane curvature: Geometry, coordination chemistry, and molecular engineering. *Current Opinion in Solid State and Materials Science*. 2013;17(4):151-163.

121. Yang L, Gordon VD, Trinkle DR, et al. Mechanism of a prototypical synthetic membrane-active antimicrobial: Efficient hole-punching via interaction with negative intrinsic curvature lipids. *Proceedings of the National Academy of Sciences*. 2008;105(52):20595-20600.

122. Engler AC, Wiradharma N, Ong ZY, Coady DJ, Hedrick JL, Yang Y. Emerging trends in macromolecular antimicrobials to fight multi-drug-resistant infections. *Nano Today*. 2012;7(3):201-222.

123. Hurdle JG, O'neill AJ, Chopra I, Lee RE. Targeting bacterial membrane function: An underexploited mechanism for treating persistent infections. *Nature Reviews Microbiology*. 2011;9(1):62.

124. Meng H, Kumar K. Antimicrobial activity and protease stability of peptides containing fluorinated amino acids. *J Am Chem Soc*. 2007;129(50):15615-15622.

125. Strömstedt AA, Pasupuleti M, Schmidtchen A, Malmsten M. Evaluation of strategies for improving proteolytic resistance of antimicrobial peptides by using variants of EFK17, an internal segment of LL-37. *Antimicrob Agents Chemother*. 2009;53(2):593-602.

126. Fazren Azmi, Mariusz Skwarczynski, Istvan Toth. Towards the development of synthetic antibiotics: Designs inspired by natural antimicrobial peptides. *Current Medicinal Chemistry*. 2016;23(41):4610-4624. http://www.eurekaselect.com/openurl/content.php?genre=article&issn=0929-8673&volume=23&issue=41&spage=4610. doi: 10.2174/0929867323666160825162435.

127. Xi Y, Ge J, Guo Y, Lei B, Ma PX. Biomimetic elastomeric polypeptide-based nanofibrous matrix for overcoming multidrug-resistant bacteria and enhancing full-thickness wound healing/skin regeneration. *ACS nano*. 2018;12(11):10772-10784.

128. Chen W, Chang H, Lu J, et al. Self-assembly of antimicrobial peptides on gold nanodots: Against multidrug-resistant bacteria and wound-healing application. *Advanced Functional Materials*. 2015;25(46):7189-7199.

129. Xiong M, Lee MW, Mansbach RA, et al. Helical antimicrobial polypeptides with radial amphiphilicity. *Proceedings of the National Academy of Sciences*. 2015;112(43):13155-13160.

130. Xiong M, Han Z, Song Z, et al. Bacteria-assisted activation of antimicrobial polypeptides by a random-coil to helix transition. *Angewandte Chemie International Edition*. 2017;56(36):10826-10829.

131. Xiong M, Bao Y, Xu X, et al. Selective killing of helicobacter pylori with pH-responsive helix–coil conformation transitionable antimicrobial polypeptides. *Proceedings of the National Academy of Sciences*. 2017;114(48):12675-12680.

132. Pires DP, Cleto S, Sillankorva S, Azeredo J, Lu TK. Genetically engineered phages: A review of advances over the last decade. *Microbiol.Mol.Biol.Rev.* 2016;80(3):523-543.

133. Lu TK, Koeris MS. The next generation of bacteriophage therapy. *Curr Opin Microbiol*. 2011;14(5):524-531.

134. Lu TKT, Koeris MS, Chevalier BS, Holder JW, McKenzie GJ, Brownell DR, inventorsRecombinant phage and methods. patent 9.234.227 B2. 2016.

135. Lu TK, Collins JJ. Engineered bacteriophage targeting gene networks as adjuvants for antibiotic therapy. *Proceedings of the National Academy of Sciences*. 2009;106(12):4629-4634.

136. Sanches LM, Petri DFS, de Melo Carrasco, Leticia Dias, Carmona-Ribeiro AM. The antimicrobial activity of free and immobilized poly (diallyldimethylammonium) chloride in nanoparticles of poly (methylmethacrylate). *Journal of Nanobiotechnology*. 2015;13(1):58. https://search.proquest.com/docview/1780100604. doi: 10.1186/s12951-015-0123-3.

137. Merril CR, Biswas B, Carlton R, et al. Long-circulating bacteriophage as antibacterial agents. *Proceedings of the National Academy of Sciences*. 1996;93(8):3188-3192.

138. de Melo Carrasco L, Sampaio J, Carmona-Ribeiro A. Supramolecular cationic assemblies against multidrug-resistant microorganisms: Activity and mechanism of action. *International journal of molecular sciences*. 2015;16(3):6337-6352.

139. Rosa H, Petri DF, Carmona-Ribeiro AM. Interactions between bacteriophage DNA and cationic biomimetic particles. *The Journal of Physical Chemistry B*. 2008;112(51):16422-16430.

140. Xavier G, Carmona-Ribeiro A. Cationic biomimetic particles of polystyrene/cationic bilayer/gramicidin for optimal bactericidal activity. *Nanomaterials*. 2017;7(12):422.

141. Zetterberg MM, Reijmar K, Pränting M, Engström Å, Andersson DI, Edwards K. PEG-stabilized lipid disks as carriers for amphiphilic antimicrobial peptides. *Journal of Controlled Release*. 2011;156(3):323-328. https://www.sciencedirect.com/science/article/pii/S0168365911006419. doi: 10.1016/j.jconrel.2011.08.029.

142. Torchilin V. *Handbook of nanobiomedical research: Fundamentals, applications, and recent developments.* Vol 3. World scientific; 2014.

143. Carmona-Ribeiro A. Self-assembled antimicrobial nanomaterials. *International journal of environmental research and public health*. 2018;15(7):1408.

144. Magesh G, Bhoopathi G, Nithya N, Arun AP, Kumar ER. Tuning effect of polysaccharide chitosan on structural, morphological, optical and photoluminescence properties of ZnO nanoparticles. *Superlattices and Microstructures*. 2018;117:36-45.

145. Sanyasi S, Majhi RK, Kumar S, et al. Polysaccharide-capped silver nanoparticles inhibit biofilm formation and eliminate multi-drug-resistant bacteria by disrupting bacterial cytoskeleton with reduced cytotoxicity towards mammalian cells. *Scientific reports*. 2016;6:24929.

146. Emberger M, Koller J, Laimer M, et al. Original article. *Journal of the European Academy of Dermatology and Venereology*. 2011;25(2):227-231.

https://onlinelibrary.wiley.com/doi/abs/10.1111/j.1468-3083.2010.03766.x. doi: 10.1111/j.1468-3083.2010.03766.x.

147. Ryge TS, Frimodt-Møller N, Hansen PR. Antimicrobial activities of twenty lysine-peptoid hybrids against clinically relevant bacteria and fungi. *Chemotherapy*. 2008;54(2):152-156. https://www.karger.com/Article/Abstract/119707. doi: 10.1159/000119707.

148. Molchanova N, Hansen PR, Damborg P, Nielsen HM, Franzyk H. Lysine-Based α-Peptide/β-Peptoid peptidomimetics: Influence of hydrophobicity, fluorination, and distribution of cationic charge on antimicrobial activity and cytotoxicity. *ChemMedChem*. 2017;12(4):312-318. https://onlinelibrary.wiley.com/doi/abs/10.1002/cmdc.201600553. doi: 10.1002/cmdc.201600553.

149. Sen Gupta A. Bio-inspired nanomedicine strategies for artificial blood components. *Wiley Interdisciplinary Reviews: Nanomedicine and Nanobiotechnology*. 2017;9(6):e1464.

150. Molinaro R, Corbo C, Martinez JO, et al. Biomimetic proteolipid vesicles for targeting inflamed tissues. *Nature materials*. 2016;15(9):1037.

151. Hammer DA, Robbins GP, Haun JB, et al. Leuko-polymersomes. *Faraday Discuss*. 2008;139:129-141.

152. Parodi A, Quattrocchi N, Van De Ven, Anne L, et al. Synthetic nanoparticles functionalized with biomimetic leukocyte membranes possess cell-like functions. *Nature nanotechnology*. 2013;8(1):61.

153. Fang RH, Zhang L. Biomimetic nanosponges as a broad-spectrum countermeasure to biological threats. *Journal of the Homeland Defense and Security Information Analysis Center*. 2019;6(3):14-19.

154. Hu CJ, Fang RH, Copp J, Luk BT, Zhang L. A biomimetic nanosponge that absorbs pore-forming toxins. *Nature nanotechnology*. 2013;8(5):336.

155. Ivanova, Vladimir Baulin Vy T. H. Pham Vi Khanh Truong Anna Orlowska Shahram Ghanaati Mike Barbeck Patrick Booms Alex J. Fulcher Chris M. Bhadra Ric¿ardas Buividas C. James Kirkpatrick Pauline Doran David E. Mainwaring Saulius Juodkazis Russell J. Crawford Elena P. Race for the surface: Eukaryotic cells can win. . 2016. https://www.openaire.eu/search/publication?articleId=od_____3351::649f2cf1b00afc194778802d7892b893.

156. Jha AK, Prasad K, Kumar V, Prasad K. Biosynthesis of silver nanoparticles using eclipta leaf. *Biotechnology Progress*. 2009;25(5):1476-1479. https://onlinelibrary.wiley.com/doi/abs/10.1002/btpr.233. doi: 10.1002/btpr.233.

157. von Woedtke T, Jülich W-, Hartmann V, Stieber M, Abel PU. Sterilization of enzyme glucose sensors: Problems and concepts. *Biosensors and Bioelectronics*. 2002;17(5):373-382. https://www.sciencedirect.com/science/article/pii/S0956566301003104. doi: 10.1016/S0956-5663(01)00310-4.

158. Li Z, Ding Y, Li S, Jiang Y, Liu Z, Ge J. Highly active, stable and self-antimicrobial enzyme catalysts prepared by biomimetic mineralization of copper hydroxysulfate. *Nanoscale*. 2016;8(40):17440-17445.

APPENDICES

APPENDIX A

Detailed Experimental Protocols

A.1 Synthesis of Nanosilver Composite Ultralow Crosslinking Microgels (Ag-ULCs)

This protocol was developed in collaboration with Erin Sproul, PhD and modified from Liu et al (2012) [30]. The objective of this protocol is to combine ultralow crosslinked pNIPAm microgels (ULCs) with antimicrobial nanosilver in a covalent reaction to create nanosilver composite ULCs (Ag-ULCs).

A.1.1 Materials

Materials needed to successfully conduct this synthesis are as follows:

- Purified pNIPAm ULCs (3.5 mg/mL)
- Silver Nitrate ($AgNO_3$), MW 196.87 g/mol, purity 99.8%
- Sodium borohydride ($NaBH_4$), MW 37.83 g/mol, purity 95%
- Ultrapure water

A.1.2 Procedure Details

1. Stir 100 mL of 3.5 mg/mL ULCs in ultrapure water in a clean and dry Erlenmeyer flask at 450 rpm and purge with nitrogen
2. Add 0.05 g $AgNO_3$ and continue to stir under nitrogen for at least 30 minutes at room temperature.
    a. Volume needed calculated from 100 mM stock of $AgNO_3$
3. Measure 0.15 g $NaBH_4$ and suspend in water
    a. Note: NaBH4: 0.16 M Solution Prep
        i. Prepare IMMEDIATELY before use - NaBH4 has very low lifetime in H2O

ii. Scaling calculation: x mg*(5 mL H2O/30 mg) = x/6 mL H2O

iii. To measure:

1. Pre-weigh holding tube
2. Inside glove box, obtain NaBH4 and place into holding tube
3. Weigh tube afterwards and determine NABH4 weight and scale H2O as needed

4. Add the NaBH4 to the reaction mixture and stir 10 minutes.
    a. The reaction should occur immediately and change the solution color to brown
5. Split the resulting brown dispersion into centrifuge tubes and add an equal amount of ultrapure water to each
6. Centrifuge at 3700x g for 20 minutes.
7. Remove supernatant and wash
8. Repeat steps 6-7 for 3 total washes
9. Resuspend in 70 mL of 2 mM sodium citrate to create 5 mg/mL solution

A.2 Synthesis of Thrombin-sensitive Nanogels (TSNs)

This objective of this protocol is to fabricate TSNs, which consist of NIPMAM crosslinked with a thrombin-cleavable peptide sequence. This protocol was adapted from a combination of established microgel synthesis methods and work by Du et. al [74]

A.2.1 Materials:

Reagents needed to successfully conduct this synthesis are as follows:

- NIPMAM, 85% of 140 mM monomer concentration
- Thrombin-cleavable Peptide (>95% purity), 5% of 140 mM monomer concentration

- TEMED, 95 mM final concentration
- APS, 125 mM final concentration
- Acrylic Acid (AAc), 10% of 140 mM monomer concentration
- Note: Reagent amounts are variable depending on total reaction volume.

A.2.2 Detailed Procedure:

1. Dissolve NIPMAM into ultrapure water and incubate with TEMED. Dissolve thrombin-cleavable peptide into ultrapure water.
    a. Note: Make sure to reconstitute thrombin-cleavable peptide in DMSO beforehand
2. Add enough water to desired total reaction volume
3. Add to reaction vessel with stirbar and allow to stir at 450 rpm under nitrogen purge for 1 hour at room temperature
4. 10 minutes before initiation, add AAc.
5. Add APS and allow to react for 24 hours at room temperature.
6. Purification achieved by dialysis in 1000 kDa tubing over 72 hours in ultrapure water followed by lyophilization.
7. Resuspend at desired working concentration in ultrapure water.

APPENDIX B

Supplemental Nanosilver Composite Platelet-like Particle (Ag-PLP) Studies

B.1 *In vitro* Optimization of Ag-PLP Dose

In these studies, an optimal dosage of Ag-PLPs was assayed. To achieve this, cell spheroids were seeded into a clot sandwich and allowed to proliferate and migrate. After 3 days, area of cell spread was measured.

B.1.1 Methods and Materials

This experiment was conducted as described by Nandi et al with clot compositions of 2 mg/mL fibrin, 10% volume HEPES, 0.1 U/mL thrombin and differing concentrations of particle treatments (0.25 mg/ml and 0.5 mg/mL). [87] Particle treatments used for this study are ULCs, Ag-ULCs (Ag), 7% BIS microgels (7% BIS) and their PLP counterparts ULC-PLP (ULC + AB), Ag-PLP (Ag + AB), and 7% BIS-PLP (7% BIS + AB). HDFn cells were used at passages 10-12 and groups were cultured in triplicate. Cell spread area was measured using ImageJ., with a % change of area calculated with using day 0 as comparison reference. Statistical analysis was conducted in GraphPad Prism with 2-way ANOVA.

B.1.2. Results

Overall, an inhibitory effect on cell migration is observed with ULC-PLPs (ULC + AB) and Ag-PLP (Ag + AB) groups when particle treatment concentration is 0.5 mg/mL and an enhanced effect on cell migration is observed for ULC-PLPs and Ag-PLPs when particle treatment concentration is 0.25 mg/mL. For 0.5 mg/mL data, the only statistical differences observed were at t=24 hrs when comparing ULCs to 7% BIS and Ag-ULCs (Ag) to 7% BIS. For 0.25 mg/mL data, no statistically significant differences are detected until t = 24 hrs when comparing ULC-PLPs to Ag-ULCs. At t= 48 hrs, statistically significant differences were

observed when comparing ULC-PLPs to ULCs, Ag-ULCs and 7% BIS and when comparing Ag-PLPs to Ag-ULCs. At t=72 hrs, statistically significant differences are observed when comparing ULC-PLPs to ULCs,7% BIS, Ag-ULCs, and Ag-PLPs, and Ag-PLPs to ULCs, Ag-ULCs, 7% BIS and 7% BIS-PLPs. (**Figure B.1)**

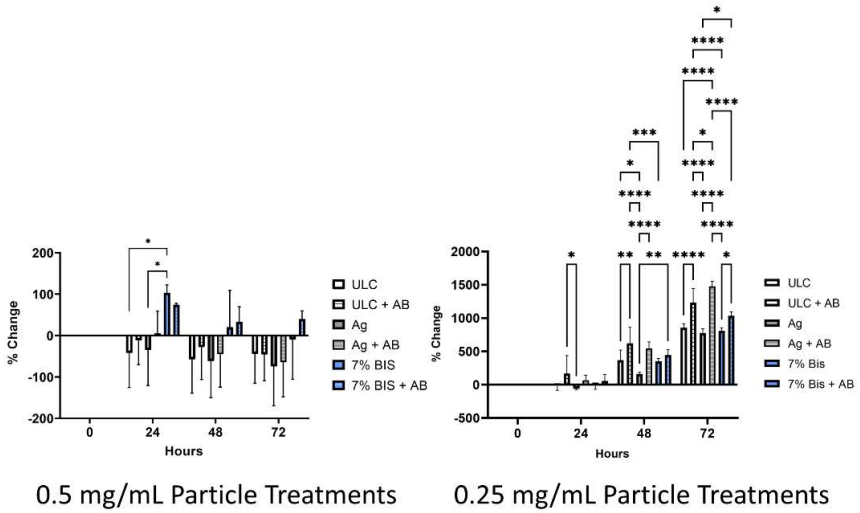

Figure B.1: Average % Change over the course of 72 hours since spheroid seeding. When particle concentration is 0.5 mg/mL, an inhibitory effect is observed with ULC-PLP (ULC + AB) and Ag-PLP (Ag + AB) groups, although this is concentration we have determined as optimal in previous studies. When the particle concentration is 0.25 mg/mL, instead, we observe the expected enhanced cell migration area increase in ULC-PLP (ULC + AB) and Ag-PLP (Ag + AB) groups. n=3-5 spheroids per group. * = $p \leq 0.05$, ** = $p \leq 0.01$, *** = $p \leq 0.001$, **** = $p \leq 0.0001$

B.2 Evaluation of Cytotoxicity of Ag-ULCs

Although nanosilver is known to be well-tolerated by eukaryotic cells [56], the production methods are considered harsh on eukaryotic cells and may leave residual harsh reagents [26]. Thus, these studies were conducted to determine *in vitro* cytotoxicity of Ag-ULCs on human dermal

fibroblasts (HdFn). Because the antimicrobial mechanism of nanometal is contact based, cells were cultured on top of films made of Ag-ULCs.

B.2.1 Methods and Materials

15 mm circle cover glass was cleaned by sonication in a series of solution for 10 minutes per solution. The solution order is as follows: alconox, de-ionized water, acetone, 200 proof ethanol, isopropanol. The cover glass was then allowed to air dry. To create microgel films, each cover glass is functionalized by 1% APTMS in EtOH and shaken for 2 hours in a 12 well plate. Then, the cover glass is washed 3 times. From there, 0.1 mg/mL microgel solutions are deposited into the plate and then centrifuged at 3700 rpm at 4° C for 10 minutes with a final wash. The films are then allowed to air dry until use.

Prior to use with cells, the films are rehydrated and then soaked in 20% ethanol for 30 minutes and then washed and immediately aspirated 3 times with water. The films are then allowed to soak in water once more to extract any residual ethanol. To promote cell adhesion, the films are then collagen coated at a density of 10 μg/cm^2 and allowed to sit at 37° C in an incubator for 3-4 hours or overnight at 4° C. The following day, HdFn is then seeded at 20k cells/ mL into each well, incubated for 24 hours and then live/dead stained. A negative control group was included and consisted of cells incubated in the presence of 70% ethanol in the media. Images were taken on an EVOS Auto FL at 10x magnification. Cells were counted manually and each group was cultured in triplicate. Statistical analysis was conducted in GraphPad Prism with 2-way ANOVA and Tukey's multiple comparisons test.

B.2.2 Results

No statistically significant differences were detected between the positive control, ULC and Ag-ULC groups. Additionally, no statistically significant difference between ULCs and Ag-

ULCs were detected. Statistically significant differences were detected in comparisons between the negative control and all other groups. These results indicate that Ag-ULCs do not result in significant cytotoxicity.

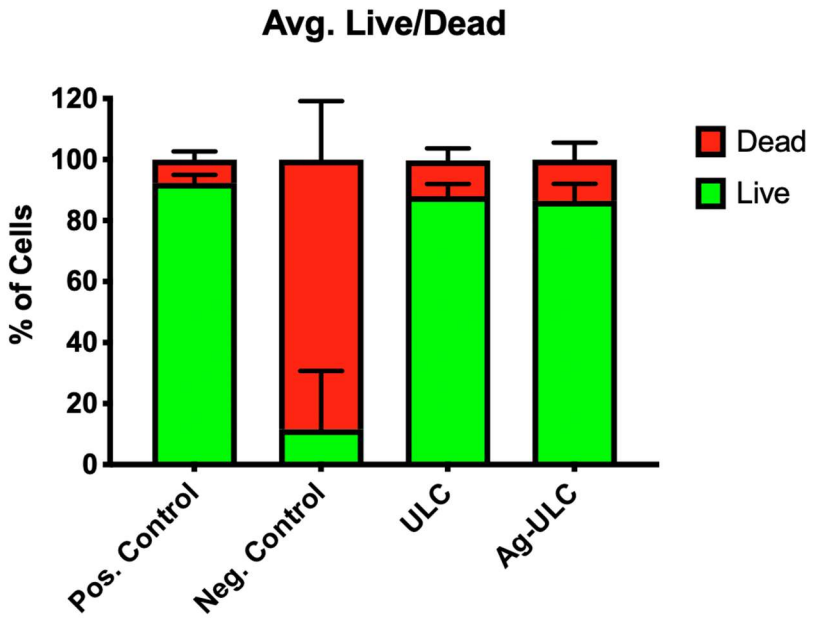

Figure B.2: Summary of Average Live/Dead % of cells. No statistically significant differences were detected between the positive control, ULCs, and Ag-ULCs. n=3 images per well, 3 wells per group

B.3 Preliminary Studies of Ag-ULC Storage Stability

Ag-PLPs have been demonstrated to be a promising material with hemostatic and wound healing enhancement properties. However, there remains a need to determine storage effects on the stability of the Ag-ULC body. This section presents the preliminary findings of these studies.

B.3.1 Materials and Methods

Ag-ULCs were stored at varying temperatures (4° C and 25° C) and in different forms (lyophilized and fluid) over the course of 1 month and aliquoted at the following time points: t= 0, 2 weeks, and 1 month. Aliquots were then analyzed for particle deformability by AFM.

To prepare samples for AFM imaging, cover glass was first cleaned by sonication and then functionalized by APTMS as described in Appendix B.2.1. Ag-ULC solution concentrations were 0.01 mg/mL, 0.004 mg/mL, and 0.002 mg/mL. The samples were then allowed to air dry. Air topography imaging was conducted on a MFP 3D Bio AFM (Asylum). Particle diameter and height were then measured by height trace on ImageJ for at least 27 particles per sample. Statistical analysis was conducted on GraphPad Prism with one-way ANOVA comparisons and Tukey's multiple comparisons test.

B.3.2 Results

Statistically significant differences were detected in particle diameter between Ag-ULCs stored in fluid at t=1 mo compared with all other time points. No statistically significant differences in average particle height were detected. Although a statistically significant difference is detected at =1 mo for Ag-ULCs stored in fluid, it is notable that it is for an increased diameter, indicating increased particle deformability.

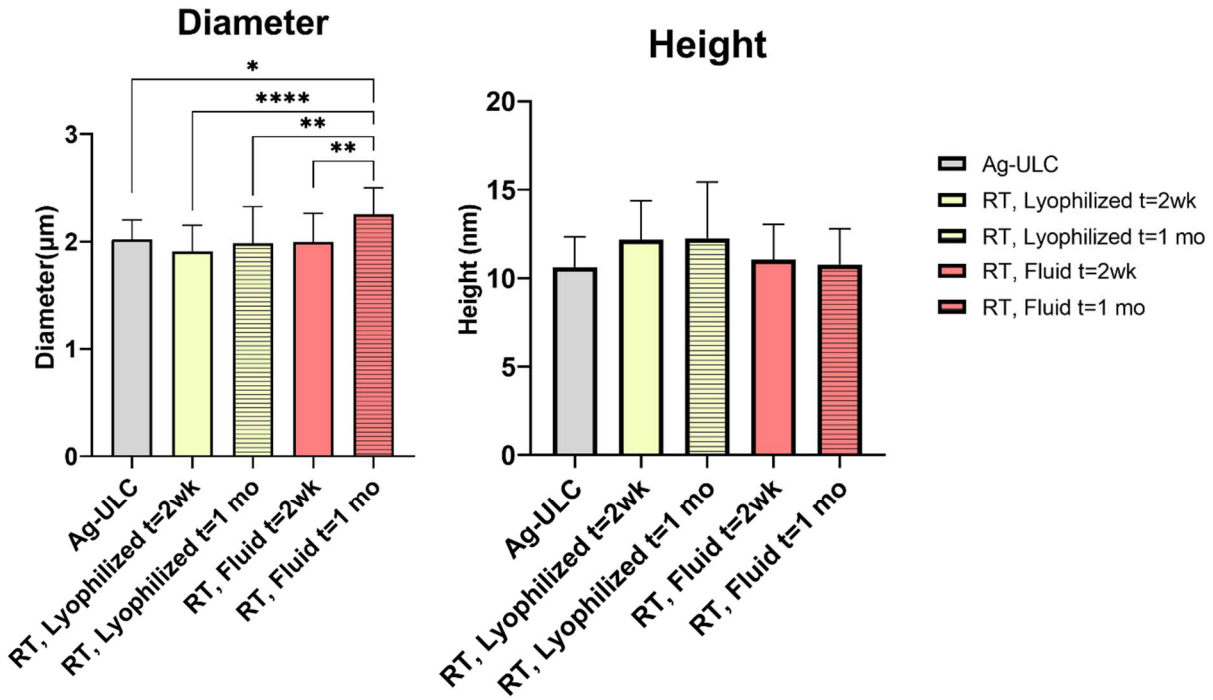

Figure B.3: Average particle dry diameter and heights. No statistically significant differences were detected for heights. Statistically significantly higher diameter was detected for Ag-ULCs stored as a fluid at room temperature compared to all other samples. n= 27-30 microgels. * = $p \leq 0.05$, ** = $p \leq 0.01$, **** = $p \leq 0.0001$

APPENDIX C

Biomimetic Antimicrobial Material Strategies for Combating Antibiotic Resistant Bacteria

This appendix is a literature review published on biomimetic antimicrobial material strategies used to combat antibiotic resistant bacteria. The work described in this appendix is already published in *Biomaterials Science:* Chee, E., & Brown, A. C. (2020). Biomimetic antimicrobial material strategies for combating antibiotic resistant bacteria. Biomaterials Science, 8(4), 1089-1100.

C.1 Introduction

The discovery of the antibiotic penicillin by Alexander Fleming in 1928 has long revolutionized the field of medicine [88] . However, continued use of penicillin, and similar antibiotic drugs, have led to the rise of strains of antibiotic resistant bacteria, which has since motivated the need for alternative treatments. According to the Centers for Disease Control (CDC), antibiotic resistant bacteria affect at least 2 million individuals annually in total[2]. In particular, high threat antibiotic strains exist across several species. Most notably, there exists Methicillin-resistant *Staphylococcus aureus* (also known as MRSA), leading to approximately 80,000 infections annually, and drug-resistant *Streptococcus pneumoniae*, leading to approximately 1.2 million infections annually [25]. These antibiotic resistant bacteria can greatly worsen prognosis for patients for whom bacterial infection is a high-risk factor, such as those with chronic injuries, burns, or compromised immune systems.

In the human body, bacterial infections are fought off by the immune system. In particular, neutrophils, monocytes and macrophages are key in fighting off bacterial

pathogens as these three cell types are those most involved in phagocytosis and ultimately clearing the body of said pathogens [89]. Additionally, immune cell responses can be augmented by platelets. During the immune response, platelets will change expression of signaling molecules that direct neutrophil and monocyte behavior to form aggregates consisting of platelets, neutrophils, and monocytes. In turn, this process activates the neutrophils and monocytes towards responding to invasion by bacteria. Furthermore, platelets themselves are able to bind to bacteria and release antimicrobial substances [3]. Because these mechanisms are already functional under *in vivo* conditions, biomimetic methods for recapitulating such behavior has been very attractive as a means of designing new strategies for fighting off antibiotic resistant bacteria. Thus, researchers have explored incorporation of these antimicrobial mechanisms in order to combat antibiotic resistant bacteria for a multitude of applications.

Commonly used strategies to combat antibiotic resistant bacteria include molecular based strategies, biopolymers, micro-organisms and materials derived from naturally antimicrobial substances such as platelet-rich plasma (PRP) [56,90-92]. These strategies are summarized in **Table C.1**. Molecular based strategies are focused around functionalizing materials with molecular substances that are antimicrobial. Notable materials within this field include antimicrobial peptides (AMP) and nanometal particles (including gold, silver, and zinc oxide) [56]. Biopolymer strategies are based around functionalizing polymeric materials towards antimicrobial activity. Notable antimicrobial strategies include molecular structure modifications, incorporation of leukocyte migration inducing materials, and incorporation of antimicrobial substances [92]. Antimicrobial derived substances are based around incorporating the use of biologically natural antimicrobial

substances. Notable within this field are platelet rich plasma (PRP) and essential oil-incorporated materials. [29,93] Bacteriophages are also a notable strategy for combatting bacterial infection due to their high efficiency in killing bacteria [28] .

While these strategies have shown great potential for antimicrobial efficacy, modifications of synthesis methods, molecular structure, or antimicrobial range could potentially improve efficacy, delivery profiles, and associated toxicity. Some molecular strategies are often associated with difficult or time-intensive synthesis means and, in the case of nanometals, harmful components that may still remain in residual amounts. Strategies based around antimicrobial peptides also face issues with ensuring that peptides are not broken down until delivery to intended treatment sites [94]. Polymeric-based strategies can face similar issues depending on the synthesis methods (e.g.: residual presence of harsh organic solvents). For derived substances, there are issues with means of supply of raw materials and consistent processing. For example, PRP relies on a patient source, which can face regulatory barriers and donor shortages. Furthermore, while PRP has shown potential for antimicrobial applications, Fernandez-Moure has reported that clinical trials utilizing PRP have reported varying levels of antimicrobial efficacy and even recurrence of infections in certain applications (e.g: chronic injury treatment) [1,95,96]. Additionally, essential oils, while reported to have components that are antimicrobial against bacteria strains like MRSA, also require some fabrication precautions to prevent essential oil droplets from forming masses during incorporation into other materials [92] .

In this review, we discuss current biomimetic antimicrobial strategies including surface mimicry, biomimetic functionalization of existing strategies, and biomimetic assemblies. The strategies discussed in this review are summarized in **Table C.2**. Surface

mimicry consists of strategies based around mimicking the structure of known naturally antimicrobial surfaces such as cicada wing and crab carapace. Biomimetic functionalization of existing strategies consists of the use of biomimetic materials to enhance existing antimicrobial strategies. In particular, these strategies seek to modify existing approaches in order to reduce cytotoxicity, improve delivery profile, and to improve antimicrobial efficacy. As an example, nanometal cytotoxicity can be reduced by using reduction reactions mimetic of chemical processes in microorganisms and plants. Biomimetic assemblies consist of antimicrobial materials that have been constructed into assemblies with other components, such as leukocyte mimetic materials that consist of polymeric particles enclosed with leukocyte membranes. Due to this structure, the resulting assembly can result in better targeted delivery towards sites of infection by mimicking leukocyte targeting mechanisms. These biomimetic methods present potential for versatile solutions for combatting infection by antibiotic resistant bacteria across a wide range of applications and treatment delivery means.

Table C.1 Overview of Current Antimicrobial Material Strategies

Category	*Strategy*	*Description*	*Pros*	*Cons*	*References*
Molecular	Nanometal	Creation of nanosized particles of metal and metal oxides.	-Wide range of affected bacteria -Less toxic than bulk antimicrobial metal	-Has varying dose-dependent cytotoxic effects. -Synthesis process can result in toxic byproducts.	56
	Antimicrobial peptides (AMPs)	Creation of AMPs for combat against drug resistant bacteria	-Capable of targeting drug resistant bacteria -Based on peptides naturally produced in animals	-High toxicity -Low in vivo efficacy -Difficult to scale up	56, 91
	Bacteriophages	Viruses capable of selectively killing bacteria	-Low toxicity -Targeting does not overlap with antibiotic drugs	-Can become resisted by bacteria -Narrow range of effect	27, 28, 133, 134
Biopolymers	Molecular structure modification	Polymers designed with molecular structure that is mimetic of AMPs	-Allows for tunable polymer with antimicrobial activity -Has potential for efficient scale-up of peptides	-Heterogeneity of chain length and copolymerization -Antimicrobial capability and toxicity dependent on amphiphilic balance	90
	Inclusion of pro-leukocyte migratory materials	Polymers including materials that encourage the migration of leukocytes at implantation sites.	-Directs local immune system cells towards sites of infection	-Requires specific molecular structure or substances	92
	Inclusion of antimicrobial materials	Polymeric materials incorporated with antimicrobial materials such as AMPs and nanometals	-Allows for delivery of antimicrobial materials on both macro- and micro-scales -Allows for tunable construction with nanofiber production methods	-Associated disadvantages of incorporated materials (e.g.: cytotoxicity of nanometals, solvent residues) -May reduce antimicrobial activity (e.g.: AMP nanofiber production)	56, 92
Antimicrobial Derived Substances	Platelet rich plasma (PRP)	The use of PRP towards treating infected sites while enhancing tissue regeneration	-Autologous treatment -Has seen use in clinical trials	-Varying efficacy -Potential regulatory barriers	1, 29, 95, 96
	Essential oils	Incorporation of extracts from plants into materials for antimicrobial function	-Easy to obtain synthesis materials	-Requires specific fabrication set up to prevent oil aggregation during incorporation into materials	93

Table C.2 Overview of Antimicrobial Biomimetic Strategies

Category	*Strategy*	*Description*	*Pros*	*Cons*	*References*
Surface Mimicry	Nanopillars	Patterning of surfaces with nanopillars; mimicking the surface geometry of insect wings	-Mechanical mechanism -Translatable across materials	-Requires optimization of surface geometry with regards to pillar length and density. -Cannot be used for applications inside the body	97, 100, 155
	Nanogrooves/wrinkles	Patterning of surfaces with nanogrooves or nanowrinkles, mimicking the surface of shark skin and crab carapace	-Mechanical mechanism -Translatable across materials	- Requires optimization of depth for nanogrooves as bacteria can settle at the bottom of grooves. -Cannot be used for applications inside the body	99, 58,102-104
Biomimetic Functionalization	Optimization of nanometal synthesis to reduce toxicity	Enhanced biocompatibility functionalization of nanometal-based strategies by use of organism mimetic molecules to reduce cytotoxicity	-Can circumvent the need for synthetic synthesis of nanometals -Dopamine based catechol structure allows for chemical versatility for in situ production	-Effectiveness of reduced cytotoxic effects dependent on incorporation means (e.g.: surface adhesion vs. copolymerization) -Does not remove inherent cytotoxicity of nanometal	57, 59, 105-119
	Antimicrobial peptide modification for improved delivery	Modification of AMP function by alternate structures (e.g.: as fibers in materials or the molecular structure itself)	-Provides alternatives to purely nanometal-based strategies -Improves stability and delivery of antimicrobial molecules such as AMPs or enzymes	-Time-intensive fabrication methods -Harsh components involved in fabrication (e.g.: solvents, radiation)	120-131
	Bacteriophages	Functionalization of bacteriophage function by genetic engineering to enhance antimicrobial ability or biocompatibility	-Can improve antimicrobial efficacy of bacteriophages -Tunable to desired functions. (e.g.: longer circulation time)	-Time-intensive production methods -Standard production methods have low yields of modified bacteriophages	27, 132-135, 137
Biomimetic Assemblies	Biomimetic assembled particles	Creation of materials by methods that mimic natural assembly of lipids into membranes, including polymers and nanometals	-Versatile in material components -Addresses issues with existing strategies such as nanometal and polymer cytotoxicity	-May not be as effective on bacteria species with thicker or less negatively charged cell walls -Antimicrobial activity may be compromised due to decreased contact area	138-144
	Antimicrobial peptide-based particles	Creation of antimicrobial peptide-based particles by assembly with membranes surrounding AMP core.	-Allows for enhanced delivery of AMP by reducing potential contact with proteases -Reduced cytotoxicity	-Antimicrobial activity limited to surface-based interactions -Reduced antimicrobial activity in comparison to free form AMP	145-147
	Cell mimetic materials	Materials designed around mimicking the function of cells capable of combating infections	-Compatible with physiological environment -Can allow for improved delivery of existing antimicrobial material strategies	-Requires significant continued investigation of function as antimicrobial delivery or efficacy of antimicrobial activity -Some methods require extraction of membranes from pre-existing cells.	36, 148-154

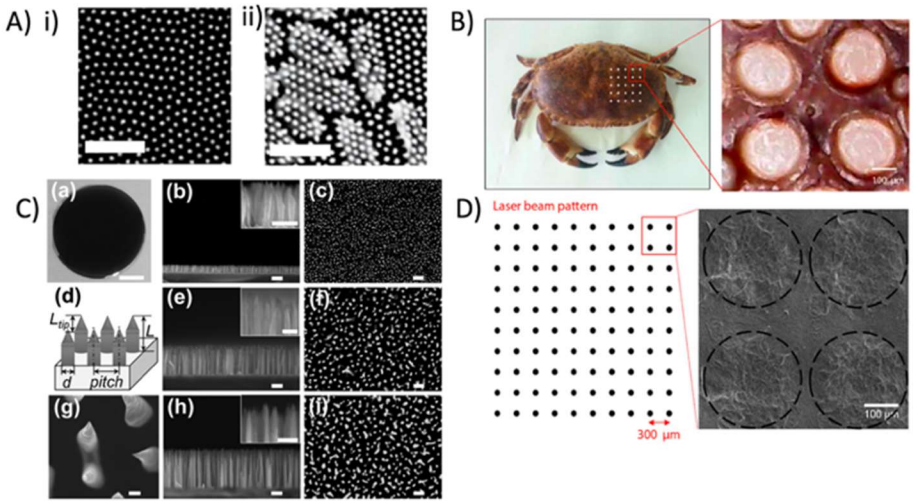

Figure C.1: A visual overview of nanopillar and nanowrinkle surface geometry. Section A &C) Comparison of SEM images of natural nanopillar geometry of cicada wing to biomimetic nanopillar surface geometry of varying density and pillar length. All scale bars are for 1 μm. Reproduced with permission [1,2]. Sections B & D) Comparison of natural crab carapace nanowrinkle geometry to SEM image of biomimetic patterned nanowrinkles. Reproduced with permission[101].

C.2 Surface Mimicry

Surface mimicry consists of modifying surfaces to mimic naturally antimicrobial surfaces. Most commonly utilized in this field is mimicry of insect wings (particularly of cicadae, damselflies, and dragonflies), shark skin, and the carapace of *Cancer pagurus* [2,97-99]. The surface geometry of insect wing, *Cancer pagurus,* and their respective biomimetic materials are summarized in Figure D.1. These surfaces are known to be self-cleaning due to naturally high hydrophobicity. In addition, these surfaces also kill bacteria by disrupting physical attachment, which prevents the formation of biofilms [2,100]. In insect

wings, disruption of physical attachment is achieved by nanopillar structures present on the wings. In the shark skin and *Cancer pagurus* carapace, the surface structure is instead nanogrooves and nanowrinkles, respectively. Biomimetic strategies using nanopillar geometry, nanogrooves, or nanowrinkles are summarized in this section.

C.2.1 Nanopillar Geometry

The nanopillar geometry of insect wings more specifically consists of thick and blunt geometry in high density on the surface. Bacteria will attach to the nanopillars in the space in between nanopillars and remain suspended, which induces mechanical stresses on the cell membrane and wall that will eventually result in membrane rupture [101]. However, Ivanova et al. has reported that cicada wing surface does not prevent attachment of pathological bacteria, though it was able to prevent the formation of biofilms [2]. Thus, current work with nanopillar surfaces focuses on better optimizing the geometry for higher antimicrobial activity. Michalska et al. utilized mimicry of this nanopillar geometry of insect wings by patterning on black silicon, but with a modification of the nanopillar geometry such that the nanopillars themselves will instead penetrate the bacteria directly [98]. Different lengths and density of nanopillars and their effects on resulting antimicrobial activity were investigated. Antimicrobial activity was reported as dependent on nanopillar length and somewhat density dependent, with no significant antimicrobial activity in surfaces with nanopillars shorter than 0.4 μm, an increasing density dependence of antimicrobial activity with 0.7-2.5 μm nanopillars, and density-independent enhanced antimicrobial activity with 3.6-6.7 μm nanopillars [98]. Overall, these results demonstrate that nanopillar geometry and density are important factors for enhancing antimicrobial activity and that the nanopillar geometry can have sufficient antimicrobial activity needed to deal with

antibiotic resistant bacteria once the geometry is modified from the normal geometry observed on actual insect wing.

C.2.2 Nanogrooves and Nanowrinkles

While nanopillar surface geometry has been frequently investigated as a means of mimicking the antimicrobial behaviour of insert wings, there remains an issue of optimization towards antimicrobial efficacy, with base nanopillar geometry still allowing for attachment of bacteria and findings showing dependence on nanopillar dimension parameters. Thus, other biomimetic geometries such as the nanogroove geometry of shark skin and nanowrinkle geometry of crab carapace have also been investigated in the literature [58,97,99,102].

The nanogroove geometry of shark skin consists of a ridged surface with 2 μm width and spacing and 3 μm heights [99]. Unlike nanopillars, this surface structure disrupts any attachment of cells and bacteria entirely. However, an accumulation of bacteria in the bottom of grooves has been reported. Sakamoto et al. have observed a decrease in bacteria presence when cultured on top of shark skin mimetic surfaces when the depth of the nanogrooves is shallow (0.4 μm) [99,103]. These findings imply that the nanopillar mimetic geometry may also require further optimization for enhanced antimicrobial activity.

Similarly, crab carapace geometry consists of a surface with protrusions much like ridges. However, these nanowrinkles originate from a hierarchical geometry, in which there are smaller winkles along the fold of larger wrinkles, with wrinkle frequency ranging from 50 nm to 500 μm [104]. Work by Efimenko et al. has demonstrated that surfaces with this geometry are capable of an antibiofouling capability that prevents attachment of microorganisms, which includes bacteria [104]. Papi et al. created a graphene-oxide based hydrogel material that was patterned with this geometry by laser printing and demonstrated enhanced antimicrobial capability against several

species of relevant bacteria (e.g.: S. aureus and E. Coli) when the hydrogel is printed with the crab carapace surface geometry [58]. Overall, antimicrobial results for surfaces using nanogrooves and nanowrinkles show potential as antimicrobial materials.

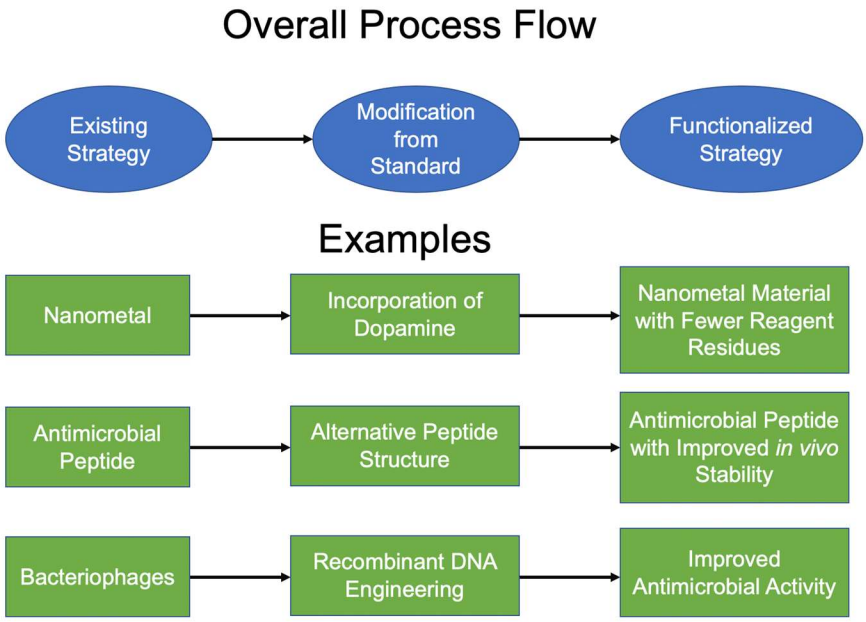

Figure C.2: Overview of biomimetic functionalization of existing antimicrobial strategies.

C.3 Biomimetic Functionalization of Existing Antimicrobial Strategies

Beyond surface mimicry, another major strategy for creating novel antimicrobial materials is to utilize biomimetic functionalization approaches to address limitations of existing antimicrobial strategies. In particular, this section will discuss improvement of nanometals, antimicrobial peptides, and bacteriophages. These strategies, while promising as means for combatting antimicrobial resistant strains of bacteria, have issues with cytotoxicity or effective delivery. Thus, the strategies in this section will discuss means to overcome these shortcomings.

For this section, we will discuss the functionalization of naturally antimicrobial substances including nanometal, antimicrobial peptides, and bacteriophages. For nanometals, we focus on

methods of synthesis that reduce the cytotoxicity associated with the reactions. These strategies include the use of dopamine and green methods of synthesis and all focus on reducing the toxicity of nanometals by reducing the amount of residue reactants. For antimicrobial peptides, modifications in peptide structure have been investigated to enhance delivery. These alternate structures can entail either the form of delivery (e.g: molecules vs. as a material) or modification of the molecular structure itself. For bacteriophages, genetic engineering has been the primary means of enhancing function. These modifications can range from expanding targeting capacity to enhancing selectivity of the bacteriophages. [56,57,59,105-110] **Figure C.2** summarizes the types of strategies that are described in this section.

C.3.1 Optimization of Nanometal Synthesis to Reduce Toxicity:

Metals such as silver and gold have been known to exhibit broad antimicrobial activity for some time by targeting multiple cellular processes in bacteria cells. However, bulk metals can cause cytotoxicity, therefore, nanometals have been widely investigated as an alternative to bulk metals due to decreased cytotoxicity. This effect is achieved by the nanoscale particle size, which vastly decreases the overall metal content as well as increases the total surface area that can come into contact with bacteria [56]. However, syntheses of nanometals typically entail the chemical reduction of metal ions, which can be left in residue after production and are harmful to the physiological environment if they remain during delivery to the body [56]. Therefore, there is a need to optimize nanometal synthesis to decrease toxic byproduct production. Mussel mimetic materials, which are naturally nontoxic and have the ability to serve as a reduction agent, have been used frequently to reduce the cytotoxicity of nanometals by providing an alternative synthesis method. The reductive property of mussel inspired materials is due to the content of dopamine in their adhesive proteins and dopamine's catechol structure, which consists of a

benzene ring with two hydroxyl side groups [57,59,105-108]. Because of this reductive capacity, dopamine and dopamine-inspired materials are a popular choice for less harmful production of nanosilver nanoparticles (NPs). Additionally, dopamine-based synthesis strategies have seen use for improving other existing antimicrobial strategies, such as serving as a selective delivery vessel for peroxides [108]. Other methods of nanometal synthesis with reduced cytotoxicity include green methods of nanometal synthesis. Dopamine and other green synthesis based methods for reducing cytotoxicity are discussed in subsequent sections.

C.3.2 Dopamine-based Methods for Reducing Cytotoxicity:

Dopamine has frequently been used as a means of less harmful production of antimicrobial nanometals, particularly nanosilver. Under artificial synthetic means, the production of nanosilver entails the use of silver ions and harsh solvents. Residual ions or solvents can have damaging effects on nonpathogenic cells [57,59,105,106]. However, because silver is known to be antibiotic against many pathogenic species, the material still has great appeal and has thus led to great interest in seeking means to synthesize nanosilver by less toxic means [56]. Many investigators have utilized the reductive property of dopamine to create composite materials with antimicrobial nanosilver with reduced cytotoxicity.

Methods of incorporation of dopamine into materials vary from direct surface functionalization by dopamine [57,59,105] to hydrogels that have been conjugated with dopamine proteins [107] or copolymerized with dopamine-incorporated monomers, particularly dopamine methacrylamide (DMA). [106,108,109] For fabrication of antimicrobial functionalized surfaces, base materials are treated with a solution of dopamine for many hours and then immersed in silver nitrate solution [57,59,105]. Kung et al., Liu et al., and Wu et al., show that the manufacturing process can be applied across different materials and report significant antimicrobial activity [57,59,105]. When

incorporated into hydrogels, DMA is typically produced and then included as a copolymer component. Once the dopamine composite hydrogel is complete, nanosilver is then incorporated by contact with silver nitrate solution [106]. GhavamiNejad et al. created such a composite hydrogel for wound healing applications using a zwitterionic hydrogel incorporated with silver nanoparticles. The composite material was reported to have significant antimicrobial activity for bacterial culture over the course of 24 hours [106].

Though silver is the main focus of functionalization, dopamine has been used to reduce cytotoxicty of other antimicrobial materials as well. Cheng et al. used dopamine to deposit zinc-oxide nanoparticles onto Poly(ethylene terepthlate) (PET) films and has reported significant antimicrobial activity [109]. Additionally, dopamine's biochemical properties can also be used as a means of delivery of other antimicrobial substances. Wang et al., fabricated peptide composite hydrogels by conjugating ε-poly-L-lysine (EPL) to polyethylene glycol (PEG) using dopamine [107]. Additionally, dopamine has been used to engineer a delivery system of hydrogen peroxide to address the issue of hydrogen peroxide transportation and stabilization. While known to be antimicrobial, hydrogen peroxide is relatively volatile, which can make transportation of viable solutions over long distances difficult. Additionally, hydrogen peroxide is very strong as an antimicrobial agent and is typically diluted to 3%, which can further contribute to problems with storing large volumes of ready to use solutions. [110] To address these issues, Meng et al. fabricated dopamine inspired hydrogels that can be repeatedly activated to produce hydrogen peroxide depending on environment pH. These dopamine-mimetic hydrogels utilize the catechol groups of dopamine to generate hydrogen peroxide by autoxidation and were reported to completely reduce bacteria colony formation after 24 hours at concentrations significantly lower than the market 3% hydrogen peroxide solutions [108]. Overall, dopamine-based materials allow for chemically

versatile means of including antimicrobial function using known antimicrobial materials, particularly nanometals.

C.3.3 Additional Green Synthesis Methods:

Due to residue of harmful reagents and involvement of ions that come from synthetic synthesis of metal nanoparticles, there has been much interest in the investigation of alternate methods of nanometal synthesis, including dopamine based strategies as discussed above. Beyond dopamine based strategies, other green synthesis schemes have also been explored, including the use of naturally derived reduction agents or the direct use of microorganisms. In nature, there exist several components and microorganisms capable of reducing ions into nanoparticles. Examples include compounds derived from plant matter essence, such as citrus fruit peels, coffee, tea, lemon verbena, and sorghum bran, which contain organic molecular structures capable of contributing to reduction reactions [111-116]. Production of nanoparticles by these methods produce no known toxic material [112].

Microorganisms capable of contributing to reduction reactions include bacteria, fungi, and algae [117-119]. However, the synthesis of nanometal particles by use of microorganisms is difficult to scale up, with algae seeing some greater appeal as the culture conditions are not as demanding as bacteria or fungi. Ebrahiminezhad et al. achieved a synthesis of silver nanoparticles by use of supernatant fluid from *Chloerlla vulgaris* algae culture. Increasing concentrations of these silver particles was directly correlated to increasing antimicrobial activity and increasing cytotoxicity [112,119]. Overall, green syntheses show potential towards improving production of antimicrobial material strategies by providing an alternate means to producing nanometals via more ecologically favourable and less cytotoxic methods.

C.3.4 Antimicrobial Peptide Modifications for Improved Delivery

Antimicrobial peptides have been seen as a promising potential platform for combatting antimicrobial resistant strains of bacteria due to killing bacteria by disrupting necessary lipid components instead of metabolic mechanisms [120-123] . However, they can be difficult to deliver due to their sensitivity to amphiphilic balance and difficult to administer due to in vivo toxicity at high doses. [124-126] Xi et al. investigated the use of antimicrobial peptides with enhanced functionalization for better biocompatibility. This functionalization was achieved by focusing on making the material biomimetic of the application environment, in this case, skin in wound healing applications, by creating a peptide composite polymer and then electrospinning the composite material into a matrix mimetic of skin extracellular matrix. The peptide composite material created was reported to significantly inhibit bacterial growth with incorporation of as little as 10% antimicrobial peptides. Notably, lower cytotoxic effects were also observed in the presence of 10% antimicrobial peptide incorporated material, which indicates potential antimicrobial efficacy with reduced cytotoxicity due to lower antimicrobial peptide content [127]. Also notable is the conjugation of antimicrobial peptides to carrier materials for stabilization and modulation of potential cytotoxic effects [56,91]. To diminish the harsh effects of antimicrobial peptides, Chen et al. investigated inducing self-assembly of the antimicrobial peptide SFT onto the surface of nanogold particles, using the nanogold as a stabilizing agent. These gold-peptide composites were reported to effectively inhibit growth of multi drug resistant strains and disrupt bacterial membrane structure [128]

In addition, direct modification of antimicrobial peptide structure has been investigated. As an example, Xiong et al. created antimicrobial peptide mimics that relied on radial amphiphilicity as opposed to facial amphiphilicity. This structural difference allows for a

reduction in self aggregation and was reported to have better stability in physiologically relevant buffers (e.g.: human serum, fetal bovine serum). The peptide mimetics were also found to have significant antimicrobial activity against drug resistant strains of *E. Coli*, *S. aureus*, and *Bacillus cereus* [129]. Helix-coil structure has also been investigated as a means of allowing antimicrobial peptides to gain pH activated antimicrobial ability. This structural modification reduces the toxicity of antimicrobial peptides by increasing selectivity towards bacteria of interest (e.g.: only in active form when in pH 2 for treating *Helicobacter pylori* in the stomach). [130,131]

C.3.5 Bacteriophages:

Bacteriophages are viruses that target bacteria and kill them. They have previously seen use as a strategy towards combatting bacterial infection due to their ability to dose automatically, low inherent toxicity, and high efficacy [28]. However, without modification bacteriophage are limited by a narrow range of effect and can be resisted by bacteria via evolution of resistance [27,132,133]. To better enhance the antimicrobial capability of bacteriophages, a range of genetic modifications and engineering have been utilized, including expansion of effect range and targeting of bacteria by mechanisms different from antimicrobial drugs [132,133]. Lu et al have developed recombinant genetic engineering techniques to achieve these modifications in bacteriophages [134]. These genetic modifications can allow bacteriophages to directly infiltrate bacteria and disrupt bacterial function, such as DNA repair in *E. coli* [132,133,135]. Other modifications have been investigated including gene functionalization towards longer circulation time, reduced toxin release of lysed bacteria, and suppression of bacterial resistance to antimicrobial drugs [135-137].

Overall, functionalization of existing strategies present alternative methods of enhancing the performance of nanometals, antimicrobial molecules, and bacteriophages in a wide range of aspects including biocompatibility, delivery efficiency, and efficacy.

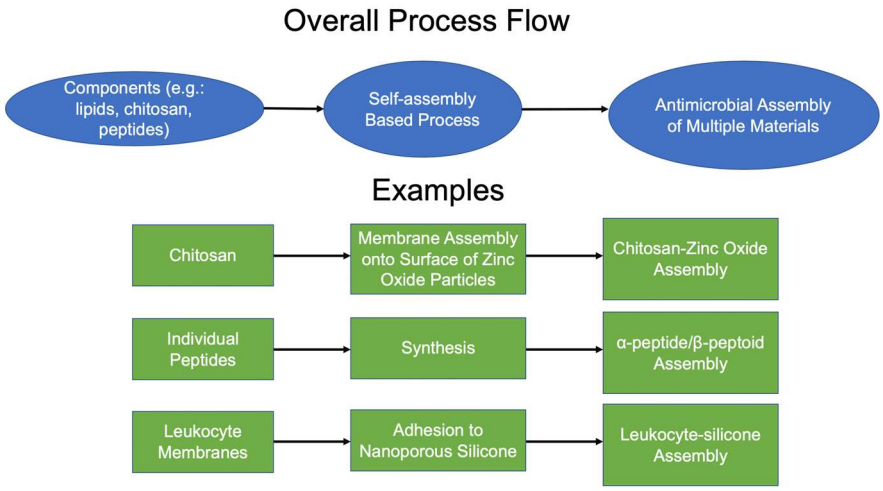

Figure C.3: Schematic of biomimetic assemblies

C.4 Biomimetic Assemblies

In this section, we will discuss antimicrobial biomimetic assemblies, which we define as antimicrobial materials that consist of an assembly of components, frequently including use of a cell-membrane like structure or cell-mimetic morphologies and function. In particular, biomimetic assembled particles, such as bioactive supramolecular assemblies, antimicrobial peptide-based particles, and cell mimetic particles will be discussed. A schematic summarizing the types of strategies discussed in this section is shown in **Figure C.3**.

C.4.1 Biomimetic Assembled Particles

Like surface mimicry discussed in earlier sections, biomimetic assembled materials can disrupt bacteria structure by mechanical means. This method of antimicrobial activity results from a charge on the material causing attachment to bacterial cell walls, which results in lysis of the bacteria [138]. Examples of such materials include the use of charged lipid layers and polymeric coatings on nanoparticles. Xavier et al. investigated the use of a cationic bilayer with polystyrene core, which has been reported to mimic histones with DNA compaction [139], with incorporation of the antimicrobial peptide gramicidin. The particles were reported to have higher positive charge when including gramicidin and had enhanced antimicrobial effects against *S. aureus* but no significant effects against *E. coli*. The authors hypothesized that this difference in efficacy may be the result of steric hindrance by the inclusion of the peptide [140]. Similar principles has been applied to assembled particles based around polymer cores by utilizing cationic polymers to provide antimicrobial function, such as Polydiallyldimethylammonium chloride (PDDA) and Poly(methyl methacrylate) (PMMA). These materials were found to be a capable of reducing bacterial cell viability to 0%, but did require higher dosage when combatting hardier species of bacteria, such as *S. aureus*. [136,141]

This type of membrane-enclosed particle can also be used with antimicrobial nanometals, antimicrobial peptides, and polymers by changing the core to which the coating materials adsorb [138,139,142]. For nanometals, incorporation is achieved by loading a porous core and then enclosing it with a biomolecular layer. This construction achieves a means to control the amount of exposure to nanometal contact and, in combination with chitosan, has been reported to achieve antimicrobial activity while improving cytotoxicity for zinc oxide and silver with a membrane structure mimetic of organisms like yeast [143-145].

C.4.2 Antimicrobial Peptide-based Particles

Antimicrobial peptide-based particles represent another class of biomimetic assemblies utilized for antimicrobial purposes. Antimicrobial peptide based particles include approaches which create particles that mimic the structure of antimicrobial peptides themselves or deliver antimicrobial peptides via particles as a means for improving delivery [126,129]. Particles based on directly mimicking the antimicrobial peptide structure are focused on altering structures in ways that can still retain antimicrobial activity while allowing the molecules to undergo less degradation and off-target interactions in the physiological environment before reaching target sites [130]. Commonly investigated designs seeking to reduce premature degradation and off-target interactions include peptide-peptoid composites and α-peptide/β-peptoids [126,146-148].

Particles can also be used to entrap antimicrobial peptides to improve their delivery and decrease systemic toxicity. By enclosing antimicrobial peptides with a membrane, peptides are allowed a means of delivery for difficult to reach targets, such as sites beyond the blood-brain barrier, and can be protected from premature degradation. Enclosed peptides have also been reported to still retain the antimicrobial efficacy of the peptide alone. Such approaches have been discussed in detail in previous sections. Overall, biomimetic assembled materials show great potential for attaining improved delivery means for a variety of antimicrobial materials.

C.4.3 Cell Mimetic Materials

An additional class of biomimetic assemblies includes cell mimetic materials, including particles which mimic various immune cell function. Native immune cells have intricate mechanisms for fighting bacterial infection. For this reason, there has been appeal in investigation towards the creation of mimetics of cells involved in infection combat, including the investigation of leukocyte-mimetic materials [149]. Molinaro et al. produced lipid nanoparticles

incorporated with leukocyte membrane proteins, which have been termed leukosomes. The leukosomes are capable of drug delivery and targeting inflamed vasculature [150]. Hammer et al. produced a hybrid particle termed as "leuko-polymersome" that consists of polymeric vesicles coated with binding motifs mimicking leukocyte interactions in the physiological environment [151]. Parodi et al. investigated the construction of porous silicone coated with leukocyte membranes, which are termed as leuko-like vectors (LLV) [152]. Both leukopolymersomes and LLVs were reported as capable of targeting inflamed endothelium, which presents potential for targeted drug delivery to infected tissue [151,152]. In general, these materials show high potential towards targeted delivery of antimicrobial agents towards sites of infection to drug resistant bacteria.

In a similar vein, cell mimetics have also been used to combat infection by reducing bacterial toxin presence. Zhang et al have developed nanosponges consisting of polymeric nanoparticles enclosed by membranes of red blood cells. This construction allows the nanosponges to mimic nonspecific binding of cell membrane components to toxins produced by the likes of MRSA and neutralize toxins. Membranes of other cells, such as white blood cells, were also found to ward against sepsis as well, presenting potential for tunability to a variety of applications. [153,154]

Platelets are also known to contribute to the infection combat process, which gives promise to the investigation of platelet-mimetic materials as an antimicrobial platform. Sproul et al. produced a platelet-mimetic particle capable of antimicrobial activity by creating nanogold composite deformable hydrogels [36]. These composites were found to have significant inhibition of bacterial growth after 24 hours but were not as effective at controlling bacterial growth as ampicillin, a clinically used antimicrobial drug [36]. While cell mimetic antimicrobial strategies

show promise in mimicry of leukocyte, red blood cell, and platelet function, further investigation is needed to more thoroughly investigate function and optimize antimicrobial capacity. For leukocyte mimetic materials, behaviour of the materials in combination with delivery of antimicrobial substances needs to be further investigated. For platelet-mimetics, further investigation is needed to optimize the antimicrobial activity.

C.5 Conclusions

Biomimetic antimicrobial strategies show great potential and versatility in addressing the rise of antibiotic resistant bacteria. These strategies can produce biocompatible means of dealing with antibiotic resistant bacteria by physical disruption, as observed with surface mimicry, biomimetic functionalization of existing antimicrobial strategies, and biomimetic assemblies. However, there remains much room for optimization.

Surface mimicry allows for disruption of bacteria by mechanical means without the need for inclusion of additional antimicrobial substances, which can allow for safer methods of combating bacterial contamination. However, there remains an issue of geometry optimization as completely mimicking natural surface geometry may not result in the desired antimicrobial capability. Additionally, there may also be dependence on the type of material used as the works involving surface mimicry all use different materials, with some utilizing materials with already reported antimicrobial properties, such as black silicone and graphene-oxide based gels [58,98,155].

Functionalization of existing strategies seeks to improve on previously investigated antimicrobial strategies. Nanosilver, though a popular choice for its antimicrobial efficacy range, is known to be cytotoxic at certain concentrations [56,91]. Similar concerns have also

been reported for substances like antimicrobial peptides and peroxides [91,110]. Despite efforts to reduce these negative effects, the concerns associated with the base antimicrobial material still linger. For silver composite surfaces produced by dopamine, it is hypothesized that this may be the result of harmful silver ions leaching off from the nanoparticles despite the less harsh synthesis provided by dopamine's reductive properties [57,59,105,106].

In a similar vein, although biomimetic syntheses can reduce the harmful aspects of the nanometal production process, the cytotoxicity problems of the ultimate nanometal product still remains. Furthermore, green syntheses have dependence on the substance used to facilitate nanoparticle production. Synthesis focused around microorganisms may demand very specific culture conditions or even present potential pathogenic effects, particularly in production by bacteria or fungi [119,156]. In addition, it has been reported that plant essence based syntheses can be significantly faster than microorganism strategies due to microorganisms requiring separate culture with varying degrees of specificity (i.e.: culture conditions for algae are less specific than those for fungi and bacteria) [112,114,117,119,156].

Biomimetic assembled particles also present potential in controlling some of the harmful effects associated with antimicrobial strategies. However, they too require further optimization. For strategies including nanometal particles, the cytotoxicity concerns are also still a major point of consideration. Additionally, the creation of these types of particles can be rigorous in the specific chemistry required to produce complex peptide structures or to produce membranes. Cell mimetic materials demonstrate the feasibility of the creation of materials mimicking cells involved in combat of infection. However, much of the investigation conducted in this field requires further study for both the

determination of potential inherent antimicrobial activity, its optimization, and potential changes in particle behaviour when loaded. For platelet mimetic materials in particular, there remains a need to investigate the incorporation of other antimicrobial materials for higher antimicrobial activity, such as stronger nanometals like nanosilver.

While versatile in potential for application, these biomimetic antimicrobial strategies may also call for further optimization for cytotoxicity depending on application. For applications focused at applying these antimicrobial materials towards use in the clinical field, the consideration of cytotoxicity is substantially more important than in other applications. Nanosilver-based strategies in particular had reported cytotoxicity concerns in this regard [56,57,59,105-107,111,112,114-119,127,157,158]. In contrast, when the application is focused around keeping substances such as medical tools and biosensors from bacterial contamination, the cytotoxicity concern may not be as relevant [157].